The influence of vertical loading on the lateral behaviour of rigid monopile foundation in clay soil

An analysis using 3D Finite Element Modeling

Rein de Voogd

Delft University of Technology

TUDelft

THE INFLUENCE OF VERTICAL LOADING ON THE LATERAL BEHAVIOUR OF RIGID MONOPILE FOUNDATION IN CLAY SOIL

AN ANALYSIS USING 3D FINITE ELEMENT MODELING

by

Rein de Voogd

To obtain the degree of Master of Science
at the Delft University of Technology
to be defended publicly on the 30th of May, 2022

Student number:	4374452	
Project duration:	March, 2021 – May, 2022	
Thesis committee:	Dr. Ir. K. Gavin	TU Delft, chair
	Dr. Ir. A. Askarinejad	TU Delft
	Dr. Ir. F. Pisanò	TU Delft
	Dr. Ir. H. Wang	TU Delft
	Ir. Y. Zhang	TU Delft

TUDelft

Delft
University of
Technology

ABSTRACT

Monopiles with large diameter (larger than 6 m) and low aspect ratio (less than 6) are increasingly used in offshore wind farms. These foundations demonstrate a rigid response under lateral loading. The validity of the existing design methods, that are based on small diameter flexible piles, has been questioned by both the industry and researchers. In addition, the monopiles are subjected to both lateral and vertical loads. The influence of vertical load on the lateral design of monopile is not clear, especially for these short rigid monopiles in clay, considering the relatively small vertical capacity compared with those in sand. In this light, this study aims to perform a comprehensive study on the influence of vertical load on the lateral response of monopile foundations in clay soil. The performance of existing design models for both small diameter flexible and larger diameter short piles are systematically evaluated in both normally consolidated and overconsolidated clay. In the end, a new mechanism based design method was proposed for modelling the lateral response of monopile foundations in clay soil.

All analysis in this study was performed using 3D finite element modeling in PLAXIS 3D software. The NGI-ADP constitutive model was adopted to simulate the nonlinear mechanical behaviour of clay. The finite element model of pile-soil system was first validated against the field and centrifuge tests performed in clay. Considered in the analysis is a short rigid pile with a diameter of 10 m (L/D = 3) and a long flexible pile with a diameter of 2 m (L/D = 15). The analyzed clay soil profiles consist of a normally consolidated clay soil and an overconsolidated clay soil with a constant undrained shear strength profile equal to 30 kPa. For each pile in each type of clay soil, a pure lateral loading scenario is performed first to assess the validity of current design methods in regards to lateral behaviour analysis of monopile foundations in clay soil. Subsequently, a combined loading scenario is performed to assess the influence of vertical loading on the lateral behaviour of rigid monopile in clay soil.

Results of the pure lateral loading scenario suggest that current design methods heavily underestimate the lateral capacity of rigid monopile foundations in both clay soil profiles analyzed. According to the findings of this study, it can be concluded that current design methods, such as API, are not fit to provide an accurate assessment regarding the lateral load response of rigid monopile in clay soil. In order to correctly assess the lateral load response of rigid monopile in clay soil, a method consisting of a 3D finite element model akin to the model used in the research or a PISA design model is advised. A potential third design method, the 1D rotational spring model, is also proposed. This is due to similar findings regarding the rotation center of a rigid monopile in clay soil as compared to results found in literature regarding rigid monopile in sandy soil.

Results of the combined loading scenario suggest that the presence of vertical loading causes a decrease in lateral and moment capacity of the rigid pile in both clay soil profiles analyzed. However, the influence is negligible when the vertical load magnitude is smaller than 50% of its bearing capacity. A more obvious influence of the applied vertical load was found at a magnitude of 75% of the bearing capacity. To quantify the influence of vertical load on a monopile foundation, a series of load analysis were performed on a real offshore wind turbine with a 5MW power capacity. It was found that the vertical load on a typical monopile foundation in clay is around 27% of its bearing capacity. According to the findings of this study, it can be concluded that the influence of vertical load on the lateral response of rigid monopiles in clay soil is limited and can be ignored in foundation design.

PREFACE

This thesis was written during the global COVID-19 pandemic. A period in time where social distancing was the norm and where the university was mostly closed. Thus, the bulk of this thesis was written at home. The thesis is a product of mostly online cooperation between me and my supervisors. Fortunately, the guidance given to me through the support of my supervisors was of excellent quality.

First and foremost, I want to thank my supervision. The guidance given to me by Huan Wang and Yuen Zhang during the research was excellent. During moments of confusion and doubt, I could always contact them and get a quick response back. This combined with their continuous dedication and positive mindset made me very grateful of the supervision during this research.

Second, I want to thank the Delft University of Technology for all the experiences and lessons learned over the course of my Master degree. I am very grateful for the people I have met and the opportunities that were made possible through the university.

Last but not least, I want to thank my parents, my sisters and my friends for their continuous support during these confusing times.

Rein de Voogd
Delft, May 2022

CONTENTS

NOMENCLATURE

ABBREVIATIONS

Abbreviation	Definition
API	American Petroleum Institute
CF	Capacity Factor
CPT	Cone Penetration Test
DSS	Direct Simple Shear
FDA	Finite Difference Analysis
FEA	Finite Element Analysis
FEM	Finite Element Method
IEA	International Energy Association
LL	Liquid Limit
NC	Normally Consolidated
NGI	Norwegian Geotechnical Institute
NREL	National Renewable Energy Laboratory
OC	Overconsolidated
OCR	Overconsolidation Ratio
PI	Plasticity Index
PL	Plastic Limit
SDS	Sustainable Development Scenario
STEPS	Stated Policies Scenario
TXC	Triaxial Compression
TXE	Triaxial Extension

SYMBOLS

Symbol	Definition
α	Interface roughness
γ	Unit weight
γ_f^C	Shear strain at failure in triaxial compression
γ_f^{DSS}	DSS shear strain at failure
γ_f^E	Shear strain at failure in triaxial extension
γ^e	Elastic shear strain
γ^p	Plastic shear strain
γ_f^p	Plastic shear strain at failure

Symbol	Definition
γ_{sat}	Saturated Unit weight
γ^t	Total shear strain
ϵ_{50}	Strain at half the maximum stress
θ	Rotation
κ	Hardening parameter
ν	Poisson's ratio
ν_p	Poisson's ratio pile
ν_u	Undrained Poisson's ratio pile
ρ_s	Solid density
σ'_v	Effective vertical stress
σ_z	Overburden pressure
τ	Shear stress
τ_0	Initial mobilized shear stress
ϕ	Friction angle
ψ	Dilation angle
A	Curve fitting parameter
a	Curve fitting parameter
B	Width
c_v	Consolidation coefficient
D	Diameter
d	Location of rotation center
D_r	Relative density
e	Loading eccentricity
e_{ini}	Initial void ratio
E_p	Young's modulus pile
E_s	Young's modulus soil
F	Force
G	Shear modulus
g	Gravitational acceleration
G_{max}	Maximum shear modulus
G_s	Specific Gravity
G_{ur}	Unloading-reloading shear modulus
H	Lateral load
H_{ult}	Lateral capacity
I_p	Inertia pile
J	Empirical parameter for the definition of ultimate soil resistance
K	Bulk modulus
k	Permeability coefficient
K_0	Coefficient of earth pressure at rest
L	Embedded length
M	Moment
M_{ult}	Moment capacity
m	Strength increase exponent

Symbol	Definition
m_b	Blade mass
m_p	Pile mass
m_{rn}	Rotor nacelle mass
m_t	Tower mass
N_p	Ultimate soil resistance coefficient
p	Soil resistance
p	Ultimate soil resistance
R	Rigidity parameter
R_{inter}	Strength reduction factor
S_u	Undrained shear strength
S_u^a	Active undrained shear strength
$S_{u,inc}^a$	Active undrained shear strength increment with depth
$S_{u,ref}^a$	Active undrained shear strength at the reference depth
S_u^{DSS}	DSS undrained shear strength
S_u^p	Passive undrained shear strength
t	Thickness
u_z	Vertical displacement
V	Vertical load
V_{ult}	Bearing capacity
W	Weight
W_p'	Buoyant weight pile
W_s'	Buoyant weight soil plug
y	Pile deflection
y_c	Pile deflection at half the ultimate soil resistance
z	Depth
z_r	Depth of reduced resistance
z_r	Reference depth

LIST OF FIGURES

LIST OF TABLES

1

INTRODUCTION

1.1. THE POTENTIAL OF OFFSHORE WIND TURBINES

Figure 1.1: 2021-2025 New onshore and offshore wind installations in Europe (WindEurope, 2021b).

For more than half a century, global consumption of energy is growing nearly every year. To put this statement into perspective, the global primary energy consumption increased from 43,248 TWh in 1965 to 162,149 TWh in 2019 (Ritchie & Roser, 2020). Global energy consumption is projected to increase nearly 50% by 2050 compared with 2020 (U.S. Energy Information Administration, 2021). As of 2020, this global energy demand is generated for 85% by the combustion of fossil fuels, i.e.: natural gas, coal and oil (BP, 2021). To answer the global energy demand in the future, the use of fossil fuels as a main source for energy generation is seen as problematic. Fossil fuels are a non-renewable resource, meaning that fossil fuel resources are finite. In addition, the scientific consensus on human caused climate change by means of the combustion of fossil fuels is greater than 99% (Lynas et al., 2021). A potential solution to problems regarding fossil fuel combustion is energy generation by means of renewable sources.
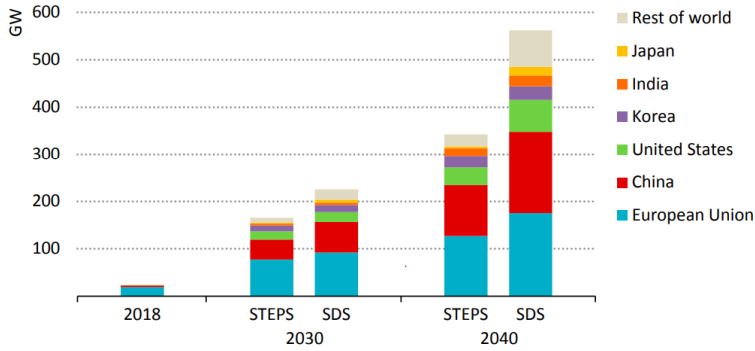
Figure 1.2: Projected global offshore wind capacity per country or region in the year 2030 and 2040 (International Energy Association, 2019).

Among all the renewable energy sources, wind energy is one of the most promising options considering that wind turbines do not release emissions that pollute air or water and do not require cooling by water. Globally, this potential of wind as a renewable energy source is being recognized. This can be seen by the increase in wind energy production by energy industries. As shown in Figure 1.1, Europe is projected to install 105 GW of new wind farms over 2021-2025 (WindEurope, 2021b). The biggest share of the new wind farms, an estimated 70%, will be installed onshore.

Even though new offshore wind farm production is lower compared to new onshore wind farms, offshore wind farm production is rapidly growing per year. Globally, the offshore wind market grew nearly 30% between 2010 and 2018 (IEA, 2019). The more advantageous wind conditions contribute highly to the remarkable potential of offshore wind energy that today's offshore wind market does not even come close to tapping in fully. The full potential of offshore wind energy production is estimated to be 420,000 TWh per year (IEA, 2019). That is to say, more than 18 times the global electricity demand today.

Another contribution is the large capacity factor associated with offshore wind energy production. The capacity factor (CF) indicates the net electricity generated, for the time considered, to the energy that could have been generated at continuous full-power operation during the same period (U.S. Nuclear Regulatory Commission, 2021). The CF is often expressed in percentages as:

$$CF = \frac{Actual\ energy\ output\ (MWh)}{Capacity\ (MW) * Time\ period\ (h)} * 100\% \qquad (1.1)$$

New offshore wind projects often have a CF in the ranges of 40 to 50% (IEA, 2019). The CF ranges of new offshore wind projects are comparable to that of efficient gas power plants, are larger than onshore wind farms and are almost double than the CF ranges associated with solar PV panels. This makes offshore wind energy generation the renewable technology that comes closest to providing a base load power generation.

Due to the high potential of offshore wind energy and the global arrangements made to reduce greenhouse gas emissions (e.g: European Commision, 2013), regions and coun-

tries worldwide are projected to take strides in the offshore market. In a stated policies or conservative scenario, the offshore wind capacity is projected to increase significantly (Figure 1.2). The global offshore wind capacity is projected to increase from 23 GW in 2018 to over 150 GW by 2030. By 2040 the global offshore wind capacity is expected to grow over 300 GW (International Energy Association, 2019).

1.2. THE USE OF MONOPILES
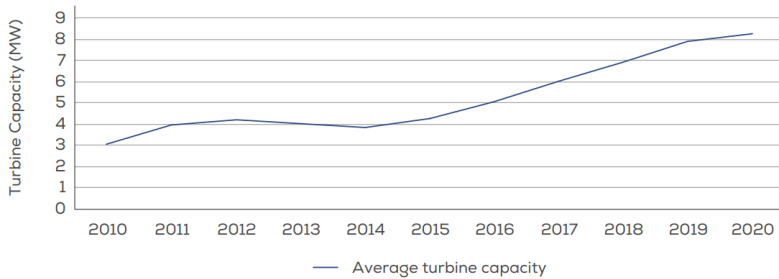
Figure 1.3: Yearly average of newly installed offshore wind turbine rated capacity (WindEurope, 2021a).
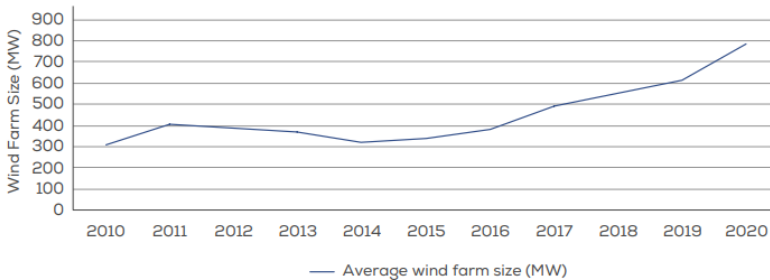
Figure 1.4: Yearly average size of commercial offshore wind farm projects (WindEurope, 2021a).

With the rapid growing offshore wind market, larger-scale offshore wind farms with bigger wind turbines are constructed in deeper waters. In the last decade, the average power capacity of offshore wind turbines in Europe has seen an almost threefold increase from an average of 3 MW in 2010 to 8.2 MW in 2020. A similar trend can be seen in the average wind farm size, growing from an average wind farm size of 300 MW in 2010 to 788 MW in 2020 (WindEurope, 2021a). Both trends are visualised in Figures 1.3 and 1.4 respectively. In 2010, the average water depth of offshore wind farms was 20 m (WindEurope, 2020). In 2020, this average increased up towards 36 m (WindEurope, 2021a). Figure 1.5 shows the spread of average water depth and distance to the shore of all offshore wind farms in Europe. From Figure 1.5, it can be interpreted that most future offshore wind farms will be designated in water depths less than 40 m.
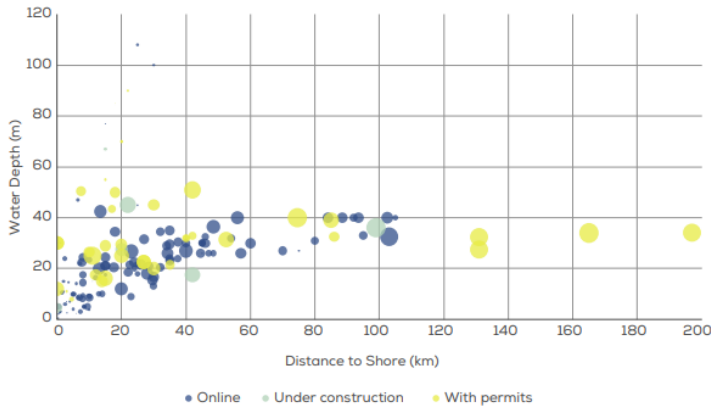
Figure 1.5: Average water depth and distance to shore of all offshore wind farms in Europe. The size of the bubble indicates the overall capacity of the site (WindEurope, 2021a).

Various foundation types (Figure 1.6) that are used in practice for offshore wind turbine construction are often categorized as either a bottom-mounted structure (i.e.: a rigid connection between the foundation system and the seabed) or a floating structure (i.e.: no rigid connection between the foundation system and the seabed). The foundation structure that is eventually adopted in practice is dependent on three criteria (Igoe et al., 2013):

- Local sea bed conditions.

- The water depth.

- Financial constraints.

Globally, the most popular foundation structure used in practice for offshore wind turbine construction is the monopile foundation. A cumulative unit of 4681 units monopile foundations have been installed. This contributes to a global share of 81.2%. This is followed by jacket structures with a 9.2% share and gravity bases with a 5% share (WindEurope, 2021a).

A monopile is a steel tube that is bored or driven in the seabed and attached to the tower via a transition piece. A monopile foundation used in the offshore wind industry often consists of a hollow steel cylinder with a diameter, D, between 4-6 m and is the common choice when it comes to offshore wind farm construction at shallow water depths less than 30 m (Arshad & O'Kelly, 2012). The embedded length, L, of the monopile foundation in the seabed is dependent on the seabed characteristics and the total load applied, though often a L of 30 m is usually marked as sufficient to meet design criteria in Europe (Musial & Ram, 2010). Common L/D ratios or aspect ratios found in monopile design consist of values ranging between 5-6 (Doherty & Gavin, 2012).

There are several reasons why monopile foundations are often chosen as the preferred foundation structure for offshore wind farms. Following the three main criteria in choosing a foundation structure (Igoe et al., 2013), the first reason is due to the local

1
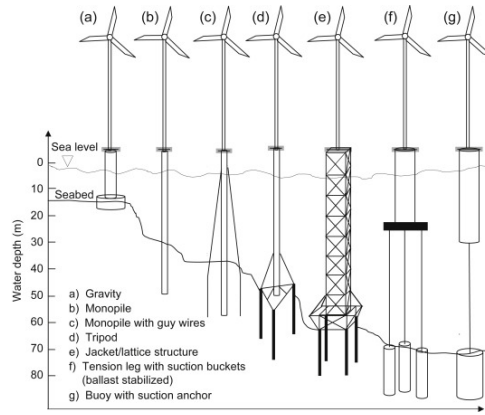
Figure 1.6: Foundation structure options with typical ranges of water depth application (O'Kelly & Arshad, 2016).

sea bed characteristics in Europe. Currently, 79% of the cumulative installed capacity of offshore wind farms comes from wind farms installed in the North Sea (WindEurope, 2021a). The sandy and gravelly nature of the North Sea seabed makes it possible to drive the monopile foundation to the required depth with minimal drilling. The second reason is the water depth. As stated previously, the average water depth of offshore wind farms is 36 m (WindEurope, 2021a). Monopile foundations are a proven and convenient option when it comes to water depths less than 40 m (Kallehave et al., 2015). Finally, the third reason is financial constraints. Foundation and installation costs of monopile foundations account for 25% of the total capital expenditure of an offshore wind project (Stehly et al., 2019). To keep costs to a minimum, the foundation structure should be easy to install and fabricate. Monopile foundations fit both these criteria.

1.3. RIGIDITY, COMBINED LOADING AND A CLAY SOIL PROFILE: THE DESIGN CHALLENGES FOR FUTURE MONOPILE DESIGN

To understand the design challenges that originate from rigid behaviour inhibited by a monopile foundation, one first needs to understand the concept of the flexibility of a monopile foundation. Researchers suggest (e.g.: Briaud et al. (1984), Budhu and Davies (1987) and Dobry et al. (1982)) that the pile response to lateral load and the governing failure mechanism is dependent on the relative stiffness between soil and pile. Poulos and Hull (1989) make use of the rigidity parameter R to classify the pile response. Mathematically, R is expressed as:

$$R = \left(\frac{E_p I_p}{E_s} \right)^{0.25} \tag{1.2}$$

With E_p and I_p the Young's modulus and inertia of the pile respectively and E_s the soil stiffness. From equation 1.2, a pile behaves rigidly if the length of the pile is less than $1.48R$ and behaves flexibly if the length of the pile exceeds $4.44R$ (Poulos & Hull, 1989).
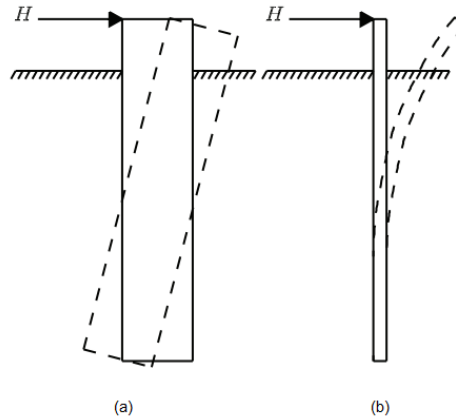
Figure 1.7: The difference between (a) rigid and (b) flexible pile behaviour (Sørensen et al., 2012).

This difference in rigid and flexible pile behaviour is illustrated in Figure 1.7.

The most common way to design a monopile subjected to offshore load scenarios is to make use of design codes by the American Petroleum Institute (API). The standard design practice adopted in API (2014) is to perform lateral load analysis on monopile foundations using the Winkler p-y load transfer model. The monopile is modeled by a beam element while the soil is modeled by nonlinear, non-interacting springs along the pile. The springs are characterized by curves that represent the soil resistance p at a given depth versus the lateral pile deflection y. The Winkler p-y model for lateral loading is visualised in Figure 1.8.

The p-y curves adopted in API (2014) for seabeds dominated by either clay or sand as soil are based on slightly modified experimental research conducted by Matlock (1970), Welch and Reese (1972) and Reese et al. (1975). The empirical basis of the proposed p-y curves consists of multiple field tests with flexible piles. However, for most monopile installations, the soil conditions of the seabed and the dimensions of the monopile are as such that a pile under lateral load inhibits a rigid behaviour with a subsequent rigid failure mechanism (Doherty & Gavin, 2012). The rigid behaviour of a monopile therefore casts doubt on the validity of applying the current p-y practice to determine the lateral behaviour of a monopile foundation.

Monopile foundations experience a vertical load (V) as a dead weight imposed by the wind turbine superstructure. A lateral load (H) is experienced by a combination of wind and wave loads acting on the tower structure. Due to the load eccentricity of the applied lateral loads on the tower structure, a moment load (M) is experienced by the monopile foundation pile head at the mudline level. Therefore, monopile foundations are subjected to combined loading (V-H-M).

As stated in section 1.2, monopile foundations used in the offshore wind industry often consist of a hollow steel cylinder with D ranging between 4-6 m, L ranging between 20-30 m and L/D ratios ranging between 5-6 (Arshad & O'Kelly, 2012). Also stated in section 1.2 is the increasing trend in turbine size for single offshore wind turbines (WindEu-

1
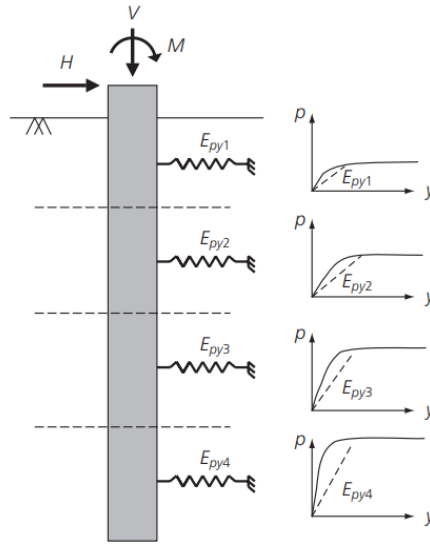
Figure 1.8: Winkler p–y model for lateral loading (Doherty & Gavin, 2012).

rope, 2021a). Due to this increasing trend, diameters of newer monopile foundations are increasing in size up to 10 m (Byrne et al., 2015). Though diameters of monopile foundation are increasing, the relatively low turbine weight resulted in the embedded length of monopile foundations to stay between the same ranges. This has caused L/D ratios to reduce to ranges between 2-3, which are more akin to L/D ratios found in shallow foundations. The interaction effect such that the lateral capacity, H_{ult}, and moment capacity, M_{ult}, are dependent on the vertical capacity, V_{ult}, has already been extensively researched and proven for shallow foundations and skirted foundations by numerous researchers (e.g.: Nova and Montrasio (1991), Butterfield and Gottardi (1994) and Bransby and Randolph (1999)). Though proven for shallow foundations and skirted foundations, the current practice is to analyse lateral behaviour and vertical behaviour of monopile foundations independently. This is due to the assumption that vertical load does not influence the lateral behaviour for a standard monopile foundation (API, 2014). With L/D ratios decreasing to similar ranges of those of shallow foundations (Byrne et al., 2015), the validity of this assumption for monopile design of large-diameter offshore wind turbines is doubtful.

Existing research on the topic of the influence of vertical loading on the lateral behaviour of a rigid monopile has thus far lead to inconclusive results (Li et al., 2020). Li (2020) extensively researched the influence of vertical loading on the lateral behaviour of rigid monopile foundations in sand by means of centrifuge modeling. The study concluded that for sand, the influence of vertical loading on the pile lateral capacity is dependent on the pile L/D ratio (Li, 2020). What is lacking however, is extensive research on the influence of vertical loading on the lateral behaviour of rigid monopile foundations in clay.

1

Clay soils tend to be complex in nature due to their overconsolidation ratio (OCR) which is of considerable influence on the stiffness of clay soils. Dependent on the location of a clay soil, the OCR can differ drastically from one potential offshore location to another. This location dependent discrepancy in clay stiffness can be seen in the OCR difference of clay soils found in seabeds globally. As an example, the type of clay soil dominated in the North Sea seabed consists of very stiff and overconsolidated (OC) clay, while the dominant clay soil found in the seabed of the Gulf of Mexico consists of soft and normally consolidated (NC) clay (Randolph & Gourvenec, 2011). Furthermore, the presence of clays with a different OCR have been reported in offshore basins in other parts of the world including West Africa, Brazil and South East Asia. With a projected global increase in offshore wind production per country (International Energy Association, 2019), future monopile foundations are bound to be embedded in different types of clay soil conditions. With additional design challenges for monopile foundations in the form of rigid pile behaviour and decreasing L/D ratios, an extensive research is required regarding the influence of vertical loading on the lateral behaviour of rigid monopile in clay soil.

1.4. RESEARCH OBJECTIVE

The research aims to investigate the design challenges and to provide geotechnical engineers with knowledge on the lateral behaviour of monopile foundations for offshore wind turbines. Hence the main objective of this research is to get a comprehensive understanding of the influence of vertical loading on the lateral behaviour of rigid monopile in clay soil.

1.4.1. MAIN RESEARCH QUESTION

To be able to reach the above stated main research objective, the following main research question is formulated:

"What is the influence of vertical loading on the lateral behaviour of rigid monopile in clay soil and how does this affect current design methods regarding lateral behaviour analysis of monopile foundations?"

1.4.2. RESEARCH SUB-QUESTIONS

In order to answer the main research question, it is essential to divide the analysis of the lateral behaviour of monopile foundations in clay soil into two scenarios. Scenario I encompasses analysis done on lateral behaviour of monopile foundations subjected to pure lateral loading in clay soil. Scenario II encompasses analysis done on lateral behaviour of monopile foundations subjected to combined loading in clay soil. This division into two scenarios allows direct comparison of computed results regarding pure lateral loading and combined loading behaviour of monopile foundations in clay soil. For each scenario, several sub-questions are formulated and designed in such a way that they contribute in small parts to answering the main research question.

1

SCENARIO I: PURE LATERAL LOADING
- How effective are current design methods in predicting the lateral behaviour of flexible and rigid pile?

- How can the use of a numerical model improve upon existing design methods regarding assessment of lateral behaviour of monopile foundation in clay soil?

- How does the lateral response of rigid monopile in clay soil differ with lateral load eccentricity?

- How does the lateral response of rigid monopile in clay soil differ with different clay soil conditions?

SCENARIO II: COMBINED LOADING
- What is the influence of the vertical load magnitude on the lateral behaviour of rigid monopile in clay soil?

- Is the influence of the vertical load on the lateral behaviour of rigid monopile in clay soil affected by different applications of lateral load eccentricity?

- Is the influence of the vertical load on the lateral behaviour of rigid monopile in clay soil affected by different clay soil conditions?

1.5. RESEARCH OUTLINE

The research will be executed in an orderly fashion such that all research sub-questions can be answered and the main objective of the research can be successfully accomplished. The research will compromise of seven chapters which are briefly outlined below. Figure 1.9 visualises the flow of the thesis and outlines the topics presented per chapter.

- **Chapter 2**: A literature study on the existing p-y models present in lateral behaviour analysis of monopile foundations in clay soil and existing research done on the main objective of the research. The aim is to give the reader a comprehensive understanding on the topic, get the reader up to date with existing research on the main objective of the research and give insight to the necessary requirements needed for the numerical model.

- **Chapter 3**: The methodology in setting up the numerical model and calculations using existing p-y models will be thoroughly explained in this chapter. Plaxis 3D software, the type of numerical model and approach in building the model will be explained, as well as the analyzed monopile geometries, soil parameters and loading conditions.

- **Chapter 4**: The validation of the numerical model used in the research will be presented and thoroughly assessed in this chapter.

1

- **Chapter 5**: Results of computations executed by the numerical model and existing methods will be presented in this chapter. The chapter will be divided into two parts consisting of analyzing pure lateral behaviour and analyzing lateral behaviour under combined loading.

- **Chapter 6**: This chapter will discuss and interpret all results and key findings from the previous chapter as well as assess the implication of the results.

- **Chapter 7**: The final chapter of the research will conclude the research by answering the main question and will provide the limitations of the research and recommendations for continuing future research.

1
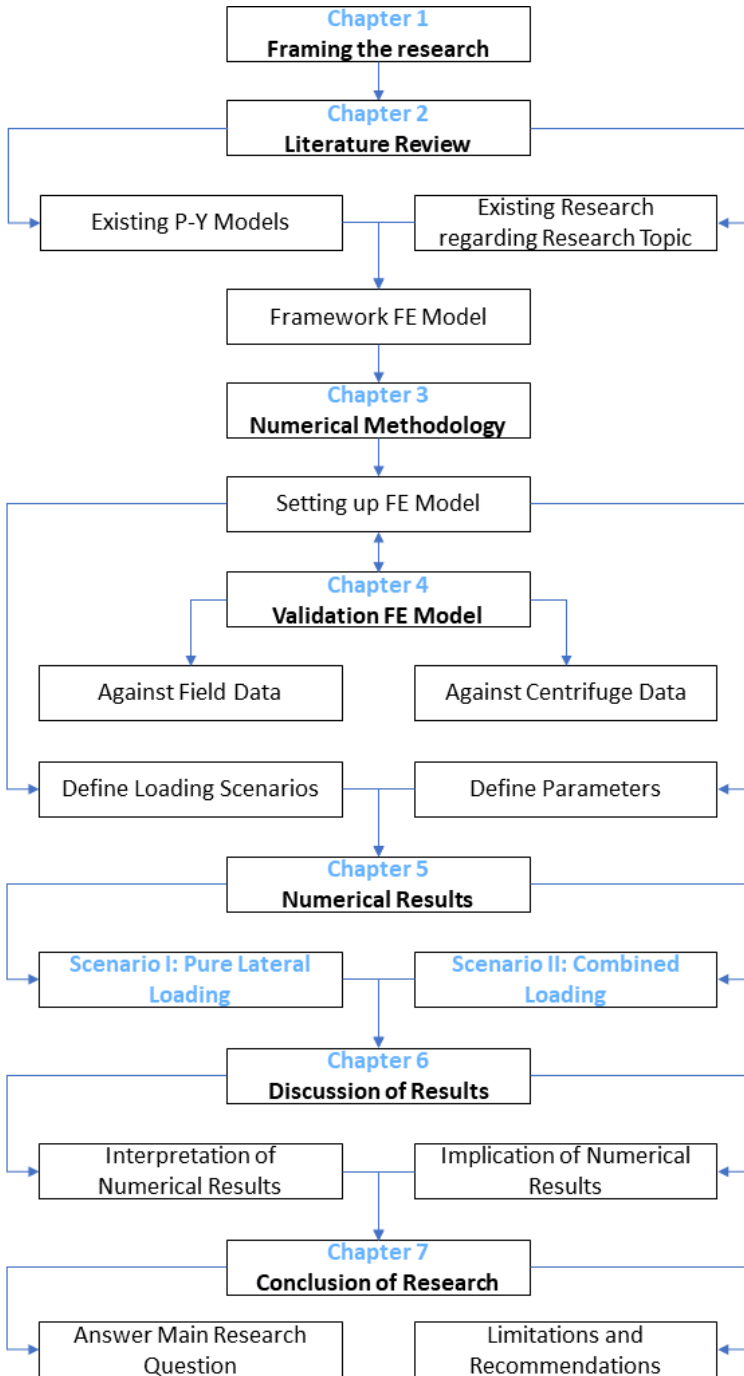
Figure 1.9: Flow of the thesis and topics presented per chapter.

2

LITERATURE REVIEW

In this chapter, an extensive literature study is performed on the existing p-y models and existing research done on the main objective of the research. The literature study is divided in three sections. Section 2.1 explores the existing p-y models present in lateral behaviour analysis of monopile foundations in clay soil. Section 2.2 provides a thorough assessment on the existing research regarding the main research objective. In section 2.3, the chapter will be drawn to its conclusion by highlighting the gaps present in the literature examined in sections 2.1 and 2.2.

2.1. P-Y MODELS FOR CLAY SOIL

2.1.1. MATLOCK (1970)

As stated in section 1.3, the most common way to design a monopile subjected to off-shore load scenarios is to make use of design codes adopted in API (2014). The approach adopted by API (2014) is based on the Winkler p-y model (Figure 1.8). Subsequent p-y curves used in API (2014) for seabeds dominated by clay soil are adopted from research conducted by Matlock (1970). Based on field tests on flexible piles performed in Lake Austin and the Sabine River in Texas, Matlock (1970) proposed constructions of p-y curves for three loading conditions:

1. short-time static loading.

2. cyclic loading.

3. subsequent reloading with forces less than previous maximums.

As this study is focused on monotonic lateral loading on a monopile, p-y models pertaining only loading condition 1 will be discussed. Table 2.1 indicates the specifications of the steel pile used in field testing and the clay soil conditions of both Lake Austin and the Sabine River as presented by Matlock (1970). In Lake Austin, the pile was subjected to static free-head lateral loading. In the Sabine River, both static free-head and restricted-head lateral loading was performed on the pile.
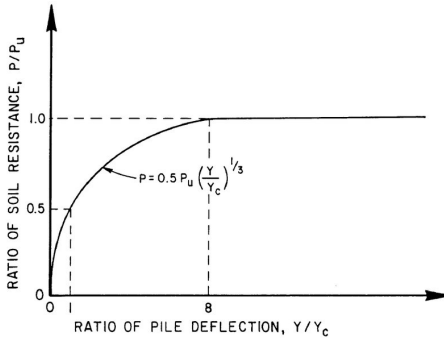
Figure 2.1: *p-y* curve for static lateral loading of a pile in soft clay as proposed by Matlock (1970).

Pile specification	Soil property
L (Embedded Length) = 12.8 m	Lake Austin clay: S_u = 38.3 kPa
D (Diameter) = 0.324 m	Sabine River clay: S_u = 14.4 kPa

Table 2.1: Specifications of the steel pile used in field testing and the clay soil properties of both Lake Austin and the Sabine River as presented by Matlock (1970).

Based on the aforementioned field tests, Matlock (1970) proposed a general form for the ultimate soil resistance per unit length, p_u:

$$p_u = N_p S_u D \tag{2.1}$$

Where: p_u = Ultimate soil resistance per unit length (kN/m)
  N_p = Ultimate soil resistance coefficient (-)
  S_u = Undrained shear strength (kPa)
  D = Diameter of the pile (m)

The value of N_p depends on the failure mechanism of the pile, i.e.: the wedge formed at shallow depths to the full flow at a deep zone. For soft clays flowing around a cylindrical pile at a considerable depth, z_r, below the surface, the value of N_p is equal to 9. Very near the surface where the soil in front of the cylindrical pile will fail in a wedge-like pattern, a value of N_p equal to 3 is recommended (Matlock, 1970). The variation in which the value of N_p ranges between its surface value and the value at depth z_r is expressed by equation 2.2:

$$N_p = 3 + \frac{\sigma_z}{S_u} + J\frac{z}{D} \tag{2.2}$$

Where: N_p = Ultimate soil resistance coefficient (-)
  σ_z = Overburden pressure from the soil (kPa)
  S_u = Undrained shear strength (kPa)
  J = Empirical parameter for the definition of ultimate soil resistance (-)
  z = Depth (m)
  D = Diameter of the pile (m)

Figure 2.1 illustrates the p-y curve for static lateral loading of a pile in soft clay as proposed by Matlock (1970). On the vertical coordinate, the soil resistance p is divided the by ultimate soil resistance p_u. On the horizontal coordinate, the pile deflection y is divided by y_c, the deflection of the pile at half the ultimate soil resistance. Matlock (1970) states that y_c can be determined by means of equation 2.3:

$$y_c = 2.5\epsilon_{50}D \qquad (2.3)$$

Where: y_c = Deflection of the pile at half the ultimate soil resistance (m)
ϵ_{50} = Strain at half of the maximum stress on a laboratory stress-strain curve (-)
D = Diameter of the pile (m)

The form of the pre-plastic proportion of Figure 2.1 can be described by equation 2.4:

$$p = 0.5p_u \left(\frac{y}{y_c} \right)^{\frac{1}{3}} \qquad (2.4)$$

2.1.2. JEANJEAN (2009)
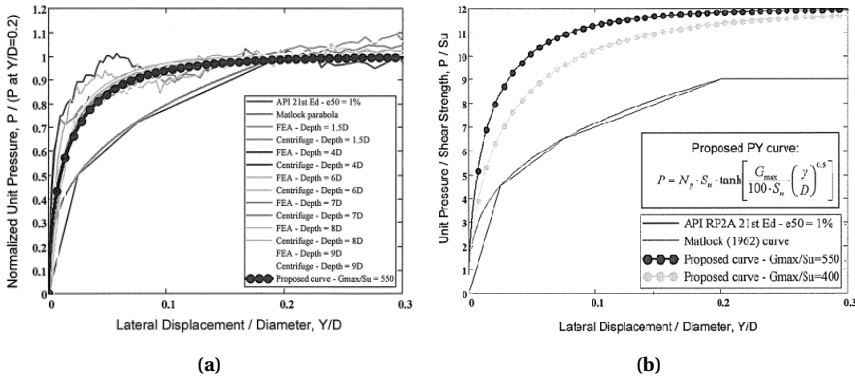
Figure 2.2: (a): Normalized p-y curves from FEA compared to Centrifuge testing as performed by Jeanjean (2009). (b): p-y curves proposed by Jeanjean (2009) compared with p-y curves proposed by Matlock (1970).

Jeanjean (2009) focused on the evaluation of lateral small-displacement soil-structure interaction for jetted conductor fatigue analysis. The study proposed a re-assessment of p-y curves for soft clay used in accordance with the models proposed in API (2000). Jeanjean (2009) argued that most software used to determine p-y curves are limited linear and non-linear elastic springs that underestimate p_u generated at the face of the pile. It was also suspected that API (2000) springs were too soft (Jeanjean, 2009).

Jeanjean (2009) makes use of a Finite Element Analysis (FEA) and centrifuge modeling to confirm the above mentioned statement. Table 2.2 indicates the pile specifications and soil properties used for both FE and centrifuge modeling as presented by

Pile specification	Soil property
L (Embedded Length) = 36.5 m	Material = Alwhite Kaolin Clay
D (Diameter) = 0.91 m	$S_u/\sigma'_v = \alpha(OCR)^{\beta}$; (Strength ratio): $\alpha = 0.19$, $\beta = 0.67$
t (Thickness) = 50.8 mm	LL (Liquid Limit) = 58%
E_p (Elastic modulus pile) = 414 MPa	PL (Plastic Limit) = 32%
	G_s (Specific Gravity) = 2.64

Table 2.2: Pile specifications and soil properties used for both FE and centrifuge modeling as presented by Jeanjean (2009).

Jeanjean (2009). The FE modeling consisted of a 3D non-linear total stress analysis with ABAQUS software. The analysis was performed using a elastic-plastic, work hardening model with Mises yield surface. The lateral loading applied to the pile consisted of static loading with no moment restraint at the load application point. The applied lateral load was increased until very large lateral displacements were achieved.

Centrifuge modeling consisted of 4 tests that included both lateral monotonic and cyclic loading of the pile in clay soil. As this study is focused on the monotonic behaviour of monopile, only the monotonic test will be discussed. The monotonic test consisted of monotonic loading of the pile until the pile head moved over 1 diameter.

Illustrated in both figures 2.2a and 2.2b, the monotonic p-y curves generated by means of FE and centrifuge modeling show that the p-y curves are stiffer than the API curves. At the full flow in the deep zone, N_p exceeds values of 9. This is due to the assumed smooth pile-soil interface by Matlock (1970). The average value of N_p is 12.7 and 13.4 for the FEA and centrifuge curves respectively (Jeanjean, 2009). Based on these results, Jeanjean (2009) proposed the following framework to calculate p_u for a soft clay soil:

$$p_u = N_p S_u \tag{2.5}$$

$$N_p = 12 - 4e^{\left(\frac{-\xi z}{D}\right)} \tag{2.6}$$

$$\xi = \begin{cases} 0.25 + 0.05\lambda, & \text{for } \lambda < 6 \\ 0.55, & \text{for } \lambda \geq 6 \end{cases} \tag{2.7}$$

$$\lambda = \frac{S_{u0}}{S_{u1}D} \tag{2.8}$$

Where: p_u = Ultimate soil resistance per unit length (kN/m)
N_p = Non-dimensional ultimate resistance coefficient (-)
S_u = Undrained shear strength (kPa)
S_{u0} = Undrained shear strength at the sea floor (kPa)
S_{u1} = Rate of undrained shear strength increase with depth (kPa)
D = Diameter of the pile (m)
z = Depth (m)

In addition, Jeanjean (2009) fitted the shape of the proposed p-y curve in figure 2.2b with empirical equation 2.9:

$$\frac{p}{p_u} = tanh \left[\frac{G_{max}}{100 S_u} \left(\frac{y}{D} \right)^{0.5} \right]$$

(2.9)

Where: p = Soil resistance per unit length (kN/m)
        p_u = Ultimate soil resistance per unit length (kN/m)
        G_{max} = Maximum shear modulus (kPa)
        S_u = Undrained shear strength (kPa)
        y = Deflection of the pile (m)
        D = Diameter of the pile (m)

2.1.3. Zhang and Andersen (2017)

Regarding the p-y models proposed by Matlock (1970), Zhang and Andersen (2017) highlighted that the proposed p-y model has been developed and calibrated mainly against the field test performed in lightly overconsolidated clay soil located at the Sabine River. The applicability of the empirical model to other soil conditions should therefore be checked (Zhang & Andersen, 2017). Regarding the p-y models proposed by Jeanjean (2009), the use of the G_{max}/S_u ratio came to discussion. By postulating the impact of the G_{max}/S_u ratio on the pile p-y response, it was anticipated that the initial stiffness of the clay soil is of influence on the p-y response of the pile (Jeanjean, 2009). Zhang and Andersen (2017) argue that not only the initial stiffness of the clay soil, but also the stress-strain response beyond the initial phase will influence the p-y response of the pile. In addition, the proposed impact of the G_{max}/S_u ratio on the pile p-y response is based on postulation and is not verified through either centrifuge modeling or numerical analysis (Zhang & Andersen, 2017).

Based on preceding research (Bransby (1999), Klar (2008) and Klar and Osman (2008)) it is demonstrated from numerical and theoretical perspectives that it is possible to link the p-y curves to a soil stress-strain response. In response, Zhang and Andersen (2017)
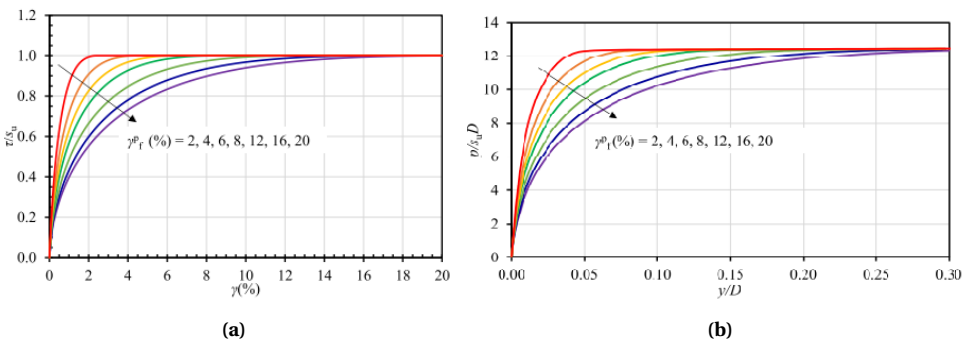
Figure 2.3: (a): Example stress-strain response (G_{max}/S_u = 250). (b): Example p-y curves with G_{max}/S_u = 250 and α = 1 (Zhang & Andersen, 2017).
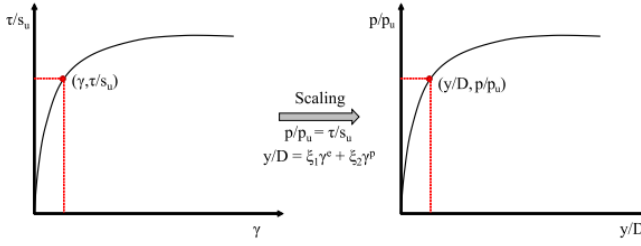
Figure 2.4: Schematic illustration of proposed p-y model by Zhang and Andersen (2017).

focused on scaling the lateral p-y response of a clay soil from laboratory stress-strain curves.

The numerical analysis involves FEA with Plaxis 3D software and a NGI-ADP constitutive model for simulating the mechanical behaviour of clay. The NGI-ADP model is a total stress soil model that can be used for simulating undrained anisotropic behaviour of clay soil and uses a Tresca yield criterion. The pile-soil interaction at the deep zone governed by the plane strain, full flow mechanism was investigated. This was done by modeling a 1 m pile slice under a horizontal rigid translation. The horizontal pile slice is analyzed in plane strain conditions (no vertical movement of the pile allowed). The plane strain condition makes it that the derived p-y springs are only relevant for the part of a pile where a localised flow-around mechanism is governing. In addition, the plane strain condition makes it that the deformation characteristics of the pile slice is better represented by the shearing in the direct simple shear mode (S_u^{DSS}).

The NGI-ADP model makes use of the following plastic hardening rule:

$$\frac{\tau}{S_u} = 2\frac{\sqrt{\gamma^p/\gamma_f^p}}{1+\gamma^p/\gamma_f^p} \tag{2.10}$$

Where: τ = Current mobilised shear stress (kPa)
S_u = Undrained shear strength (kPa)
γ^p = Current plastic shear strain (-)
γ_f^p = Plastic shear strain at failure (-)

The total shear strain, γ^t, associated with τ is the summation of the elastic and plastic shear strain (γ^e and γ^p respectively). This relationship is expanded upon in equation 2.11:

$$\gamma^t = \gamma^e + \gamma^p = \frac{\tau}{G_{max}} + \gamma^p = \frac{\tau/S_u}{G_{max}/S_u} + \gamma^p \tag{2.11}$$

The G_{max}/S_u ratio and γ_f^p can then be calibrated against site-specific data such that the actual soil response is simulated in the numerical model.

A parametric finite element analysis of varying G_{max}/S_u ratios and γ_f^p with corresponding p-y pile responses was performed. In addition, the parametric study also in-

2

cludes the influence of the pile-soil interface roughness, α, on the p-y pile response. An example of the parametric finite element analysis is shown for a G_{max}/S_u ratio equal to 250 in figures 2.3a and 2.3b. It can be seen that the shape of the p-y response of the pile bears strong similarity to the soil stress-strain response. Based on this result, Zhang and Andersen (2017) propose a p-y model illustrated in figure 2.4. In it, a point on the stress-strain curve corresponds to a point on the p-y curve. The corresponding normalized lateral displacement can then be scaled from the shear strain using the scaling coefficients ξ_1 and ξ_2, which correspond to γ^e and γ^p respectively. The scaling coefficients were both found to be dependent on α, though ξ_1 is taken as a constant for simplicity.

$$\xi_1 = 2.8 \tag{2.12}$$

$$\xi_2 = 1.35 + 0.25\alpha \tag{2.13}$$

The ultimate soil resistance p_u was also found to be related by α due to the relation between the ultimate soil resistance coefficient N_p and α based on the results of Randolph and Houlsby (1984):

$$N_p = 9 + 3\alpha \tag{2.14}$$

2.1.4. Jeanjean et al. (2017)
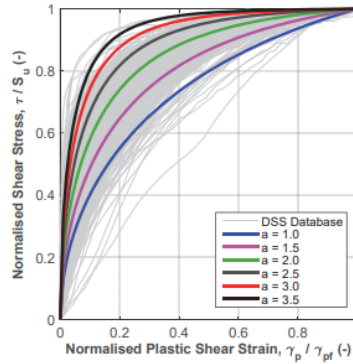
Figure 2.5: Normalised 537 stress-strain curves in database and family of curves used in FEA performed by Jeanjean et al. (2017).

Jeanjean et al. (2017) presented a new framework for the calculation of a best estimate p-y curve. Akin to Zhang and Andersen (2017), this was done by developing a scaling procedure to determine the shape of the p-y curve from the shape of the stress-strain curve obtained from a DSS test.

A FEA was performed with ABAQUS software with a Von Mises plasticity model. A plane strain condition was imposed with a rigid body constraint on the pile nodes. Final simulations were run with a pile slice with a diameter of 1 m. A hardening rule to be used with the Von Mises plasticity model was created via a database consisting of 537

DSS stress-strain curves. The curves originated from tests on samples from either the Gulf of Mexico or kaolin clay soils used in centrifuge testing. The resulting hardening rule is shown in equation 2.15:

$$\frac{\tau}{S_u} = \frac{tanh\left[a\left(\frac{\gamma^p}{\gamma_f^p}\right)^{0.5}\right]}{tanh(a)} \tag{2.15}$$

Introduced in equation 2.15 is the curve fitting parameter a. The parameter a can be chosen between values ranging between 1 and 3.5, depending on the shape of the normalized stress-strain curve. This is demonstrated in Figure 2.5, which shows the correct value of the a parameter with each corresponding shape of the normalized stress-strain curve.

Jeanjean et al. (2017) proposed the following framework for the shape of the p-y curve:

$$\frac{p}{p_u} = \frac{tanh\left[A\left(\frac{(y/D)^p}{(y/D)_f^p}\right)^{0.5}\right]}{tanh(A)} \tag{2.16}$$

$$A = 1.33 + 0.45a \tag{2.17}$$

$$(y/D)_f^p = \gamma_f^p(2.5 - ln(a)) \tag{2.18}$$

2.2. EXISTING RESEARCH ON LATERALLY LOADED PILE

2.2.1. NUMERICAL RESEARCH

PILE-CLAY SOIL INTERACTION UNDER COMBINED LOADING

Karthigeyan et al. (2007) performed a series of 3D FEA to get a better understanding of the influence of a vertical load on the lateral behaviour of a pile in clay soil. The 3D FEA was performed in GEOFEM3D software with a Von Mises constitutive model with associated flow rule for clayey soils. In it, a series of 3D FEA analyses was performed on a single free-headed pile in clay soils. Pile and soil parameters as outlined in the study by Karthigeyan et al. (2007) are presented in Table 2.3.

The response of piles under combined loads was analyzed with vertical loads equal to 0.2, 0.4, 0.6 and 0.8 V_{ult}. The combined load was applied in two stages. The first stage consisted of applying the considered vertical load. In the second stage, lateral loads were applied while the vertical load considered was kept constant. Vertical loading was performed using load control while lateral loads were applied using displacement control.

The results regarding the lateral load-displacement curve are illustrated in Figure 2.6. As shown in the figure, under combined loading, lateral loads developed at all deflections are less than the corresponding load developed under a pure lateral load scenario. Though lateral loads reduced for all vertical load scenarios, the reduction is not significant for vertical loads up to 0.6V_{ult}. Beyond a 0.6V_{ult} scenario, a significant reduction of 20% of the lateral capacity of the pile was noted at a magnitude of 0.8V_{ult} (Karthigeyan et al., 2007).
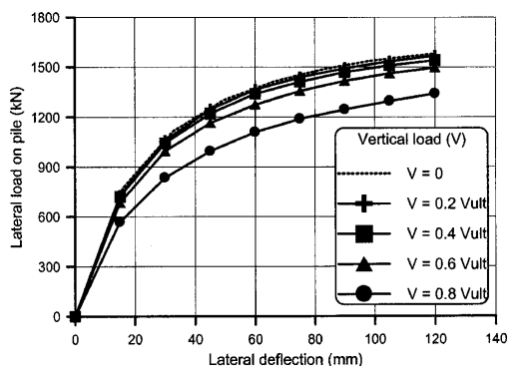
Figure 2.6: Lateral load-deflection curves of piles under combined loading in clayey soils as presented by Karthigeyan et al. (2007).

A follow-up study regarding the influence of a vertical load on the lateral pile response in clay soil was performed by Hazzar et al. (2017). In it, a 3D Finite Difference Analysis (FDA) was performed using an elastic perfectly plastic Mohr-Coulomb constitutive model in conjunction with a nonassociated flow rule. The study used a similar pile model as used by the study performed by Karthigeyan et al. (2007), though differing in geometry. Where Karthigeyan et al. (2007) opted for a pile with a square geometry, Hazzar et al. (2017) opt for a pile with a circular geometry with a diameter equal to 1 m. In addition, Hazzar et al. (2017) performed combined analysis in homogeneous clay soils (a constant S_u profile) and inhomogeneous clay soils (a varying S_u profile with constant OCR). Two cases were considered. Case 1 compromised of a shear modulus dependent on S_u ($G = 300 S_u$). Case 2 compromised of a constant shear modulus ($G = 38.5$ MPa). The procedure in analyzing the combined loading behaviour of the pile was akin to the procedure performed by Karthigeyan et al. (2007). A vertical load with either a magnitude equal to 0.25, 0.5, 0.75 or $1.0 V_{ult}$ was considered.

Figure 2.7 shows the results of the combined loading procedure performed by Hazzar et al. (2017). As shown in the figure, results are similar to the results from the combined loading procedure performed by Karthigeyan et al. (2007) (Figure 2.6). In general, both studies show a significant decrease in lateral capacity of the pile when a large vertical

Pile specification	Soil property
Size = 1200 x 1200 mm	S_u (Undrained Shear Strength) = 100 kPa
L (Embedded Length) = 10 m	ϕ (Friction Angle) = 0°
Type of pile: Concrete	ψ (Dilation Angle) = 0°
Grade of concrete: M25	E_s (Young's Modulus Soil) = 40 MPa
E_p (Young's Modulus Pile) = 25,000 MPa	v (Poisson's Ratio Soil) = 0.40
γ_p (Unit Weight) = 24 kN/m³	γ_{sat} (Unit Weight) = 18 kN/m³
v_p (Poisson's Ratio Pile) = 0.19	K_0 (Earth Pressure Coefficient) = 0.60

Table 2.3: Pile specifications and soil properties as presented in the study by Karthigeyan et al. (2007).
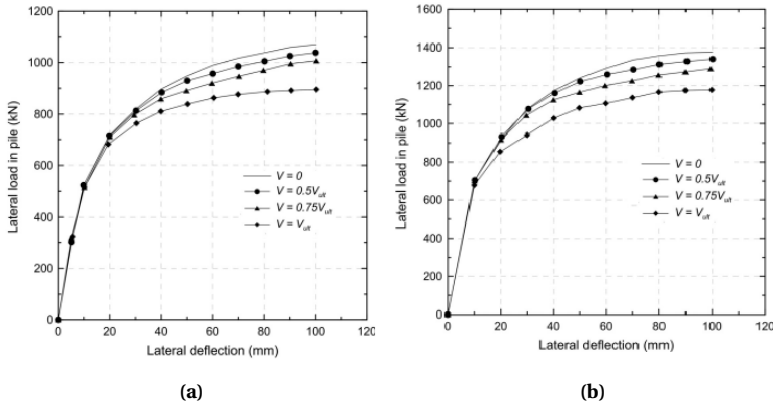
Figure 2.7: Lateral load-deflection curves of piles under combined loading: (a) case 1 (b) case 2 as presented by Hazzar et al. (2017).

load is imposed. Across the two cases analyzed, results suggest that the influence of combined loading on pile in is not affected by the homogeneity of clay soil (Hazzar et al., 2017).

RIGID PILE WITH LOWER ASPECT RATIO

In light of the design challenges regarding short rigid monopile foundations, Byrne et al. (2017) proposed the PISA design model for offshore monopiles in clay soil. This model is illustrated in Figure 2.8a. The PISA model builds upon the conventional p-y models explored in section 2.1. Much akin to the p-y approach, the PISA model also takes into account a distributed load along the embedded length of the pile. Differing from the p-y approach, the PISA model includes the application of vertical shear tractions, a base shear force and a base moment reaction to the monopile. The inclusion of these resistance components makes the PISA model more applicable towards rigid piles with lower L/D ratios, as these become increasingly significant with a reduced L/D ratio of a pile. Vertical loading applied to the monopile is assumed to be small compared to V_{ult}, and is therefore neglected in the PISA model (Byrne et al., 2017). The PISA design model for offshore wind turbines has been implemented in PLAXIS MoDeTo software. The software allows for the extraction of all the individual resistance components (Bentley, 2022).

The PISA model is compromised of a 1D FEA model (Figure 2.8b) that makes use of soil reaction curves (similar to p-y curves) acquired from 3D FEA for specific soil properties. Thus the soil reaction curves are determined on a site-specific basis. This is in contrast with standard p-y models, which make use of a set of equations within a design guidance document. Byrne et al. (2017) propose two methods of applying the PISA model. In the first method, the 'rule-based method', soil reaction curves are determined using predefined mathematical functions. The parameters are then determined from standard site investigation data. The second method, the 'numerical-based method' involves the use of a 3D FE calibration study to determine the soil reaction curves. The generated soil reaction curves are then used for the 1D FEA model for a particular offshore site.
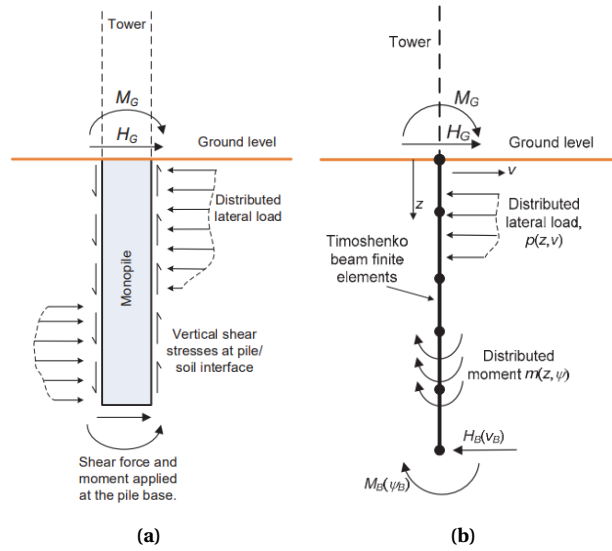
Figure 2.8: (a): Soil reaction components incorporated in the PISA design model. (b): 1D FE model employed in the PISA analysis model as presented by Byrne et al. (2017).

To highlight the approach of the PISA model and illustrate the shortcomings of conventional p-y models, Byrne et al. (2017) show an example of a numerical-based method approach towards the PISA model. The approach consisted of a 3D FEA in Cowden stiff clay soil modeled via an extended generalized Modified Cam Clay (MCC) model. The 3D FEA analyzed an elastic steel pile. Figure 2.9a shows a comparison between the PISA predicted soil reaction curves and the soil reaction curves predicted by API (2014) for a pile
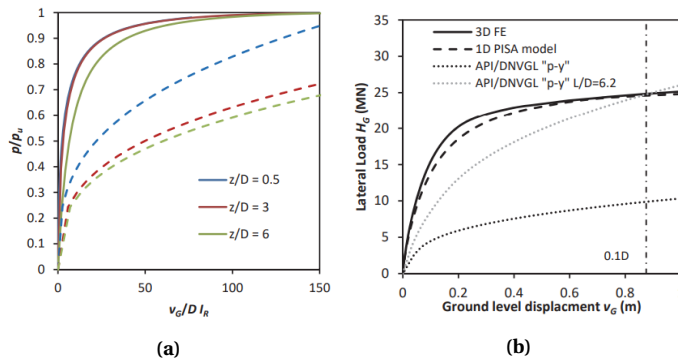
Figure 2.9: (a): Comparison between PISA parametric (solid lines) and API p-y model (dashed lines) soil reaction curves at various depths for a 10 m diameter pile. (b): Lateral load-displacement graph for the 3D FEA, 1D PISA and API predicted curves for a pile with L/D ratio equal to 4 as presented by Byrne et al. (2017).

with a L/D ratio equal to 6. The comparison highlights the underestimation of the lateral load response by API models. As shown in the figure, API models tend to under-predict the requirement of displacement needed to mobilise p_u for rigid piles with a lower L/D ratio (Byrne et al., 2017). Figure 2.9b illustrates the lateral load-displacement graph for the 3D FEA, 1D PISA and API (2014) predicted curves for a pile with L/D ratio equal to 4. The 3D FEA validates the 1D PISA response, while the API curve severely underestimates the ultimate capacity (Byrne et al., 2017). The estimated lateral capacity via 3D FEA and the 1D PISA model of a pile with L/D ratio equal to 4 is found equal to API predicted lateral capacity for a pile with L/D ratio equal to 6.2. Even with this increased length, the initial response would be significantly softer at smaller displacements than determined using the 1D PISA model or 3D FEA (Byrne et al., 2017).

LOADING ECCENTRICITY
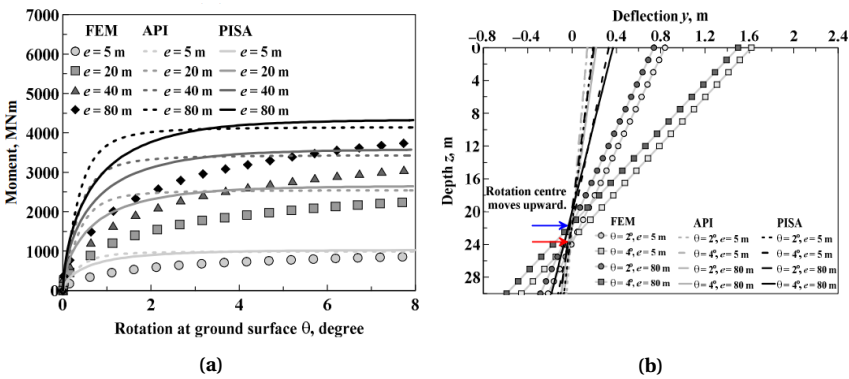
Figure 2.10: (a): Moment–rotation curves at the ground surface in 65% relative dense sand for a monopile with $D = 10$ m. (b): Pile deflection profiles under typical rotations and loading eccentricity in 65% relative density sand for a monopile with $D = 10$ m as presented by Wang et al. (2021).

Wang et al. (2021) performed 3D FE study on the lateral behaviour of large diameter, short rigid monopiles in sands with three different relative densities (D_r = 40%, 65%, 80%). The FE compromised of an analysis in ABAQUS software with different pile diameters (D = 4, 6, 8 and 10 m) and an embedded length L equal to 30 m. To quantify the lateral behaviour of the tested monopiles under different load conditions, simulations under seven different loading eccentricities of 5, 10, 20, 40, 60, 80, and 100 m were performed for each monopile. Results regarding a monopile with $D = 10$ m are shown in Figure 2.10. Figure 2.10a shows the moment-rotation curve for four loading eccentricities of 5, 10, 20 and 40 m at the ground surface in 65% relative density sand. For all monopile diameters, the moment capacity increased with increasing eccentricity (Wang et al., 2021). Figure 2.10b illustrates the pile deflection profile for loading eccentricities of 5 and 80 m in 65% relative density. An interesting observation from the pile deflection profiles is the upwards movement of the rotation center of the pile with increasing loading eccentricity (Wang et al., 2021). From Figure 2.10, it can be concluded that the loading eccentricity is of significant influence for the lateral behaviour of short rigid monopiles in sands (Wang

et al., 2021). Though Wang et al. (2021) performed the study in a sandy soil, a similar analysis performed in clay soil can be of interest towards reaching the main objective of the thesis.

2.2.2. EXPERIMENTAL RESEARCH
PILE-CLAY SOIL INTERACTION UNDER COMBINED LOADING
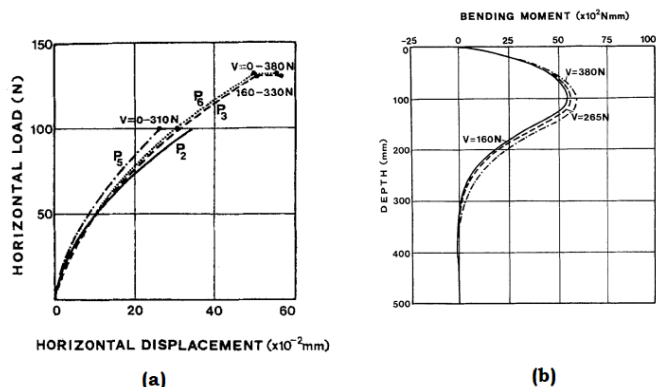
Figure 2.11: (a,b): Lateral load-displacement curves and bending moment profiles respectively as presented by Anagnostopoulos and Georgiadis (1993).

Regarding the influence of combined loading on pile response, Anagnostopoulos and Georgiadis (1993) performed six laboratory tests on closed-ended aluminum piles in soft clay. Pile and soil parameters are presented in Table 2.4. Both vertical and lateral loads were applied to the pile heads at ground elevation using dead weights. The displacement of the pile head was determined through a system of three displacement transducers. The tests involved applying a variety of vertical and lateral loads in different sequences.

Results regarding combined loading on the lateral pile response are illustrated in Figure 2.11. Both lateral load-displacement curves and bending moment profiles showed that the effect of vertical loading on the lateral pile response, regardless of loading magnitude, was rather limited. The low value in changes to both the lateral load-displacement curve and bending moment profile are deemed negligible (Anagnostopoulos & Georgiadis, 1993). This is in contrast with the results from studies performed by Karthigeyan et al. (2007) and Hazzar et al. (2017), which do imply an influence of combined loading on the lateral pile response in clay at high vertical magnitude. A possible reason for this

Pile specification	Soil property
L (Embedded Length) = 500 mm	S_u (Undrained Shear Strength) = 28 kPa
D (Diameter) = 19 mm	LL (Liquid Limit) = 42%
t (Thickness) = 1.5 mm	PL (Plastic Limit) = 24%

Table 2.4: Pile specifications and soil properties as presented by Anagnostopoulos and Georgiadis (1993).

2
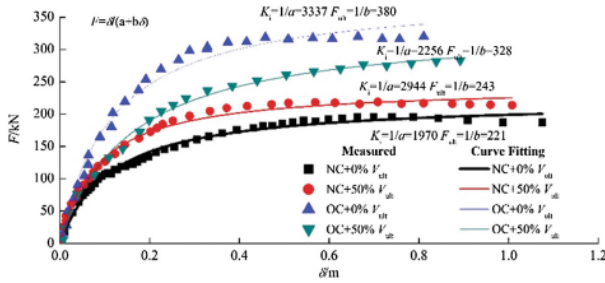
Figure 2.12: Measured and fitting results of load-displacement responses at pile head as presented by He et al. (2018).
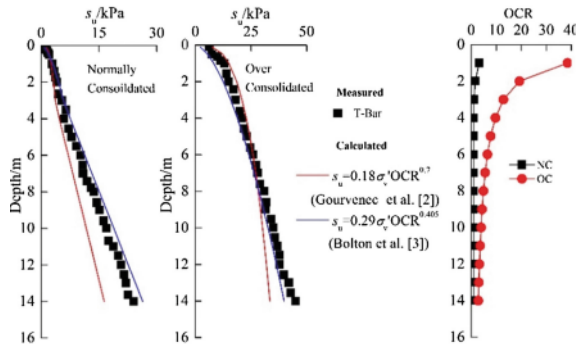
Figure 2.13: Variation of OCR and undrained shear strength with depth in NC and OC clay soil as presented by He et al. (2018).

difference is that Anagnostopoulos and Georgiadis (1993) do not look into horizontal displacements that reach or exceed $0.1D$ of the tested model pile. The reasoning behind this limited observation is not mentioned in the study. Another possible reason is the difference in model pile L/D ratios. Karthigeyan et al. (2007) and Hazzar et al. (2017) analyzed model piles with a L/B ratio equal to 8.33 and L/D ratio equal to 10 respectively. A larger L/D ratio equal to 26.3 was considered for the model pile used in testing by Anagnostopoulos and Georgiadis (1993). This can indicate that the pile L/D ratio is of influence on combined loading lateral pile response.

He et al. (2018) performed centrifuge tests to understand the lateral behaviour of a single pile in clay soil. Centrifuge modeling was performed on piles consisting of an aluminum tube in both NC and OC clay soil. Pile and soil parameters as outlined in the study are presented in Table 2.5. Clay consolidation was performed first by a preliminary consolidation stage at $1g$, followed by an in-flight consolidation stage at $40g$. After the consolidation stages, micro T-bar tests were performed to acquire S_u and OCR profile of the NC and OC clay soils as presented in Figure 2.13. The model pile was then installed and excess pore pressures were allowed to be fully dissipated before the combined loading stage. The combined loading involved vertical loading at $0.5V_{ult}$ applied by a lump

Pile specification	Soil property
L (Embedded Length) = 33 cm	Material = Speciwhite China Kaolin Clay
D (Diameter) = 2 cm	LL (Liquid Limit) = 27%
t (Thickness) = 2 mm	PI (Plasticity Index) = 61%
e (Eccentricity) = 10 cm	γ_{sat} (Unit Weight) = 16.5 kN/m^3
E_p (Young's Modulus Pile) = 72 GPa	
Yield Stress = 241 MPa	

Table 2.5: Pile specifications and soil properties as presented by He et al. (2018).

mass and monotonic lateral loading applied at the pile head.

Figure 2.12 shows the lateral load-displacement curve during combined loading in both NC and OC clay soils. The ultimate lateral capacity and initial stiffness increased by 10% and 50% respectively for a pile subjected to combined loading at $0.5V_{ult}$ in NC clay. Interestingly, the opposite effect was observed for OC clay soil with an ultimate lateral capacity and initial stiffness decrease by 13% and 33% respectively (He et al., 2018).

LOADING ECCENTRICITY

Murali et al. (2015) performed a series of centrifuge model tests to investigate the lateral response of a short aspect ratio rigid pile ($L/D = 2$) with both fixed and rotating heads in soft NC clay. Centrifuge testing was performed at 70g on piles consisting of aluminum tubes with D equal to 49.6 mm, t equal to 0.609 mm and L equal to 101.6 mm. Murali et al. (2015) investigated the influence of loading eccentricity on the lateral monotonic response of the pile subject to rotation. Considered were four different loading eccentricities of 1,2D, 1.5D, 2.5D and 3.5D. The results are illustrated in Figure 2.14. As shown in the figure, results suggest that a higher loading eccentricity causes the ultimate lateral capacity to decrease for short aspect ratio rigid piles embedded in soft NC clay (Murali et al., 2015).
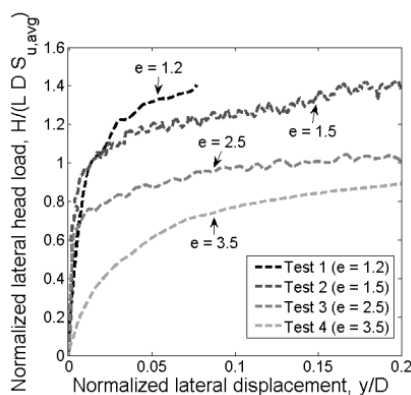
Figure 2.14: Lateral monotonic response of the test pile ($L/D = 2$) subject to rotation for four different eccentricities: 1,2D, 1.5D, 2.5D and 3.5D (Murali et al., 2015).

2.3. CONCLUSION

In chapter 2, an extensive literature review was performed on existing p-y models for lateral behaviour of piles in clay soil and existing studies regarding the main objective of the research. The conclusions drawn from the literature review are outlined below.

2

In regards to the existing p-y models for lateral behaviour of piles:

- The p-y models proposed by Matlock (1970), and subsequently API (2014), are developed and calibrated on experimental results gained from testing on flexible piles in lightly overconsolidated clay soil. The applicability of p-y models proposed by Matlock (1970) regarding rigid piles and stiffer clay soils is to be discussed.

- The p-y models proposed by Jeanjean (2009) correct a possible underestimation of the ultimate soil resistance p_u by the p-y models proposed by Matlock (1970). However, with the proposed p-y models being calibrated against flexible piles and soft clay soil, concerns regarding applicability towards rigid piles and stiffer clay soils are not addressed.

- Both the Zhang and Andersen (2017) and Jeanjean et al. (2017) proposed p-y models are calibrated against a rigid pile slice. The proposed method of scaling the stress-strain curve to p-y curves is proven to be accurate for clay soils ranging from very soft to very stiff. A concern however is the applicability of both p-y models towards short rigid piles with large diameters, since both are only calibrated against long flexible piles with a small diameter.

- None of the p-y models discussed include the possibility of analysis regarding the influence of vertical loading on the lateral behaviour of piles in clay soil.

In regards to existing research relevant to the research topic:

- In general, results from existing research regarding pile-clay soil interaction under combined loading is found to be inconsistent with varying conclusions across numerical and experimental studies.

- Existing research regarding pile-clay soil interaction under combined loading is limited to either square rigid or flexible piles with small diameters. In addition, piles used in the existing research often do not represent conditions of typical monopile properties used in the industry.

- Results from existing research regarding pile-clay soil interaction under combined loading is limited to research done on the influence on lateral load-displacement or bending moment profiles. Further possible consequences of combined loading on the lateral response of rigid pile in clay soil, i.e.: moment-rotation curves, H-M interaction diagrams or pile deflection curves are not considered.

- The PISA design model for offshore monopiles in clay soil provides a solution to the design challenge of short rigid monopile foundations. By taking into account

vertical shear tractions induced on the pile-soil interface, the PISA design model is proven to be more applicable towards short rigid monopile foundations. However, the PISA design model does not take into account the potential influence of vertical loading on the lateral behaviour of short rigid monopile in clay soil (Byrne et al., 2017).

- The research of Wang et al. (2021) regarding short rigid pile in sandy soil suggest that a higher loading eccentricity causes an increase of moment capacity and an upwards movement of the rotation center of the pile (Wang et al., 2021). Though the research is performed in sandy soil, a similar analysis performed in clay soil can be of interest towards reaching the main objective of the research.

- Results from the research presented by Murali et al. (2015) suggest that a higher loading eccentricity causes a decrease of lateral capacity for short rigid piles embedded in soft NC clay soil (Murali et al., 2015).

3

NUMERICAL METHODOLOGY

In this chapter, the methodology in setting up the 3D FE model will be thoroughly explained. The chapter is divided in three sections. Section 3.1 summarizes the background information behind the NGI-ADP constitutive model used for the FE model. Section 3.2 details the 3D FE model specifications by outlining the general modelling approach as well as the input for the modeled clay soil and pile. Section 3.3 gives background to the performed loading scenarios applied to the monopile tests by detailing the analysis and approach of the loading scenarios.

3.1. NGI-ADP
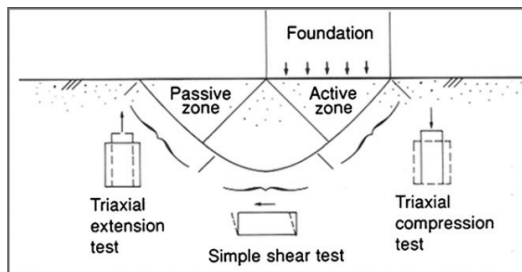
Figure 3.1: Visualisation of the proposed Bjerrum ADP framework (Bjerrum, 1973).

The constitutive model used to reach the main research objective consists of the elasto-plastic model NGI-ADP. The NGI-ADP model is used for capacity, soil deformation and soil-strucutre analysis involving undrained loading of clay (Bentley, 2020). The NGI-ADP model allows for a direct input of the undrained shear strength, S_u. This is in contrast with other constitutive models (e.g.: Mohr-Coulomb, Hardening Soil) available to use in PLAXIS software, which apply an effective stress concept from which S_u can be indirectly determined. This determination of the S_u input requires more understanding and
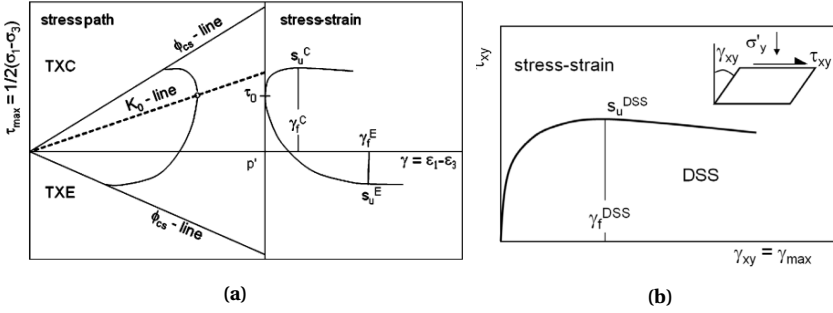
Figure 3.2: (a): Typical stress paths and stress-strain curves associated with triaxial compression and extension tests (Grimstad et al., 2012). (b): Direct simple shear test with definition of stress strain quantities (Andresen et al., 2011).

trial-and-error testing to match the model's prediction to laboratory results or a design profile of S_u. Regarding design calculations concerning undrained loading of clay, it is preferred to exactly match the design profiles of S_u. This makes the NGI-ADP model the more advantageous model to use. Loading of a monopile, laterally and vertically, in an offshore clay seabed will always be governed by undrained behaviour due to the low permeability of the clay soil preventing any pore pressure dissipation to occur during the time of interest. This fact, combined with the ease of a direct S_u input, makes the NGI-ADP constitutive model the best and efficient choice to reach the main research objective.

The NGI-ADP constitutive model makes use of the ADP framework proposed by Bjerrum (1973), which takes into account the stress path dependency of S_u. Bjerrum (1973) indicates that there is a difference in S_u profiles for active or triaxial compression (TXC) loading, Direct Simple Shear (DSS) and passive or triaxial extension (TXE) loading. This concept is illustrated in Figure 3.1. The NGI-ADP model simplifies the plane strain active and passive strength by setting them almost equal to the accompanying TXC and TXE strengths respectively ($S_u^{TXC}/S_u^a = 0.99$; $S_u^{TXE}/S_u^p = 1$). Taking into account the ADP framework proposed by Bjerrum (1973), the NGI-ADP model requires as input active, passive and DSS undrained shear strengths (S_u^a, S_u^p and S_u^{DSS}) as well as their corresponding shear strain at failure (γ_f^a, γ_f^p and γ_f^{DSS}) along the three directions of shearing. The typical stress paths and stress-strain curves associated with the three undrained loading inputs are illustrated in Figures 3.2a and 3.2b. Through interpolation between the three curves, the NGI-ADP model predicts anisotropic behaviour of a saturated clay in a general 3D stress state. Both Bjerrum (1973) and Ladd and Foott (1974) suggest that the triaxial test input for the NGI-ADP model should be anisotropicaly consolidated based on the in-situ stress (Bjerrum, 1973 and Ladd and Foott, 1974). Thus, curves illustrated in Figure 3.2a start from an initial point τ_0, the initial mobilized shear stress.

In the NGI-ADP model, the S_u varies linearly with depth from a reference point $S_{u,ref}^a$ at a reference depth z_{ref} with an input increment $S_{u,inc}^a$. The input in the model for the dependency of the stress path for the S_u value is expressed by different ratios of S_u^a. Ratios S_u^p/S_u^a and S_u^{DSS}/S_u^a are considered. The input parameter for the initial elastic
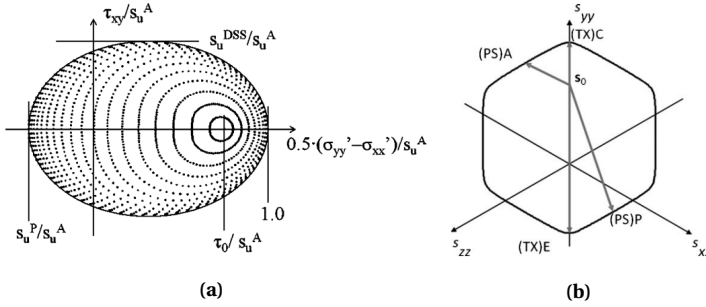
Figure 3.3: (a): Typical deviatoric plane strain plot of equal shear strain contours for the NGI-ADP model. (b): Failure criterion used in the NGI-ADP model (Grimstad et al., 2012).

stiffness parameter is given by the unloading reloading shear modulus, G_{ur}. The input consists of a ratio G_{ur}/S_u^a. Because S_u^a varies with depth, G_{ur} is also automatically dependent with depth when using the NGI-ADP model.

The NGI-ADP model is formulated for a general stress state by a modified Tresca yield criterion. This yield criterion takes into account the anisotropy of undrained loading in clay (Grimstad et al., 2012). The yield function for the NGI-ADP model, as implemented in PLAXIS 3D software, for a 3D stress space is defined as (Bentley, 2020):

$$f = \sqrt{H(\omega)\hat{J}_2} - \kappa \frac{S_u^a + S_u^p}{2} = 0 \tag{3.1}$$

Where: $\hat{J}_2$ = The modified second deviatoric invariant (-)
S_u^a = The active undrained shear strength (kPa)
S_u^p = The active undrained shear strength (kPa)
κ = The hardening parameter, as described in equation 2.10 (-)

The function $H(\omega)$ approximates the Tresca criterion and is defined as:

$$H(\omega) = cos^2\left(\frac{1}{6}arccos(1-2a_1\omega)\right) \tag{3.2}$$

$$\omega = \frac{27}{4}\frac{\hat{J}_3^2}{\hat{J}_2^3} \tag{3.3}$$

Where: $\hat{J}_2$ = The modified second deviatoric invariant (-)
$\hat{J}_2$ = The modified third deviatoric invariant (-)
a_1 = The rounding ratio S_u^{TXC}/S_u^a (-)

In Figure 3.3a, the NGI-ADP yield criterion is illustrated for a plane strain condition. The contours of the constant plastic shear strain and the elliptical failure curve ($\kappa = 1$) are plotted in the plane strain deviatoric stress plot. Figure 3.3b shows the failure criterion of the NGI-ADP model in the π plane with a default rounding ratio ($a_1 = 0.99$).This criterion is continuous and differentiable and it is described by a single function.

The input parameters discussed for the NGI-ADP model are summarized in Table 3.1. The determined values for each input parameter of the clay soil integrated in the 3D model will be expanded upon in chapter 3.2.2.

Symbol	Description	Unit
G_{ur}/S_u^a	Ratio unloading/reloading shear modulus over (plane strain) active shear strength	-
γ_f^C	Shear strain in triaxial compression	%
γ_f^E	Shear strain in triaxial extension	%
γ_f^{DSS}	Shear strain in direct simple shear	%
$S_{u,ref}^a$	Reference (plane strain) active shear strength	kN/m^2
z_{ref}	Reference level	m
$S_{u,inc}^a$	Increase of shear strength with depth	kN/m^2/m
S_u^p/S_u^a	Ratio of (plane strain) passive shear strength over (plane strain) active shear strength	-
τ_0/S_u^a	Initial mobilization	-
S_u^{DSS}/S_u^a	Ratio of direct simple shear strength over (plane strain) active shear strength	-
ν_u	Undrained Poisson's ratio	-

Table 3.1: Overview of the input parameters of the NGI-ADP model (Bentley, 2020).

3.2. 3D MODEL SPECIFICATIONS

3.2.1. GENERAL MODELING APPROACH

The numerical monopile tests described in this study are performed in PLAXIS 3D software. The tests were modeled using a half-pile geometry to reduce computation time with the pile located in the center of the mesh. An example of a finite element mesh for a rigid pile with a loading eccentricity equal to 5 m is visualised in Figure 3.4. The lateral boundary was set as 10 times the diameter of the model pile in negative and positive lateral direction respectively. The depth was set as twice the embedded length of the pile. Soil elements were modeled as ten-node tetrahedral elements. The pile wall was modeled as an half cylindrical plate using six-node triangular plate elements. The mesh is generated using the built-in PLAXIS 3D meshing procedure. The pile and soil volume near the pile are fine-meshed with a coarseness factor equal to 0.25. The remaining soil volume is coarse meshed with a coarseness factor equal to 2. For combined loading tests of the pile, the fine-mesh of the soil is extended with an increasing depth to take into account the deformation of the soil during vertical loading. A mesh analysis was performed to deduce the optimal element distribution regarding computation time and accuracy of results (appendix G). The mesh analysis concluded that a fine element distribution produced a significantly more accurate result compared to a medium element distribution. The fine element distribution produced result differed slightly in accuracy compared to a very fine element distribution. With an extra disadvantague due to the larger computation time associated with a very fine element distribution, all monopile tests described in this study are meshed with a fine element distribution. The number of nodes and elements for each model concerning pure lateral loading and combined loading scenarios are summarized in Tables 3.2 and 3.3.
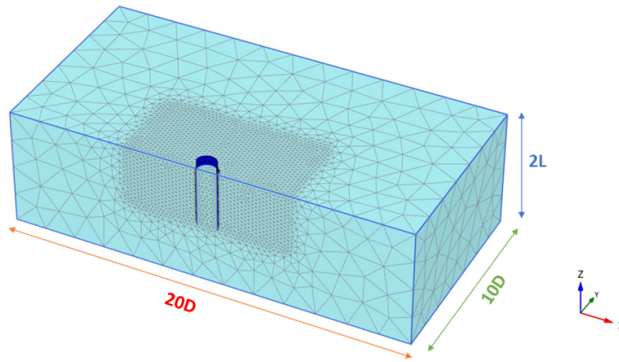
Figure 3.4: Example of a finite element mesh for a rigid pile with a diameter of 10 m ($L/D = 3$) and a loading eccentricity of 5 m in NC clay soil.

	Rigid Pile		Flexible Pile	
Loading Eccentricity	**Nodes**	**Elements**	**Nodes**	**Elements**
e = 5 m	99,060	69,747	122,869	87,488
e = 20 m	94,056	66,090	129,319	92,138
e = 40 m	60,837	87,377	101,671	71,894
e = 80 m	50,688	73,810	62,867	43,180

Table 3.2: The number of nodes and elements for each model concerning pure lateral loading.

	Rigid Pile		Flexible Pile	
Loading Eccentricity	**Nodes**	**Elements**	**Nodes**	**Elements**
e = 5 m	167,454	119,950	157,487	112,874
e = 20 m	157,250	112,340	187,884	135,023
e = 40 m	167,262	119,575	150,191	107,015
e = 80 m	157,919	112,715	104,684	73,320

Table 3.3: The number of nodes and elements for each model concerning combined loading.

3.2.2. SOIL TYPE
This section will discuss certain specific values chosen as input parameters for the modeled NC and OC clay soil using the NGI-ADP constitutive model. An overview for all selected values per input parameter for NC and OC clay soil is given in section 3.3.3.

UNDRAINED SHEAR STRENGTH S_u
The numerical monopile tests described in this study are performed in normally consolidated (NC) and overconsolidated (OC) clay soil. Ladd and Foott (1974) proposed the SHANSEP method, which is used to model S_u for certain clay soils. For modeling the S_u profile of a soft clay soil, the following simplified SHANSEP model is proposed (Ladd & Foott, 1974):

$$\frac{S_u}{\sigma'_v} = \left(\frac{S_u}{\sigma'_v}\right)_{NC} OCR^m = 0.22OCR^{0.8} \tag{3.4}$$

Where: OCR = The overconsolidation ratio (-)
$\quad\quad\quad m$ = Strength increase exponent (-)

For a NC clay soil where the OCR is equal to 1, the following relation based on equation 3.4 is used to model the S_u profile:

$$S_u = 1.5z \tag{3.5}$$

For modelling the NC clay soil using the NGI-ADP constitutive model, equation 3.5 is used by applying a value for $S^a_{u,inc}$ equal to 1.5 kPa per meter of depth. Due to the NGI-ADP implementation in PLAXIS 3D software not allowing a zero value for $S^a_{u,ref}$, a small value of 0.1 kPa is chosen at a reference depth z_{ref} of 0 m.

A homogeneous clay soil with a value for $S^a_{u,ref}$ equal to 30 kPa is chosen as implementation for an OC clay soil into the NGI-ADP model. For the homogeneous strength in clay, a value for $S^a_{u,inc}$ equal to 0 kPa and a reference depth at the lowest depth boundary of the modeled soil was chosen. This is due to the NGI-ADP model only applying $S^a_{u,inc}$ below and $S^a_{u,ref}$ above the reference depth respectively. To visualize the OCR profile of the implemented OC clay soil in the NGI-ADP model, the SHANSEP relation for lightly overconsolidated clay soil is used (Gourvenec et al., 2009):

$$\frac{S_u}{\sigma'_v} = 0.18OCR^{0.7} \tag{3.6}$$

Figures 3.5a, 3.5b and 3.5c visualize the S_u profile and OCR profile of both the NC and OC clay soil along the embedded length of the pile. The OCR profile of the NC clay is modeled using equation 3.4.
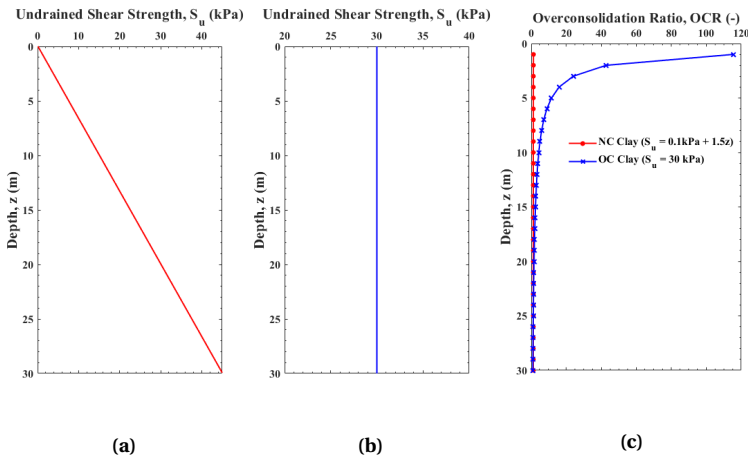
Figure 3.5: (a): S_u profile of the NC clay soil along the embedded length of the pile. (b): S_u profile of the OC clay soil along the embedded length of the pile. (c): OCR profile of both the NC and OC clay soil along the embedded length of the pile.

Though the NGI-ADP model allows for modelling anisotropic behaviour of the clay soil, for simplicity it is chosen to model both NC and OC clay soil such that the clay soil exhibits isotropic behaviour. To achieve this, both S_u^p and S_u^{DSS} are set equal to S_u^a such that the ratios S_u^p/S_u^a and S_u^{DSS}/S_u^a are equal to 1. In addition, the initial mobilization τ_0/S_u^a is set to a value of 0 to account for the triaxial input not being anisotropically consolidated.

SHEAR STRAIN γ_f

Regarding the input of the associated shear strain at which failure is obtained for the three types of undrained loading, the following general rule for near NC clays is acceptable to follow (Bentley, 2020):

$$\gamma_f^C \leq \gamma_f^{DSS} \leq \gamma_f^E \tag{3.7}$$

Bentley (2020) states that for a capacity analysis, the failure strains are not important and one may set all three values equal for simplicity. To understand the influence the magnitude of the shear failure strains might have on the lateral capacity of the monopile in clay soils, a parametric study is performed during pure lateral behaviour testing for values of γ_f^{DSS} equal to 2%, 5% and 10% respectively. Due to equation 3.7 and the lack of importance for capacity analysis (Bentley, 2020), γ_f^C and γ_f^E are set 0.001% lower and higher compared to the input for γ_f^{DSS} respectively.

SHEAR MODULUS G_{ur}
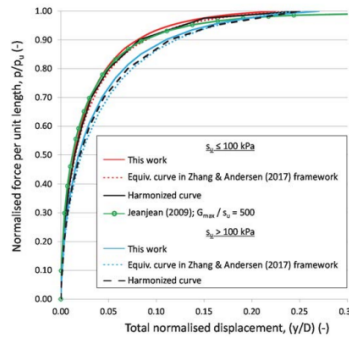
Figure 3.6: Recommended harmonised default p-y curves in absence of site-specific DSS data (Jeanjean et al., 2017).

Due to the lack of performed triaxial tests and DSS tests on clay soil, an adequate assumption had to be made for the input value of the ratio G_{ur}/S_u^a for all tests performed using the FE model. Jeanjean et al. (2017) recommends G_{max}/S_u input values in the absence of DSS test data for clay soils. For S_u values less than or equal to 100 kPa, a default DSS curve can be constructed with an input value for G_{max}/S_u equal to 500. The proposed input for G_{max}/S_u should then be combined with inputs for γ_f and a equal to 0.15 and 2.38 respectively (Jeanjean et al., 2017). Figure 3.6 illustrates that when using the proposed input, p-y curves are very similar to those proposed by Jeanjean (2009)

and Zhang and Andersen (2017) for clay soils with S_u values less than or equal to 100 kPa. Based on the proposed DSS curve by Jeanjean et al. (2017), the input value for the ratio G_{ur}/S_u^a in the NGI-ADP constitutive model is chosen to be equal to 500. This input value allows for a fair comparison between results acquired from the FE model and the discussed p-y models (section 2.1) during the pure lateral loading stage.

INPUT PARAMETERS NC AND OC CLAY SOIL

Table 3.4 summarizes all input values used in the NGI-ADP costitutive model for both NC and OC clay soil. For both NC and OC clay soil, a standard saturated unit weight γ_{sat} of 16 kN/m^3 is assumed. To model the clay soil in an undrained state, the undrained poisson's ratio ν_u is set equal to 0.495. The reduction in interface shear strength when slip occurs is accounted for by setting the strength reduction factor R_{inter} equal to 0.67.

	NC Clay Soil		OC Clay Soil	
Input Parameter	Input Value	Unit	Input Value	Unit
γ_{sat}	16	kN/m^3	16	kN/m^3
e_{ini}	1.27	-	1.27	-
G_{ur}/S_u^a	500	-	500	-
γ_f^C	1.999; 4.999; 9.999	%	1.999; 4.999; 9.999	%
γ_f^E	2.001; 5.001; 10.001	%	2.001; 5.001; 10.001	%
γ_f^{DSS}	2; 5; 10	%	2; 5; 10	%
$S_{u,ref}^a$	0,1	kN/m^2	30	kN/m^2
z_{ref}	0	m	-60	m
$S_{u,inc}^a$	1,5	kN/m^2/m	0	kN/m^2/m
S_u^P/S_u^a	1	-	1	-
τ_0/S_u^a	0	-	0	-
S_u^{DSS}/S_u^a	1	-	1	-
ν_u	0.495	-	0.495	-
R_{inter}	0.67	-	0.67	-
$K_{0,x}$	1	-	1	-
$K_{0,y}$	1	-	1	-

Table 3.4: All input values used for each input parameter in the NGI-ADP costitutive model for both NC and OC clay soil.

3.2.3. FLEXIBLE AND RIGID PILE

PILE GEOMETRY AND PROPERTIES

The pure lateral loading and combined loading tests in NC and OC clay soil will be performed on monopile foundations exhibiting rigid and flexible pile behaviour. The pile properties of the modeled rigid and flexible piles in PLAXIS 3D software are summarized in Table 3.5. Both the rigid and flexible pile are considered as cylindrical steel tubes with the young's modulus of the pile, E_p, set to 210GPa and a poisson's ratio, ν_p, set to 0.25. The rigid pile is modeled as a short length, large diameter design with an L/D ratio equal to 3. The flexible pile is modeled as such that the pile exhibits flexible behaviour by setting the diameter to a lower value equal to 2 m. The wall thickness of both piles, t, is determined using the following equation (API, 2014):

$$t \geq 6.35 + \frac{D}{100} \tag{3.8}$$

Where D is equal to the pile diameter in millimeters.

| | Rigid Pile | | Flexible Pile | |
Pile Property	Input Value	Unit	Input Value	Unit
Embedded Length, L	30	m	30	m
Pile Diameter, D	10	m	2	m
Wall Thickness, t	0.11	m	0.03	m
Aspect Ratio, L/D	3	-	15	-
Young's Modulus Pile, E_p	210	GPa	210	GPa
Poisson's Ratio, v_p	0.25	-	0.25	-
Unit Weight, γ	78	kN/m^3	78	kN/m^3

Table 3.5: The pile properties of the modeled rigid and flexible piles in PLAXIS 3D software.

3

RIGIDITY PARAMETER R
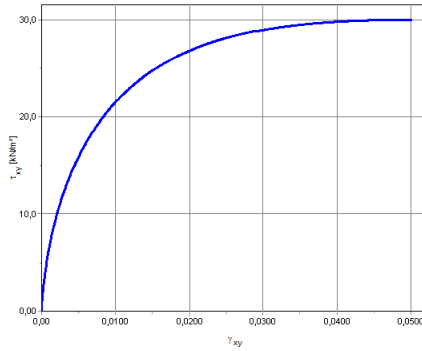
Figure 3.7: Shear stress-shear strain curve acquired from simulated DSS testing on NC and OC clay soil at a depth of $2/3L$.

To confirm the flexible and rigid pile behaviour, the standard proposed by Poulos and Hull (1989) is applied using equation 1.2. The inertia of the modeled monopile, I_p is equal to:

$$I_p = \frac{\pi(D^4 - (D - 2t)^4)}{64} \tag{3.9}$$

The soil young's modulus, E_s, of both NC and OC clay soil is determined using simulated DSS testing via the built-in SoilTest facility in PLAXIS 3D software. For both NC and OC clay soil, a representative sample at a depth of $2/3L$ is taken which both coincide with an S_u equal to 30 kPa. The sample is considered undrained and isotropically consolidated and the input is set as 0 kPa initial vertical stress, 5% maximum shear strain failure and a 1000 steps. The resulting DSS curve for both NC and OC clay soil is illustrated in Figure 3.7. From the DSS curve, the maximum shear modulus, G_{max}, is determined and transformed to E_s using equation 3.10:

$$E_s = 2G_{max}(1 + v_u) \tag{3.10}$$

Table 3.6 summarizes all R parameters for the modeled rigid and flexible pile in both NC and OC clay soil. A pile behaves rigidly if the length of the pile is less than $1.48R$

and behaves flexibly if the length of the pile exceeds $4.44R$ (Poulos & Hull, 1989). Based on the results of the simulated DSS testing, both modeled rigid pile and flexible pile are confirmed to exhibit corresponding rigid and flexible behaviour in all soil types.

Parameter	Rigid Pile		Flexible Pile	
	Value	Unit	Value	Unit
G_{max}	14,385	kPa	14,385	kPa
E_s	43,011	kPa	43,011	kPa
I_p	0.09	m^4	0.09	m^4
R	21.3	-	4.58	-
$1.48R$	31.5	-	6.78	-
$4.44R$	94.4	-	20.3	-

Table 3.6: Relevant parameters for the rigidity behaviour analysis of the modeled rigid and flexible pile in both NC and OC clay soil.

3.3. Loading Scenarios

3.3.1. Pure lateral loading

The pure lateral loading scenario consists of pure lateral loading tests on both rigid and flexible monopile models (Table 3.5) in both NC and OC clay soil conditions (Table 3.4). Pure lateral analysis includes an investigation on potential shortcomings of current practice p-y models (section 2.1) used in lateral behaviour analysis of monopile foundations. This is done by comparing the lateral capacity of the considered monopile foundations at $0.1D$ from the FE model with capacities obtained from the discussed p-y models using MATLAB software. Pure lateral analysis also includes an investigation on the influence of clay soil conditions and the loading eccentricity on the lateral behaviour of the monopile foundations in clay soil. Comparisons will be drawn for computed results at loading eccentricities of e equal to 5, 20, 40 and 80 meters respectively in both NC and OC clay soil conditions. The response of the monopile under different lateral conditions will be analyzed using the following curves:

- Lateral load-displacement curves at the ground surface/mudline.

- Pile deflection curves at 2° rotation.

- Moment-rotation curves at 2° rotation.

- Rotational stiffness degradation curves.

Pure lateral loading stages

Pure lateral loading analysis performed in the FE model consists of three stages. The initial stage establishes the initial effective vertical stress state of the modeled clay soil using the specified saturated volumetric weight. The K_0-procedure is then employed to establish the initial effective horizontal stress state in the soil. In the second stage, the pile is established in the clay soil by a "wished in-place" procedure where soil elements are replaced by pile elements with adjusted strength and stiffness parameters. It is noted that the "wished in-place" procedure is a simplification of the pile installation. The changes in soil density and the stress state around the pile that occur during jacking of the pile

are not taken into account with this procedure (Dijkstra et al., 2011). Once the pile is in place, a third stage of lateral loading is applied to the pile head. This is done by applying a large enough displacement such that a surface displacement at the ground level equal to or larger than $0.1D$ and a rotation of the pile body equal to or larger than 2° is reached.

p-y APPROACH

During the pure lateral loading scenario, a comparison will be drawn between lateral capacity results acquired from the FE model and the four p-y models incorporated in MATLAB as introduced in section 2.1. The relevant soil input parameters for all p-y models used in the pure lateral analysis are summarized in Table 3.7. Input values for ϵ_{50} and J are set as 1% and 0.5 respectively, which are satisfactory inputs for most cases (Matlock, 1970). An input value was set to 500 and 2.38 for the G_{max}/S_u ratio and a parameter respectively, as discussed in section 3.2.2. The interface roughness, α is assumed to be rough and set equal to 1.

| | Matlock (1970) | Jeanjean (2009) | Zhang and Andersen (2017) | Jeanjean et al. (2017) |
Input Parameter	Input Value	Input Value	Input Value	Input Value
ϵ_{50}	1 %	-	-	-
J	0.5	-	-	-
G_{max}/S_u	-	500	500	500
α	-	-	1	1
γ_f	-	-	2%; 5%; 10 %	2%; 5%; 10 %
a	-	-	-	2.38

Table 3.7: All relevant soil input parameters for all p-y models used in the pure lateral analysis of monopile foundations.

3.3.2. COMBINED LOADING

The combined loading scenario consists of combined loading tests on both rigid and flexible monopile models summarized in section 3.2.3, in both NC and OC clay soil conditions. Because previously discussed p-y approaches do not incorporate the possibility of analyzing the effect of vertical loading on the lateral behaviour of monopile foundations in clay soil, a comparison between the FE model and current practice p-y models can not be drawn for the combined loading scenario. The combined loading scenario analyzes the effect of vertical loading on lateral behaviour of the monopile in clay soils at different vertical load magnitudes (0.25, 0.50 and $0.75V_{ult}$). Akin to the pure lateral load scenario discussed in section 3.3.1, an analysis of combined loading is performed in NC and OC clay soil with all load eccentricities specified previously. All curves specified in section 3.3.1 are also relevant to the combined loading analysis of monopile foundations. The combined loading analysis includes the addition of an analysis on the lateral load-moment (H-M) curves of the monopile foundation. This approach allows for a direct comparison between computed results of the pure lateral loading and combined loading scenario's.

BEARING CAPACITY V_{ult}

The bearing capacity of all monopile models discussed are determined via the FE model akin to the pure lateral loading stages discussed in section 3.3.1. Instead of a lateral dis-

placement, a vertical displacement is applied at the pile head such that a surface displacement at the ground level equal or larger than $0.1D$ is reached. At a vertical displacement of $0.1D$, the corresponding value of V_{ult} is then taken as such. Additionally, the determined bearing capacity will be compared to bearing capacities computed using the API model (API, 2014):

$$V_{ult} = Q_{sf} + Q_{bf} - W'_{pile} \tag{3.11}$$

$$Q_{sf} = \pi D \int_0^L \alpha S_u \, dz \tag{3.12}$$

$$Q_{bf} = \frac{\pi D^2}{4} q_{bf} \tag{3.13}$$

Where: V_{ult} = Bearing capacity of the pile (kN)
$\quad\quad\quad Q_{sf}$ = Shaft resistance (kN)
$\quad\quad\quad Q_{bf}$ = Base resistance (kN)
$\quad\quad\quad W'_{pile}$ = Submerged weight of the pile (kN)
$\quad\quad\quad q_{bf}$ = Maximum stress mobilized at the pile base (kPa)

API (2014) recommends the use of the alpha method and q_{bf} value of $9S_u$ to determine the bearing capacity of the pile in clay soil. The alpha method is outlined in equation 3.14 (API, 2014):

$$\alpha = \begin{cases} \frac{1}{2} \left(\frac{S_u}{\sigma'_{v0}} \right)^{-\frac{1}{2}}, & \text{for } S_u < \sigma'_{v0} \\ \frac{1}{2} \left(\frac{S_u}{\sigma'_{v0}} \right)^{-\frac{1}{4}}, & \text{for } S_u > \sigma'_{v0} \end{cases} \tag{3.14}$$

Combined loading stages
Combined loading analysis performed in the FE model consisted of four stages. The first two stages are akin to the first two stages applied during pure lateral loading analysis discussed in section 3.3.1. Once the pile is set in place, the desired vertical load is applied to the pile head in stage three via a surface vertical load equal to either 0.25, 0.50 or $0.75V_{ult}$ respectively. A fourth stage of lateral loading is then applied to the pile head by applying a large displacement such that a surface displacement at the ground level equal to or larger than $0.1D$ and a rotation of the pile body equal to or larger than 2° is reached. During the lateral loading of the pile head in stage four, the vertical load applied on the pile head during stage three is kept constant.

3.3.3. Loading stages summarized
Table 3.8 summarizes the outlined loading stages of the pure lateral and combined loading scenario of the FE model discussed in sections 3.3.1 and 3.3.2 respectively.

	Stage	Description	Lateral Displacement	Vertical Load
Pure Lateral Loading	1	Establish initial effective vertical stress state	-	-
	2	Establish pile via "wish in-place" procedure	-	-
	3	Apply lateral load to the pile head	$0.1D$; 2°	-
Combined Loading	1	Establish initial effective vertical stress state	-	-
	2	Establish pile via "wish in-place" procedure	-	-
	3	Apply vertical load to the pile head	-	0.25, 0.50 or 0.75 V_{ult}
	4	Apply lateral load to the pile head	$0.1D$; 2°	0.25, 0.50 or 0.75 V_{ult}

Table 3.8: Loading stages of the pure lateral and combined loading scenario of the FE model.

4

NUMERICAL VALIDATION

This chapter presents the validation of the FE model against measured field and centrifuge test data of both flexible and short rigid piles in soft clay respectively. Sections 4.1 and 4.2 present both the field and centrifuge tests respectively. Also presented are the input parameters and the simulation test results using the FE model. Section 4.3 concludes the chapter by presenting the verdict on the validation of the FE model for use of further analysis.

4.1. FIELD TESTS OF FLEXIBLE PILES IN SOFT CLAY

4.1.1. DESCRIPTION OF PERFORMED FIELD TESTS

Zhu et al. (2017) performed field tests on two laterally loaded flexible piles which were driven offshore in a soft clay seabed. The field tests were performed at the Guishan offshore wind farms in the Pearl River Estuary located in the Guangdong Province in China (Zhu et al., 2017). The two piles, referred to as GK04 and GK08 respectively, are open ended Q345B steel piles with pile properties and geometries summarized in Table 4.1. The dominating soil strata supporting both GK04 and GK08 consisted of soft clay soils with soil properties summarized in Table 4.2.

	GK04		GK08	
Pile Property	**Value**	**Unit**	**Value**	**Unit**
Embedded Length, L	57.4	m	52.5	m
Pile Diameter, D	2.2	m	2.2	m
Wall Thickness, t	0.03	m	0.03	m
Loading Eccentricity, e	12.6	m	13.5	m
Aspect Ratio, L/D	28.7	-	23.9	-
Young's Modulus Pile, E_p	213	GPa	213	GPa
Poisson's Ratio, ν_p	0.25	-	0.25	-
Unit Weight, γ	78	kN/m^3	78	kN/m^3

Table 4.1: Pile properties and geometries of the laterally loaded GK04 and GK08 piles (Zhu et al., 2017)).

Soil Property	Value	Unit
Saturated Unit Weight , γ_{sat}	16.7	kN/m^3
Specific Gravity, G_s	2.68	-
Permeability Coefficient, k	6.6E-09	m/s
Bulk Modulus, K	2.1	MPa
Consolidation Coefficient, c_v	1.4E-06	m^2/s

Table 4.2: Soil properties of the soft clay seabed (Zhu et al., 2017)).

4.1.2. INPUT PARAMETERS OF THE FE MODEL
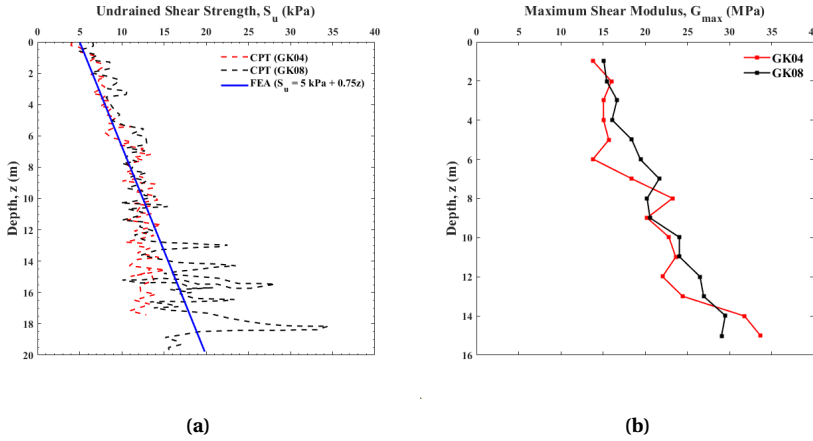
Figure 4.1: (a): S_u profile of clay soil supporting piles GK04 and GK08 (Zhu et al., 2017)) compared with the FE S_u profile estimate. (b): G_{max} profile of clay soil supporting piles GK04 and GK08 (Zhu et al., 2017)).

Figure 4.1a shows the S_u profile acquired from CPT data of clay soil in the field. Based on both profiles, an estimated S_u profile for the FE model, $S_u = 5kPa + 0.75z$, is formulated. Comparing the estimated FE S_u profile and the CPT data, it can be concluded that the estimation is a good fit with regards to both GK04 and GK08 S_u profiles respectively. Figure 4.1b shows the acquired G_{max} profile of clay soil supporting piles GK04 and GK08. Based on Figures 4.1a and 4.1b, Zhu et al. (2017) suggest that the average value of G_{max}/S_u at different depths can be calculated as 1,900 for both GK04 and GK08. Thus, for the input of G_{ur}/S_u^a in the FE model, a corresponding input value of 1,900 is chosen. Due to the lack of DSS data presented by Zhu et al. (2017), a value for γ_f^{DSS} had to be estimated. This was done by applying a trial-and-error process for a best-fit curve in correspondence with results by Zhu et al. (2017) for both GK04 and GK08 piles respectively. A value for γ_f^{DSS} equal to 5% was determined as a reasonable input for the FE model. Table 4.3 summarizes all input parameters and values for the FE model used in the validation process.

Input Parameter	Input Value	Unit
γ_{sat}	16.7	kN/m^3
e_{ini}	1.27	-
G_{ur}/S_u^a	1,900	-
γ_f^C	4.999	%
γ_f^E	5.001	%
γ_f^{DSS}	5	%
$S_{u,ref}^a$	5	kN/m^2
z_{ref}	0	m
$S_{u,inc}^a$	0.75	kN/m^2/m
S_u^p/S_u^a	1	-
τ_0/S_u^a	0	-
S_u^{DSS}/S_u^a	1	-
ν_u	0.495	-
R_{inter}	0.67	-
$K_{0,x}$	1	-
$K_{0,y}$	1	-

Table 4.3: Input parameters for the validation of the FE model in correspondence with Zhu et al. (2017)

4.1.3. RESULTS

Figure 4.2: Validation of the FE model against field tests performed by Zhu et al. (2017) regarding pile head lateral load-displacement curves of flexible piles GK04 and GK08.

Figure 4.2 presents the comparison of the measured pile head lateral load-displacement response of flexible piles GK04 and GK08 with the predicted results using the FE model and API model. From Figure 4.2, it is shown that the FE model reasonably captures the measured field test results for both flexible piles. The pile head response as predicted by using API p-y models was found to be over-conservative. API p-y models underestimate the lateral pile head load at $0.1D$ pile head displacement by ~160% and ~ 170% for flexible piles GK04 and GK08 respectively.

4.2. CENTRIFUGE TESTS OF SHORT RIGID PILES IN SOFT CLAY

4.2.1. DESCRIPTION OF PERFORMED CENTRIFUGE TESTS

Murali et al. (2015, 2019) performed four centrifuge tests of laterally loaded short rigid piles in soft NC clay. Four different load eccentricities of e = 1.2, 1.5, 2.5 and 3.5D were considered. Pile load tests with loading eccentricities corresponding to 1.2D and 3.5D were performed in clay bed 1, while the remaining two pile load tests were performed in clay bed 2. The model piles were considered equivalent in prototype scale to that of hollow steel piles. Properties of the model piles in prototype scale are summarized in Table 4.4. The soil properties of the kaolin clay used during centrifuge testing are summarized in Table 4.5.

Pile Property	Value	Unit
Embedded Length, L	7.1	m
Pile Diameter, D	3.47	m
Wall Thickness, t	0.0125	m
Loading Eccentricity, e	1.2D; 1.5D; 2.5D; 3.5D	m
Aspect Ratio, L/D	2	-
Young's Modulus Pile, E_p	200	GPa
Poisson's Ratio, v_p	0.25	-
Unit Weight, γ	78	kN/m^3

Table 4.4: Pile properties and geometries of the laterally loaded short rigid piles in prototype scale (Murali et al., 2015 and Murali et al., 2019).

Soil Property	Value	Unit
Saturated Unit Weight, γ_{sat}	15.5	kN/m^3
Specific Gravity, G_s	2.6	-
Liquid Limit, LL	63	%
Plasticity Index, PI	33	%

Table 4.5: Soil properties of the kaolin clay used for centrifuge testing (Murali et al., 2015 and Murali et al., 2019).

4.2.2. INPUT PARAMETERS OF THE FE MODEL

Figures 4.3a and 4.3b show the S_u profile acquired from T-bar test data performed by Murali et al. (2015, 2019) of clay beds 1 and 2 respectively. Based on both profiles, an estimated S_u profile for the FE model, $S_u = 1kPa + 1.1z$, is formulated. Figures 4.3a and 4.3b show a comparison between the estimated FE S_u profile and the T-Bar test data. As shown in the figures, it can be concluded that the estimation is a reasonably good fit with regards to both clay beds 1 and 2 S_u profiles respectively. Murali et al. (2015, 2019) suggest an average value between 100-200 for G_{max}/S_u based on the works of Aubeny and Grajales (2015). However, an estimation of 50 was used by Murali et al. (2015, 2019) to take into account the low strength of the clay soil used during centrifuge testing. For the FE model, an input value of 50 for G_{ur}/S_u^a with a corresponding shear strain at failure γ_f^{DSS} equal to 5% was found to give a reasonable fit for modelling clay bed 1. For clay bed 2, a lower input for γ_f^{DSS} equal to 3% and an input value of 100 for G_{ur}/S_u^a was found to improve the best-fit curve. Table 4.6 summarizes all input parameters and values for the FE model used in the validation process.

(a)   **(b)**
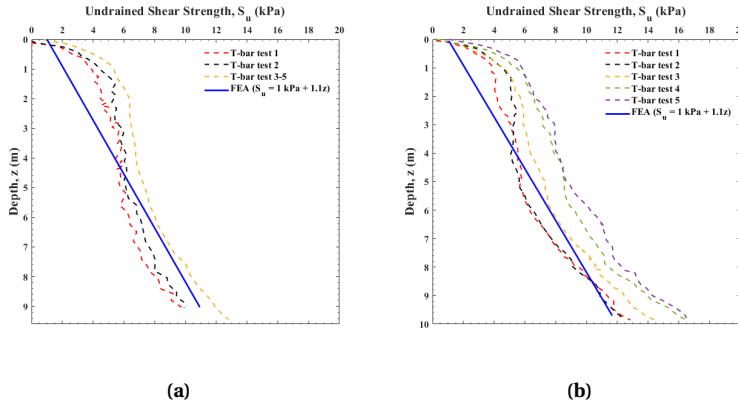
Figure 4.3: S_u profile of clay beds (a) 1 and (b) 2 compared with the FE S_u profile estimate (Murali et al., 2015 and Murali et al., 2019).

| | Clay Bed 1 | | Clay Bed 2 | |
Input Parameter	Input Value	Unit	Input Value	Unit
γ_{sat}	15.5	kN/m^3	15.5	kN/m^3
e_{ini}	1.27	-	1.27	-
G_{ur}/S_u^a	50	-	100	-
γ_f^C	4.999	%	2.999	%
γ_f^E	5.001	%	3.001	%
γ_f^{DSS}	5	%	3	%
$S_{u,ref}^a$	1	kN/m^2	1	kN/m^2
z_{ref}	0	m	0	m
$S_{u,inc}^a$	1.1	kN/m^2/m	1.1	kN/m^2/m
S_u^p/S_u^a	1	-	1	-
τ_0/S_u^a	0	-	0	-
S_u^{DSS}/S_u^a	1	-	1	-
ν_u	0.495	-	0.495	-
R_{inter}	0.67	-	0.67	-
$K_{0,x}$	1	-	1	-
$K_{0,y}$	1	-	1	-

Table 4.6: Input parameters for the validation of the FE model in correspondence with Murali et al. (2015, 2019).

4.2.3. RESULTS

Figures 4.4 and 4.5 present the comparison of the measured pile head lateral load-displacement response of the short rigid piles in clay beds 1 and 2 respectively with the predicted results using the FE model. From Figures 4.4 and 4.5, it is shown that the FE model reasonably captures the measured centrifuge test results for all short rigid piles. Differences in response can be attributed to the approximation of the S_u profile, G_{max}/S_u input and γ_f^{DSS} input. The pile head response as predicted by using API p-y models was found to be heavily over-conservative, with a much softer response predicted for all short rigid piles.
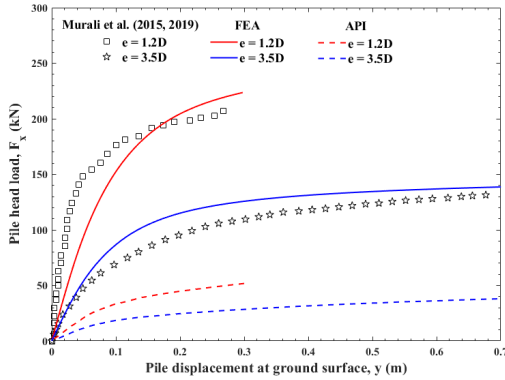
Figure 4.4: Validation of the FE model against centrifuge tests performed by Murali et al. (2015, 2019) regarding pile head lateral load-displacement curves of short rigid piles in clay bed 1 ($e = 1.2D$ and $3.5D$).
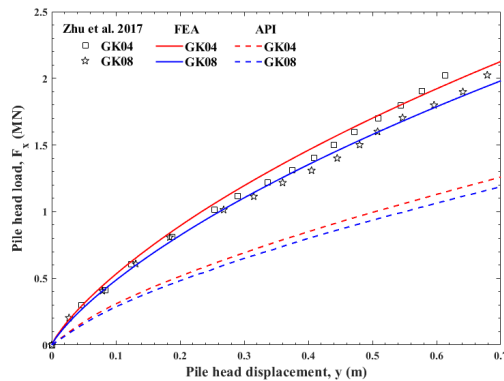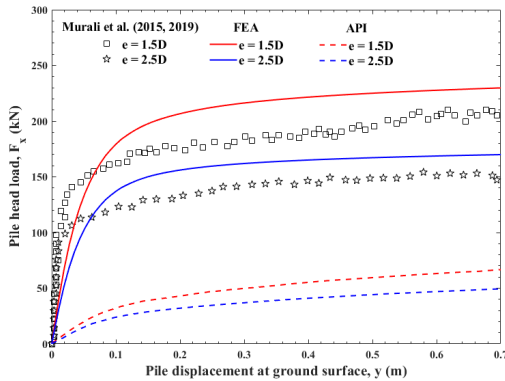

Figure 4.5: Validation of the FE model against centrifuge tests performed by Murali et al. (2015, 2019) regarding pile head lateral load-displacement curves of short rigid piles in clay bed 2 ($e = 1.5D$ and $2.5D$).

4.3. CONCLUSION

Based on comparisons between measured field test data of flexible piles and centrifuge data of short rigid piles in NC soft clay, it can be concluded that the FE model captures the response of aforementioned piles reasonably well, thus validating the FE model for use of further analysis. The standard practice API method was found to be over-conservative in regards to the response of both flexible and short rigid pile under lateral load. The result brings in to question the use of the API method for the aforementioned piles.

5

NUMERICAL RESULTS

This chapter presents the numerical results of computations executed by the FE model and existing p-y models (as summarized in section 2.1) according to the loading scenarios outlined in section 3.3. Section 5.1 presents the results of the analysis regarding the pure lateral loading scenario. Section 5.2 presents the results of the analysis regarding the combined loading scenario.

5.1. PURE LATERAL LOADING

5.1.1. LATERAL LOAD-DISPLACEMENT CURVES

INFLUENCE OF γ_f^{DSS}

Figures 5.1a and 5.1b present the response of flexible and rigid pile under lateral load with loading eccentricity e = 5 m in NC clay soil. The NC clay soil has a varying γ_f^{DSS} input of 2%, 5% and 10% respectively. As shown in the figure, increasing the input of γ_f^{DSS} causes a softer initial lateral response for both flexible and rigid pile. The described influence was found to be more prevalent on the rigid pile.

Figures 5.1c and 5.1d further detail the influence of γ_f^{DSS} on the lateral pile response. The figures show the pile head lateral load at y = 0.1D and y = 0.01D per γ_f^{DSS} input for flexible and rigid pile. Due to the softer initial response, the pile head lateral load at y = 0.1D will decrease with increasing γ_f^{DSS} input. Comparing the pile head lateral load at 0.1D with a γ_f^{DSS} input equal to 2% and 10%, a decrease of ~20% is observed for flexible pile in NC clay soil. A decrease of ~10% is observed for rigid pile in NC clay soil.

Another interesting observation is the influence of the γ_f^{DSS} input on the initial lateral response of rigid pile. Comparing the rigid pile head lateral load response at y = 0.01D with a γ_f^{DSS} input equal to 2% and 10%, a decrease of ~37% is observed. This result regarding small pile displacement might be of interest for the industry. As highlighted in appendix A, similar flexible and rigid pile lateral load responses are observed with different loading eccentricities and in OC clay soil. For simplicity, further analysis performed on flexible and rigid pile will be associated with a γ_f^{DSS} input equal to 5%.
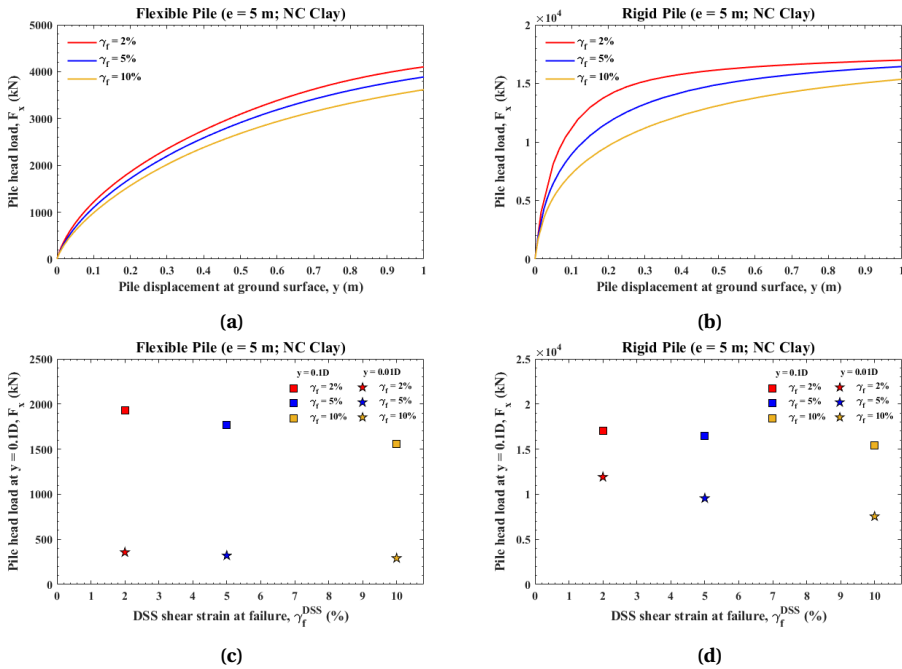
Figure 5.1: (a,b): Response of flexible and rigid pile respectively under lateral load with $e = 5$ m in NC clay soil with varying γ_f^{DSS} input ($\gamma_f^{DSS} = 2\%, 5\%, 10\%$). (c,d): Pile head lateral load at $y = 0.1D$ and $y = 0.01D$ per γ_f^{DSS} input for flexible and rigid pile respectively.

INFLUENCE OF LOADING ECCENTRICITY

Figure 5.2 presents the response of flexible and rigid pile under lateral load in NC and OC clay soil. The loading eccentricity varies with $e = 5, 20, 40$ and 80 m respectively. As shown in the figure, the loading eccentricity is found to be of significant influence in regards to the lateral response of flexible and rigid pile in both NC and OC clay soil. It can be seen that an increase in loading eccentricity results in a decrease of the pile head lateral load at failure. Tables 5.1 and 5.2 highlight the pile head lateral load at $y = 0.1D$ and change in pile head load per loading eccentricity regarding flexible and rigid pile behaviour respectively. As shown in the tables, the influence of the loading eccentricity is found to be similar regardless of the type of pile behaviour or clay soil.
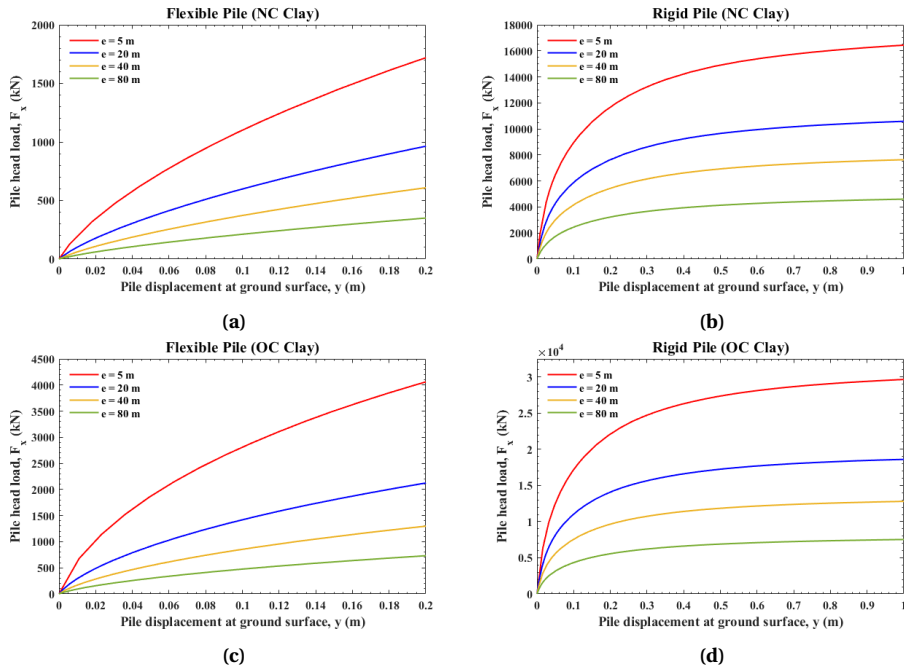
Figure 5.2: Response of flexible and rigid pile under lateral load with varying loading eccentricity e = 5, 20, 40 and 80 m respectively in: (a,b) NC clay soil and (c,d) OC clay soil.

	NC Clay Soil		OC Clay Soil	
Loading eccentricity	**Pile head load at y = 0.1D**	**Change in pile head load**	**Pile head load at y = 0.1D**	**Change in pile head load**
e = 5 m	1767 kN	-	4155 kN	-
e = 20 m	990 kN	-44%	2131 kN	-49%
e = 40 m	617 kN	-65%	1333 kN	-68%
e = 80 m	356 kN	-80%	732 kN	-82%

Table 5.1: Pile head lateral load at $y = 0.1D$ and change in pile head lateral load per loading eccentricity in regards to flexible pile in NC and OC clay soil.

	NC Clay Soil		OC Clay Soil	
Loading eccentricity	**Pile head load at y = 0.1D**	**Change in pile head load**	**Pile head load at y = 0.1D**	**Change in pile head load**
e = 5 m	16,470 kN	-	29,687 kN	-
e = 20 m	10,587 kN	-36%	18,610 kN	-37%
e = 40 m	7641 kN	-54%	12,800 kN	-57%
e = 80 m	4617 kN	-72%	7533 kN	-75%

Table 5.2: Pile head lateral load at $y = 0.1D$ and change in pile head lateral load per loading eccentricity in regards to rigid pile in NC and OC clay soil.

COMPARISON WITH EXISTING p-y MODELS
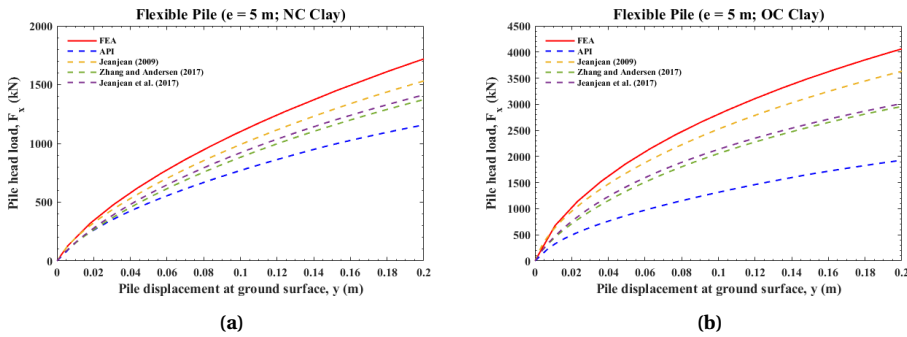
Figure 5.3: Predicted response of flexible pile under lateral load per model with loading eccentricity e = 5 m in: (a) NC clay soil and (b) OC clay soil.

Figure 5.3 presents an example of a comparison between the FE model and existing p-y models (section 2.1). The figure shows the predicted response of flexible pile under lateral load per model with loading eccentricity e = 5 m in NC and OC clay soil. Table 5.3 further details the comparison of the FE model and the standard p-y model. As shown in the figure and the table, standard p-y models reasonably capture the results of the FE model in regards to flexible pile behaviour in NC clay soil conditions. All p-y models were found to be over-conservative with Jeanjean (2009) and API (2014) models being the least and most over-conservative respectively.

Most p-y models were also found to reasonably capture the results of the FE model in regards to flexible pile behaviour in OC clay soil conditions. All p-y models were found to be over-conservative. The API (2014) model severely underestimates the lateral response of the flexible pile in OC clay soil with regards to the FE model. The underestimation of the lateral behaviour of the flexible pile in OC clay soil is likely attributed to the calibration of the API model in NC clay soil conditions, as discussed in section 2.1.1. As highlighted in appendix B, results in regards to flexible pile behaviour were found similar for other loading eccentricities analyzed.

Method of analysis	NC Clay Soil		OC Clay Soil	
	Pile head load at y = 0.1D	Difference between FE model	Pile head load at y = 0.1D	Difference between FE model
FEA	1767 kN	-	4155 kN	-
API	1164 kN	-34%	1934 kN	-54%
Jeanjean (2009)	1532 kN	-13%	3633 kN	-13%
Zhang and Andersen (2017)	1384 kN	-22%	3006 kN	-28%
Jeanjean et al. (2017)	1421 kN	-19%	3053 kN	-27%

Table 5.3: Pile head lateral load at y = 0.1D per method of analysis and difference between the FE model and p-y model predicted result regarding flexible pile with e = 5 m in NC and OC clay soil.
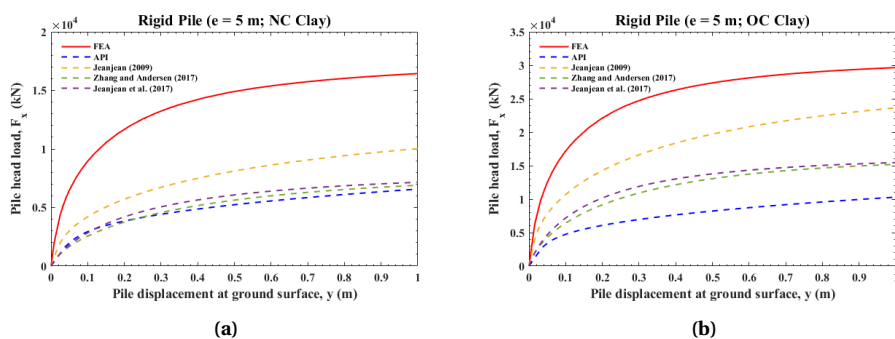
Figure 5.4: Predicted response of rigid pile under lateral load per model with loading eccentricity $e = 5$ m in: (a) NC clay soil and (b) OC clay soil.

Figure 5.4 shows the predicted response of rigid pile under lateral load per model with loading eccentricity $e = 5$ m in NC and OC clay soil. Table 5.4 further details the comparison of the FE model and the standard p-y model. As shown in the figure and the table, all standard p-y models severely underestimate the lateral response of the rigid pile in NC and OC clay soil conditions. As discussed in chapter 2, this can be attributed to the discussed p-y models not accounting for the affect of vertical shear tractions on the lateral response of rigid pile. As highlighted in appendix B, results in regards to rigid pile behaviour were found similar for other loading eccentricities analyzed.

Method of analysis	NC Clay Soil		OC Clay Soil	
	Pile head load at y = 0.1D	Difference between FE model	Pile head load at y = 0.1D	Difference between FE model
FEA	16,470 kN	-	29,687 kN	-
API	6578 kN	-60%	10,313 kN	-65%
Jeanjean (2009)	10,031 kN	-39%	23,610 kN	-21%
Zhang and Andersen (2017)	6906 kN	-58%	15,208 kN	-49%
Jeanjean et al. (2017)	7160 kN	-57%	15,476 kN	-48%

Table 5.4: Pile head lateral load at $y = 0.1D$ per method of analysis and difference between the FE model and p-y model predicted result regarding rigid pile with $e = 5$ m in NC and OC clay soil.

SOIL REACTION CURVES

Figures 5.5a and 5.5b present the 3D finite element and 1D lateral load response of flexible and rigid pile respectively with loading eccentricity $e = 5$ m in NC clay soil. The 3D result and 1D result employing the numerical soil reaction curves was acquired by using MoDeTo software. As shown in the figures, the lateral load applied to the flexible pile is almost fully resisted by the lateral soil resistance (characterized by the 1D p-y spring curve). However, the 1D p-y spring curve extracted from the 3D FEA underestimates the lateral response of the rigid pile. This is because the lateral load applied to the rigid pile is not only being resisted by the lateral soil resistance but also the base shear, base moment and vertical shear tractions. Similar observations were made by Byrne et al. (2017), as discussed in section 2.2. Figure 5.5c shows the contribution of the pile base shear, base moment and vertical shear tractions to the ultimate lateral pile capacity of
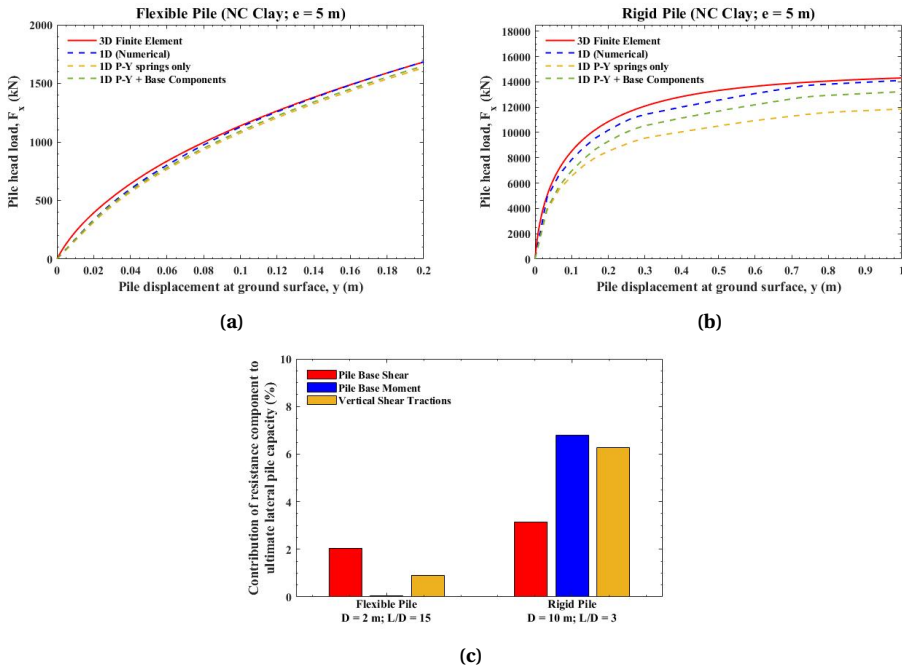
Figure 5.5: (a,b): 3D Finite element and 1D lateral load response of flexible and rigid pile respectively with loading eccentricity $e = 5$ m in NC clay soil. 3D result and 1D result employing numerical soil reaction curves acquired using MoDeTo software. (c): Contribution of the pile base shear, base moment and vertical shear tractions to the ultimate lateral pile capacity of flexible and rigid pile respectively.

the flexible and rigid pile. As shown in the figure, the contribution of the aforementioned three resistance components is found more significant for the lateral rigid pile capacity. Among the three resistance components, the base moment shows the greatest contribution to the lateral rigid pile capacity (up to ~7%). This is followed by the vertical shear tractions (up to ~6%) and the base shear component (up to ~3%).

As discussed in section 2.2, conventional p-y models do not take into account the affect of the base shear, base moment and vertical shear tractions on the lateral pile response. Comparing Figure 5.4 with Figure 5.5, results suggest that the underestimation of the lateral response of the rigid pile by the discussed p-y models can be attributed to omitting the three resistance components in the analysis.

5.1.2. PILE DEFLECTION CURVES
Figures 5.6a and 5.6b present the deflection profile of rigid pile per loading eccentricity in NC and OC clay soil respectively. As shown in the figures, the modeled rigid monopile undergoes a typical rigid rotation under the applied lateral loading. The variation of the rotation center of rigid pile per loading eccentricity in NC and OC clay soil is shown in Figure 5.6. In NC clay soil conditions, the rotation center varies slightly with a range of

(a)   **(b)**

(c)
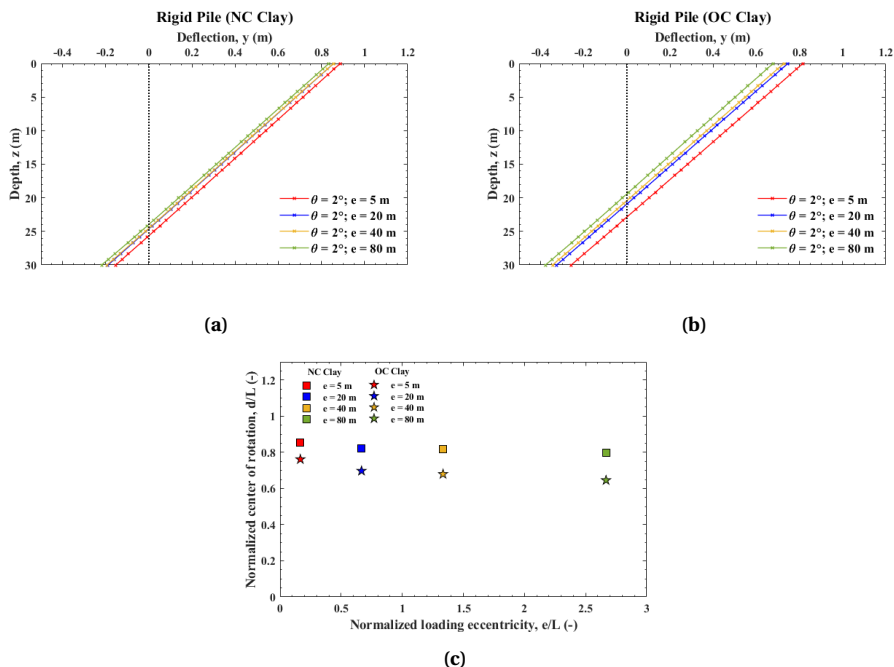
Figure 5.6: (a,b): Deflection profile of rigid pile per loading eccentricity with applied rotation θ = 2° in NC and OC clay soil respectively. (c): Variation of the rotation center per loading eccentricity of rigid pile in NC and OC clay soil.

0.85-0.8L below the ground surface. In OC clay soil conditions, the rotation center tends to move towards the ground surface with increasing loading eccentricity. The rotation center varies with a range of 0.76-0.64L below the ground surface. In addition, it is observed that the center of rotation moves upwards with increasing loading eccentricity in NC and OC clay soil conditions. The upwards movement was observed to be more prevalent in OC clay soil.

The FEA shows that a change in loading eccentricity leads to a small change in the depth of the rotation center for rigid pile in NC and OC clay soil. Based on this result, a further analysis regarding the influence of loading eccentricity on the moment at the rotation center is performed in section 5.1.3.

5.1.3. MOMENT-ROTATION CURVES

Figure 5.7 presents the moment-rotation curve at the ground surface of rigid pile under lateral load in NC and OC clay soil. The loading eccentricity varies with e = 5, 20, 40 and 80 m respectively. Table 5.6 further details the moment-rotation response of rigid pile in NC and OC clay soil respectively. As shown in the figure and the table, an increase in loading eccentricity results in a significant increase of moment response in both NC and OC clay soil.

Figure 5.8 presents the moment-rotation curve at the rotation center of rigid pile
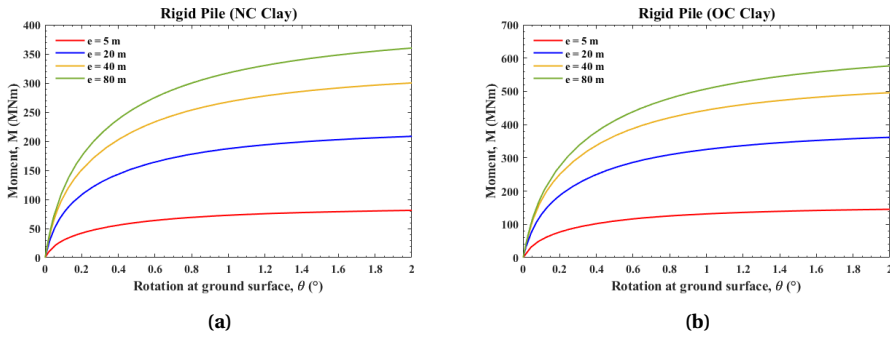
Figure 5.7: Moment-rotation curve at the ground surface of rigid pile under lateral load with varying loading eccentricity e = 5, 20, 40 and 80 m respectively in: (a) NC clay soil and (b) OC clay soil.
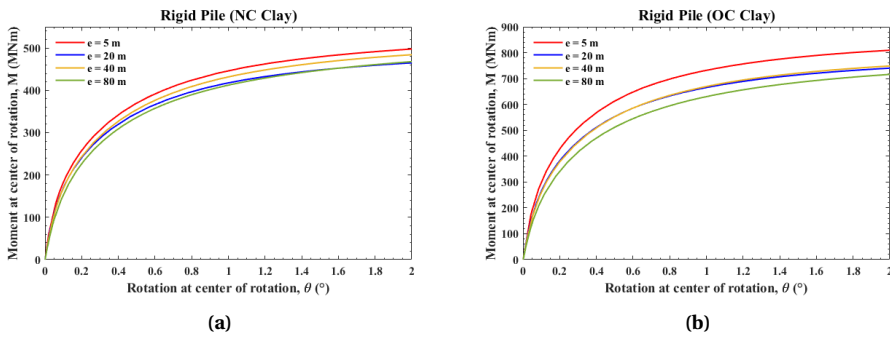
Figure 5.8: Moment-rotation curve at the rotation center of rigid pile under lateral load with varying loading eccentricity e = 5, 20, 40 and 80 m respectively in: (a) NC clay soil and (b) OC clay soil.

under lateral load in NC and OC clay soil. The loading eccentricity varies with e = 5, 20, 40 and 80 m respectively. Table 5.6 further details the moment-rotation response at the rotation center of rigid pile in NC and OC clay soil. As shown in the figure and the table, the moment at the rotation center remains fairly stable with increasing loading eccentricity for both NC and OC clay soil. A bigger deviation is observed per loading eccentricity in OC clay soil. The FEA shows that a change in loading eccentricity leads to a fairly stable moment-rotation response at the rotation center for rigid pile in NC and OC clay soil. This result and the results in section 5.1.2 suggest that the response of a rigid pile under pure lateral loading can be simplified to that of a beam hinged at the rotation center. This observation holds true in both NC and OC clay soil.

	NC Clay Soil		OC Clay Soil	
Loading eccentricity	Moment ($\theta = 2°$)	Change in moment	Moment ($\theta = 2°$)	Change in moment
e = 5 m	81 MNm	-	146 MNm	-
e = 20 m	208 MNm	+157%	362 MNm	+148%
e = 40 m	300 MNm	+270%	498 MNm	+241%
e = 80 m	360 MNm	+344%	577 MNm	+295%

Table 5.5: Moment and change in moment per loading eccentricity at a failure condition of $\theta = 2°$ for rigid pile in NC and OC clay soil respectively.

	NC Clay Soil			OC Clay Soil		
Loading eccentricity	Moment at rotation center ($\theta = 2°$)	Deviation in moment	Location of rotation center	Moment at rotation center ($\theta = 2°$)	Deviation in moment	Location of rotation center
e = 5 m	497 MNm	-	0.85L	811 MNm	-	0.76L
e = 20 m	465 MNm	-7%	0.82L	742 MNm	-9%	0.70L
e = 40 m	473 MNm	-5%	0.82L	751 MNm	-7%	0.68L
e = 80 m	468 MNm	-6%	0.80L	717 MNm	-12%	0.64L

Table 5.6: Moment and change in moment at the center of rotation per loading eccentricity for rigid pile in NC and OC clay soil respectively.

5.1.4. ROTATIONAL STIFFNESS DEGRADATION CURVES
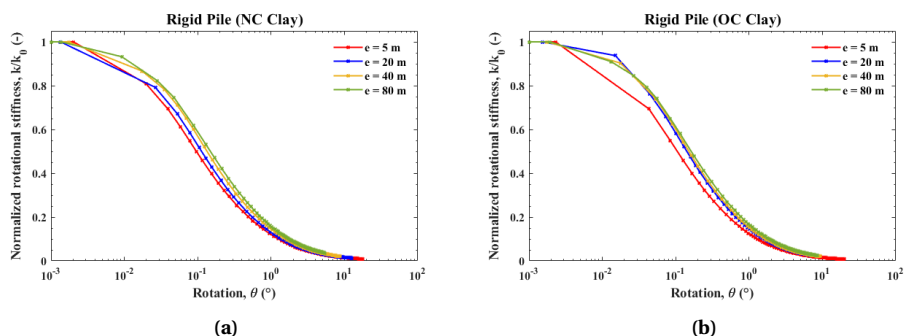
Figure 5.9: normalized rotational stiffness degradation curve of rigid pile per loading eccentricity in: (a) NC clay and (b) OC clay.

Figure 5.9 presents the normalized rotational stiffness degradation curve of rigid pile per loading eccentricity in NC and OC clay soil. As shown in the figure, the influence of loading eccentricity on the normalized rotational stiffness of rigid pile under lateral load is almost non-existent. Increasing the applied loading eccentricity causes the normalized rotational stiffness degradation curve to become more steep, but the observed influence is of low value. Thus, the influence of increasing loading eccentricity on the normalized rotational stiffness can be considered negligible for a rigid pile in both NC and OC clay soil.

5.2. COMBINED LOADING

5.2.1. BEARING CAPACITY
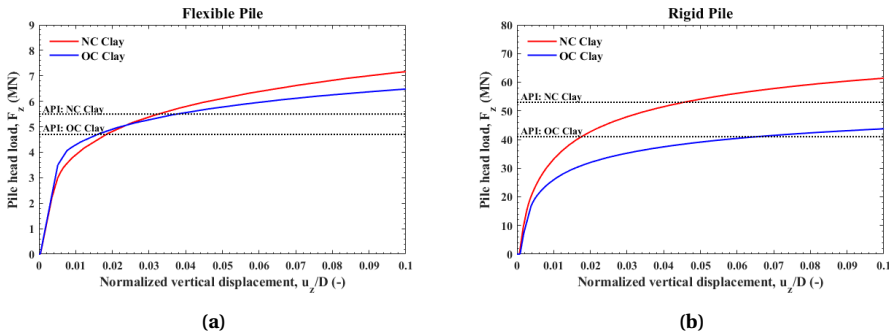
Figure 5.10: Vertical load-displacement curve of: (a) flexible pile and (b) rigid pile in NC and OC clay soil.

Figure 5.10 presents the vertical load-displacement curve of flexible and rigid pile in NC and OC clay soil. A comparison is drawn between the FEA predicted response and the bearing capacity as predicted by API (2014) models. As shown in the figure, the API computed bearing capacity tends to underestimate the capacity in regards to the FEA computed bearing capacity. However, the underestimation tends to vary depending on the pile rigidity and soil type. An interesting observation is that although the API model is calibrated on flexible pile behaviour, the predicted predicted bearing capacities for a rigid pile are quite comparable and close to the result computed by the FE model. Tables 5.7 and 5.8 further detail the applied vertical load to the pile head during the combined loading stage of rigid and flexible pile in NC and OC clay soil.

Soil type	Rigid Pile				
	V_{ult} FEA (MN)	V_{ult} FEA (kPa)	$0.25V_{ult}$ (kPa)	$0.50V_{ult}$ (kPa)	$0.75V_{ult}$ (kPa)
NC clay	62	782	196	391	587
OC clay	44	557	140	279	418

Table 5.7: Applied vertical load to pile head during combined loading stage of rigid pile in NC and OC clay soil.

Soil type	Flexible Pile				
	V_{ult} FEA (MN)	V_{ult} FEA (kPa)	$0.25V_{ult}$ (kPa)	$0.50V_{ult}$ (kPa)	$0.75V_{ult}$ (kPa)
NC clay	7.2	2280	570	1140	1710
OC clay	6.5	2063	516	1032	1548

Table 5.8: Applied vertical load to pile head during combined loading stage of flexible pile in NC and OC clay soil.

5.2.2. LATERAL LOAD-DISPLACEMENT CURVES
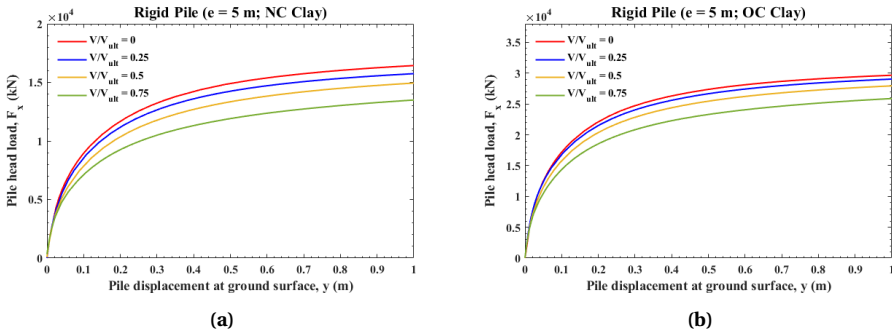
Figure 5.11: Response of rigid pile under combined loading with loading eccentricity e = 5 m in: (a) NC clay soil and (b) OC clay soil.

Figure 5.11 presents the response of rigid pile under combined loading with loading eccentricity e = 5 m in NC and OC clay soil. As shown in the figure, applying a vertical load to the pile head during lateral loading of the pile causes the initial lateral response to become softer. This tends to decrease the lateral capacity in both NC and OC clay soil. The magnitude of the described influence of combined loading is dependent on the magnitude of the vertical load applied. This is further detailed in Tables 5.9 and 5.10. As shown in the tables, increasing the magnitude of the applied vertical load causes in turn a greater decrease of the lateral capacity in both NC and OC clay soil. At applied vertical load magnitudes below $0.50V_{ult}$, the observed decrease in lateral capacity tends to be of low value (up to 11%). A more obvious influence of the applied vertical load is seen at a magnitude of $0.75V_{ult}$. The decrease in lateral capacity ranges between 18-21% and 13-24% in NC and OC clay soil conditions respectively.

	NC Clay Soil						
Loading eccentricity	H_{ult} (V/V_{ult} = 0)	H_{ult} (V/V_{ult} = **0.25**)	H_{ult} (V/V_{ult} = **0.50**)	H_{ult} (V/V_{ult} = **0.75**)	Deviation of H_{ult} (V/V_{ult} = **0.25**)	Deviation of H_{ult} (V/V_{ult} = **0.50**)	Deviation of H_{ult} (V/V_{ult} = **0.75**)
e = 5 m	16,470 kN	15,763 kN	14,941 kN	13,542 kN	-5%	-9%	-18%
e = 20 m	10,587 kN	10,511 kN	9829 kN	8576 kN	-1%	-7%	-19%
e = 40 m	7641 kN	7444 kN	6910 kN	6074 kN	-3%	-5%	-21%
e = 80 m	4617 kN	4649 kN	4262 kN	3700 kN	+1%	-8%	-20%

Table 5.9: Lateral capacity H_{ult} and deviation of H_{ult} per applied combined loading step and loading eccentricity for rigid pile in NC clay soil.

	OC Clay Soil						
Loading eccentricity	H_{ult} (V/V_{ult} = 0)	H_{ult} (V/V_{ult} = **0.25**)	H_{ult} (V/V_{ult} = **0.50**)	H_{ult} (V/V_{ult} = **0.75**)	Deviation of H_{ult} (V/V_{ult} = **0.25**)	Deviation of H_{ult} (V/V_{ult} = **0.50**)	Deviation of H_{ult} (V/V_{ult} = **0.75**)
e = 5 m	29,687 kN	29,073 kN	27,963 kN	25,936 kN	-2%	-6%	-13%
e = 20 m	18,610 kN	18,599 kN	17,575 kN	15,671 kN	0%	-6%	-16%
e = 40 m	12,800 kN	12,675 kN	11,845 kN	10,523 kN	-1%	-8%	-18%
e = 80 m	7533 kN	7398 kN	6688 kN	5764 kN	-2%	-11%	-24%

Table 5.10: Lateral capacity H_{ult} and deviation of H_{ult} per applied combined loading step and loading eccentricity for rigid pile in OC clay soil.

Figure 5.12: Normalized V-H diagrams in regards to a failure criterion of $y = 0.1D$ of rigid pile and flexible pile under combined loading in: (a,b) NC clay soil and (c,d) OC clay soil.

Figure 5.12 presents the normalized V-H diagrams in regards to a failure criterion of $y = 0.1D$ of rigid pile and flexible pile under combined loading in NC and OC clay soil. As shown in the figure, normalized V-H diagrams regarding flexible monopile foundations are not influenced by the applied vertical load during combined loading. However, normalized V-H diagrams regarding short rigid monopile foundations are obviously influenced by vertical loading. Under combined loading, the lateral capacity of the rigid pile in NC and OC clay soil tends to decrease. In line with the results regarding lateral load-displacement curves, a more obvious influence of the applied vertical load is seen at a magnitude of $0.75V_{ult}$.

5.2.3. Pile deflection curves

(a)

(b)

(c)
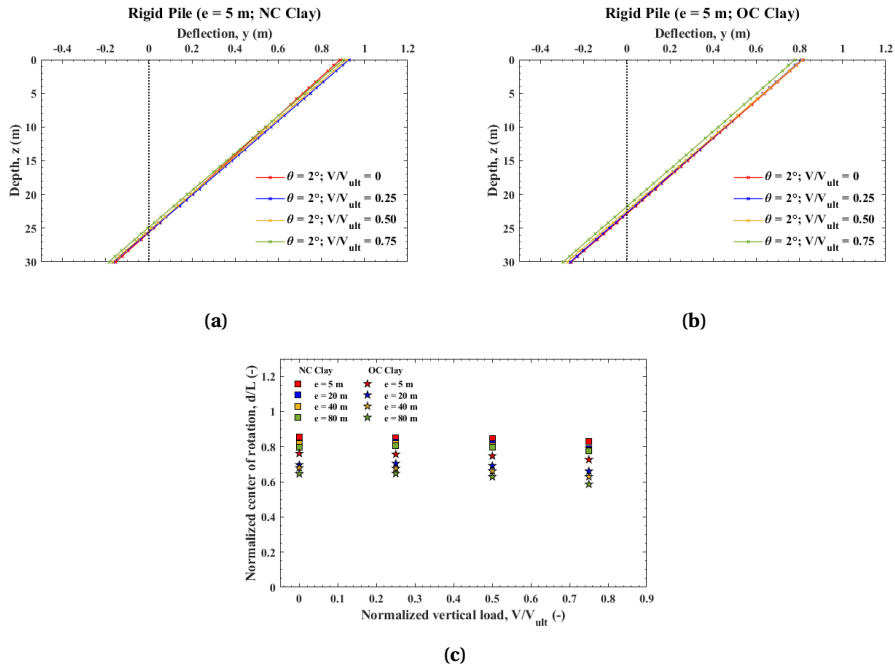
Figure 5.13: (a,b): Deflection profile of rigid pile under combined loading with applied loading eccentricity e = 5 m in NC and OC clay soil respectively. (c): Variation of the rotation center per applied vertical load and loading eccentricity of rigid pile in NC and OC clay soil.

Loading eccentricity	NC Clay Soil				OC Clay Soil			
	Location of rotation center (V/V_{ult} = 0)	Location of rotation center (V/V_{ult} = 0.25)	Location of rotation center (V/V_{ult} = 0.50)	Location of rotation center (V/V_{ult} = 0.75)	Location of rotation center (V/V_{ult} = 0)	Location of rotation center (V/V_{ult} = 0.25)	Location of rotation center (V/V_{ult} = 0.50)	Location of rotation center (V/V_{ult} = 0.75)
e = 5 m	0.85L	0.85L	0.85L	0.83L	0.76L	0.76L	0.75L	0.73L
e = 20 m	0.82L	0.82L	0.82L	0.79L	0.70L	0.70L	0.70L	0.66L
e = 40 m	0.82L	0.82L	0.81L	0.78L	0.68L	0.68L	0.66L	0.63L
e = 80 m	0.80L	0.80L	0.80L	0.78L	0.64L	0.64L	0.63L	0.59L

Table 5.11: Location of the rotation center per applied vertical load step and loading eccentricity of rigid pile in NC and OC clay soil.

Figure 5.13 presents the deflection profile of a rigid pile under combined loading with applied loading eccentricity e = 5 m in NC and OC clay soil. As shown in the figure, only a small influence is observed even under a large vertical load (V/V_{ult} = 0.75). In both NC and OC clay soil, the rotation center tends to move slightly more towards the ground surface when a vertical load equal to 0.75V_{ult} is applied to the pile head. In OC clay soil conditions, this influence seems to be more prevalent. The observed influence is further detailed in Table 5.11. As shown in the table, the influence of the vertical load at 0.75V_{ult} is as such that the range in which the rotation center varies decreases to 0.83-0.78L below

the ground surface in NC clay soil. In OC clay soil, the range in which the rotation center varies decreases to 0.73-0.59L below the ground surface.

The FEA shows that combined loading of a rigid pile leads to a negligible change in the depth of the rotation center for rigid pile in NC and OC clay soil. Based on this result, a further analysis regarding the influence of combined loading on the moment at the rotation center is performed in section 5.2.4.

5.2.4. MOMENT-ROTATION CURVES
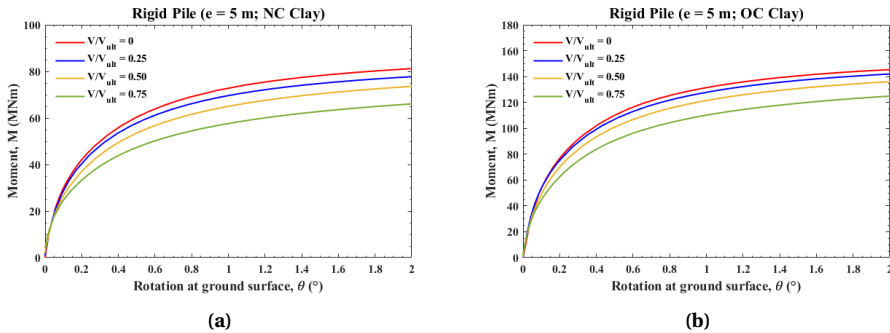
Figure 5.14: Moment-rotation curve at the ground surface of rigid pile under combined loading with loading eccentricity $e = 5$ m in: (a) NC clay soil and (b) OC clay soil.

Figure 5.14 presents the moment-rotation curve at the ground surface of rigid pile under combined loading with loading eccentricity $e = 5$ m in NC clay and OC clay soil. As shown in the figure, the moment response under combined loading has a similar trend as the lateral load response under combined loading as shown in Figure 5.11. Combined loading of the pile causes the initial moment response to become softer. This tends to

				NC Clay Soil			
Loading eccentricity	M_{ult} ($V/V_{ult} = 0$)	M_{ult} ($V/V_{ult} = 0.25$)	M_{ult} ($V/V_{ult} = 0.50$)	M_{ult} ($V/V_{ult} = 0.75$)	Deviation of M_{ult} ($V/V_{ult} = 0.25$)	Deviation of M_{ult} ($V/V_{ult} = 0.50$)	Deviation of M_{ult} ($V/V_{ult} = 0.75$)
$e = 5$ m	81 MNm	78 MNm	74 MNm	66 MNm	-4%	-9%	-19%
$e = 20$ m	208 MNm	207 MNm	193 MNm	166 MNm	0%	-7%	-20%
$e = 40$ m	300 MNm	292 MNm	270 MNm	235 MNm	-3%	-10%	-22%
$e = 80$ m	360 MNm	362 MNm	330 MNm	284 MNm	0%	-8%	-21%

Table 5.12: Moment capacity M_{ult} and deviation of M_{ult} per applied combined loading step and loading eccentricity for rigid pile in NC clay soil.
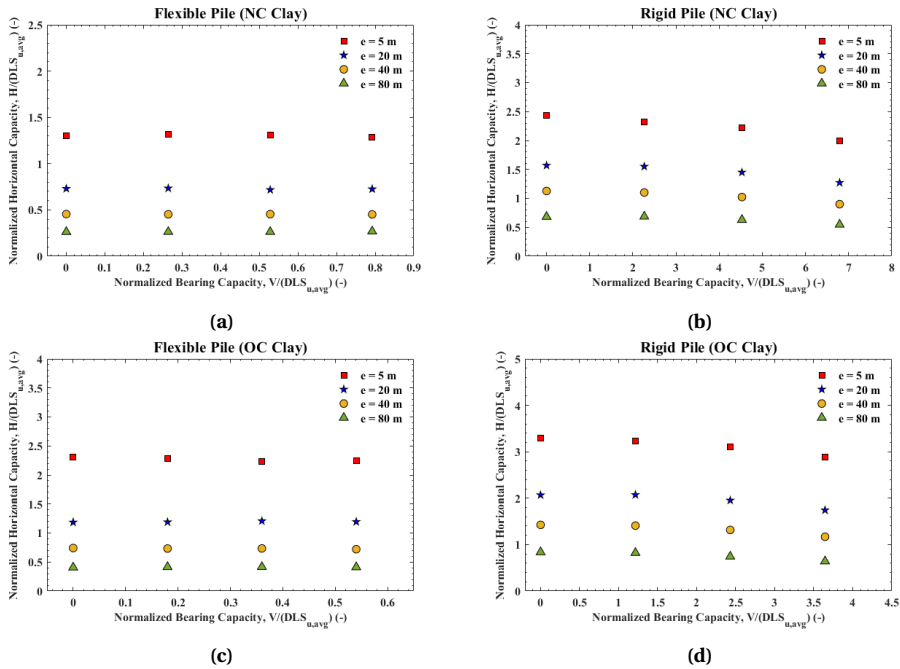
				OC Clay Soil			
Loading eccentricity	M_{ult} ($V/V_{ult} = 0$)	M_{ult} ($V/V_{ult} = 0.25$)	M_{ult} ($V/V_{ult} = 0.50$)	M_{ult} ($V/V_{ult} = 0.75$)	Deviation of M_{ult} ($V/V_{ult} = 0.25$)	Deviation of M_{ult} ($V/V_{ult} = 0.50$)	Deviation of M_{ult} ($V/V_{ult} = 0.75$)
$e = 5$ m	146 MNm	142 MNm	137 MNm	125 MNm	-3%	-6%	-14%
$e = 20$ m	362 MNm	360 MNm	338 MNm	296 MNm	0%	-7%	-18%
$e = 40$ m	498 MNm	488 MNm	451 MNm	393 MNm	-2%	-10%	-21%
$e = 80$ m	577 MNm	561 MNm	499 MNm	418 MNm	-3%	-14%	-28%

Table 5.13: Moment capacity M_{ult} and deviation of M_{ult} per applied combined loading step and loading eccentricity for rigid pile in OC clay soil.

(a)   **(b)**

Figure 5.15: Moment capacity at the rotation center per applied vertical load and loading eccentricity for rigid pile in: (a) NC clay soil and (b) OC clay soil.

Loading eccentricity	NC Clay Soil						
	M_{ult} at rotation center ($V/V_{ult}=0$)	M_{ult} at rotation center ($V/V_{ult}=0.25$)	M_{ult} at rotation center ($V/V_{ult}=0.50$)	M_{ult} at rotation center ($V/V_{ult}=0.75$)	Deviation $M_{ult} - M_{ult}$ ($e=5$ m) ($V/V_{ult}=0.25$)	Deviation $M_{ult} - M_{ult}$ ($e=5$ m) ($V/V_{ult}=0.50$)	Deviation $M_{ult} - M_{ult}$ ($e=5$ m) ($V/V_{ult}=0.75$)
$e=5$ m	497 MNm	475 MNm	446 MNm	394 MNm	-	-	-
$e=20$ m	465 MNm	463 MNm	427 MNm	365 MNm	-3%	-4%	-7%
$e=40$ m	473 MNm	471 MNm	435 MNm	372 MNm	-1%	-3%	-6%
$e=80$ m	468 MNm	471 MNm	426 MNm	365 MNm	-1%	-4%	-7%

Table 5.14: Moment capacity M_{ult} and deviation of M_{ult} at rotation center per applied combined loading step and loading eccentricity for rigid pile in NC clay soil.

Loading eccentricity	OC Clay Soil						
	M_{ult} at rotation center ($V/V_{ult}=0$)	M_{ult} at rotation center ($V/V_{ult}=0.25$)	M_{ult} at rotation center ($V/V_{ult}=0.50$)	M_{ult} at rotation center ($V/V_{ult}=0.75$)	Deviation $M_{ult} - M_{ult}$ ($e=5$ m) ($V/V_{ult}=0.25$)	Deviation $M_{ult} - M_{ult}$ ($e=5$ m) ($V/V_{ult}=0.50$)	Deviation $M_{ult} - M_{ult}$ ($e=5$ m) ($V/V_{ult}=0.75$)
$e=5$ m	811 MNm	789 MNm	745 MNm	671 MNm	-	-	-
$e=20$ m	742 MNm	741 MNm	688 MNm	589 MNm	-6%	-8%	-12%
$e=40$ m	751 MNm	732 MNm	674 MNm	577 MNm	-7%	-10%	-14%
$e=80$ m	717 MNm	697 MNm	617 MNm	510 MNm	-12%	-17%	-24%

Table 5.15: Moment capacity M_{ult} and deviation of M_{ult} at rotation center per applied combined loading step and loading eccentricity for rigid pile in OC clay soil.

decrease the moment capacity in both NC and OC clay soil. Akin to the lateral load response, the moment capacity is dependent on the magnitude of the vertical load applied. This is further detailed in Tables 5.12 and 5.13. As shown in the tables, increasing the magnitude of the applied vertical load causes in turn a decrease of the moment capacity in both NC and OC clay soil. At applied vertical load magnitudes below $0.50V_{ult}$, the observed decrease in moment capacity tends to be of low value with an observed decrease in moment capacity up to 14% depending on the vertical load magnitude, loading eccentricity and clay soil condition. A more obvious influence of the applied vertical load is seen at a magnitude of $0.75V_{ult}$. The decrease in moment capacity ranges between 19-22% and 14-28% in NC and OC clay soil conditions respectively.
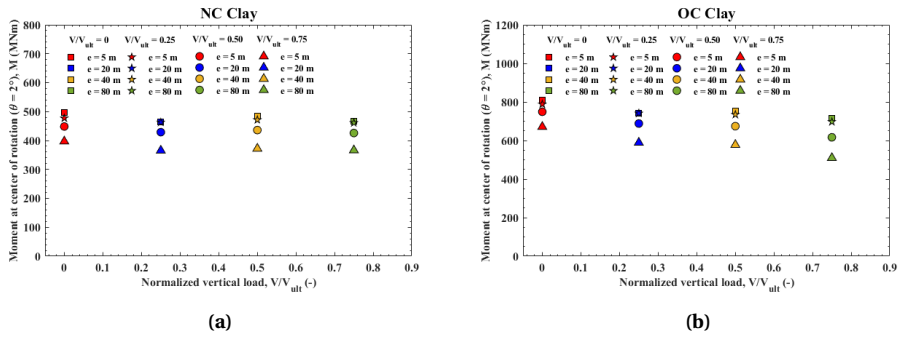
Figure 5.15 presents the moment capacity at the rotation center per applied vertical load and loading eccentricity for rigid pile in NC and OC clay soil. As shown in the figure, combined loading of the pile decreases the moment capacity at the rotation center. Akin to the moment-rotation curves at ground surface, the moment capacity at the rotation
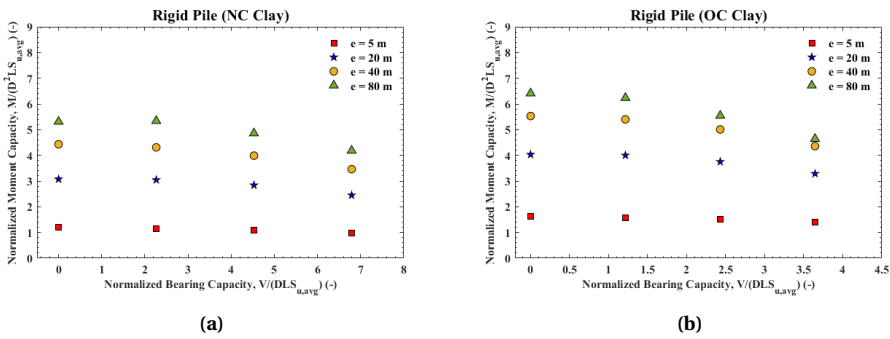
Figure 5.16: Normalized V-M diagrams in regards to a failure criterion of $\theta = 2°$ of rigid pile under combined loading in: (a) NC clay soil and (b) OC clay soil.

center is dependent on the magnitude of the vertical load applied. Tables 5.14 and 5.15 further detail the moment-rotation response at the rotation center for rigid pile in NC and OC clay soil. As shown in the tables, the moment-rotation response at the rotation center tends to be fairly stable with increasing magnitude of applied vertical load and loading eccentricity in NC clay soil. However, the moment capacity at the rotation center tends to become more unstable with increasing magnitude of applied vertical load in OC clay soil conditions.

The FEA shows that combined loading of a rigid pile leads to a fairly stable moment-rotation response at the rotation center for rigid pile in NC and OC clay soil. This result and the results in section 5.2.3 suggest that the response of a rigid pile under combined loading can be simplified to that of a beam hinged at the rotation center. This observation holds true in both NC and OC clay soil.

Figure 5.16 presents the normalized V-H diagrams in regards to a failure criterion of $\theta = 2°$ of rigid pile under combined loading in NC and OC clay soil. As shown in the figure, normalized V-M diagrams regarding short rigid monopile foundations are obviously influenced by vertical loading. Under combined loading, the moment capacity of the rigid pile in NC and OC clay soil tends to decrease. In line with the results regarding the moment-rotation curves, a more obvious influence of the applied vertical load is seen at a magnitude of $0.75V_{ult}$.

5.2.5. Rotational Stiffness Degradation Curves
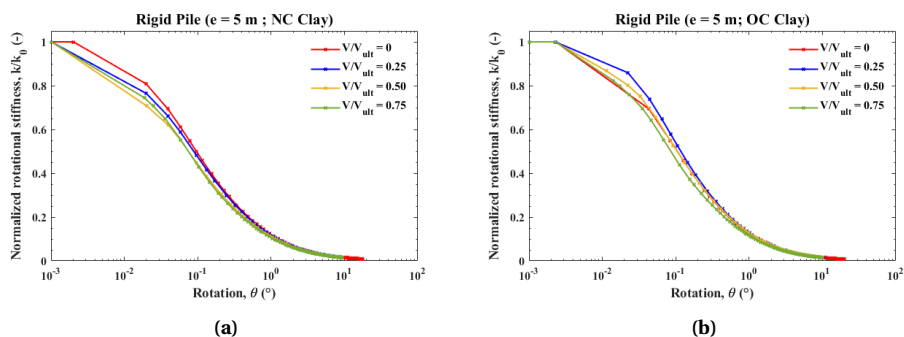
Figure 5.17: (a,b): Normalized rotational stiffness degradation curve of rigid pile under combined loading with loading eccentricity e = 5 m in NC and OC clay soil respectively.

Figure 5.17 presents the normalized rotational stiffness degradation curve of rigid pile under combined loading with loading eccentricity e = 5 m in NC and OC clay soil. As shown in the figure, the influence of combined loading of rigid pile on the normalized rotational stiffness degradation curve is almost non-existent in both NC and OC clay soil conditions. Increasing the applied vertical load magnitude causes the rotational stiffness degradation curve to become more steep, but the observed influence is of low value. Thus, the influence of combined loading on the normalized rotational stiffness degradation curve can be considered negligible for a rigid pile in both NC and OC clay soil. Similar observations were observed regarding rigid pile under combined loading with varied loading eccentricities, as highlighted in appendix F.

5.2.6. H-M Curves

Figure 5.18 presents the normalized H-M diagrams in regards to a failure criterion of y = 0.1D of rigid pile and flexible pile under combined loading in NC and OC clay soil. As shown in the figure, normalized H-M diagrams regarding flexible monopile foundations are not influenced by the applied vertical load during combined loading. However, H-M diagrams regarding short rigid monopile foundations are obviously influenced by vertical loading. Normalized H-M curves regarding short rigid monopile foundations tend to move towards the origin with increasing magnitude of the vertical load applied to the pile head in both NC and OC clay soil conditions. In line with the results observed in sections 5.2.2 and 5.2.4, the movement of the normalized H-M curves towards the origin tends to be more obvious at applied vertical load magnitudes higher than $0.50V_{ult}$.
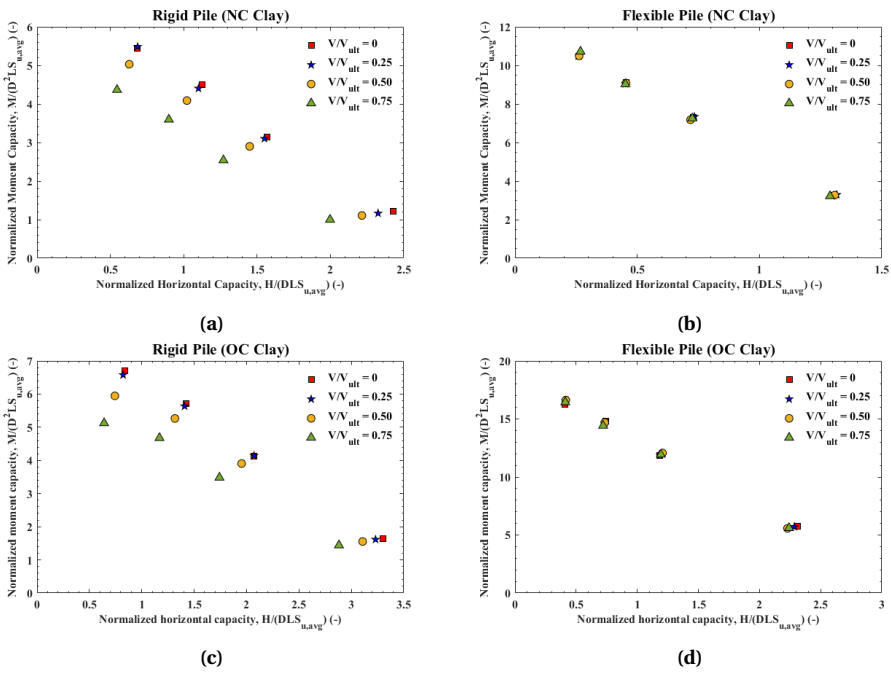
Figure 5.18: Normalized $H\text{-}M$ diagrams in regards to a failure criterion of $y = 0.1D$ of rigid pile and flexible pile under combined loading in: (a,b) NC clay soil and (c,d) OC clay soil.

6

DISCUSSION

This chapter will discuss all results and key findings from numerical computations performed in chapter 5. In section 6.1, the results from chapter 5 will be interpreted by answering the sub-research questions proposed in section 1.4.2. In section 6.2, the implication of the results will be discussed. A real turbine analysis is performed in section 6.2.1. The implication on the foundation design of rigid monopile in clay soil is assessed in section 6.2.2.

6.1. INTERPRETATION OF RESULTS

The results from chapter 5 will be interpreted by answering the sub-research questions proposed in section 1.4.2. Section 6.1.1 will answer the sub-research questions regarding the pure lateral loading scenario. Section 6.1.2 will answer the sub-research questions regarding the combined loading scenario.

6.1.1. PURE LATERAL LOADING

Interpretations and key findings regarding sub-questions concerning the pure lateral loading scenario are addressed below.

Sub-research question: *"How effective are current design methods in predicting the lateral behaviour of flexible and rigid pile?"*

- In regards to flexible pile behaviour, the results from computations using existing p-y models and the FE model suggest that existing p-y models are reasonably effective in predicting the lateral response of a flexible pile under lateral loading in clay soil. As compared to the prediction computed by the FE model, all existing p-y models analyzed in the research were found to be over-conservative in their prediction of the lateral response. This interpretation held true across all applied loading eccentricities and clay soil conditions. Jeanjean (2009) p-y model was observed to compute the least over-conservative prediction. API (2014) p-y model was observed to compute the most over-conservative prediction.

- In regards to rigid pile behaviour, the results from existing p-y models and the FE model suggest that existing p-y models severely underestimate the lateral response of a flexible pile under lateral loading in clay soil. As compared to the prediction computed by the FE model, all existing p-y models analyzed in the research were found to be heavily over-conservative in their prediction of the lateral response. This interpretation held true across all applied loading eccentricities and clay soil conditions.

Sub-research question: *"How can the use of a numerical model improve upon existing design methods regarding assessment of lateral behaviour of monopile foundation in clay soil?"*

- The input of the NGI-ADP constitutive model is as such that a variety of laboratory results regarding site-specific clay specimen can directly be used as input parameters for the FE model. In addition, regarding the assessment of short rigid pile behaviour under lateral loading, the FE model takes into account vertical shear tractions induced on the pile-soil interface and allows for the application of a vertical load during lateral loading of pile.

- In comparison to data regarding field and centrifuge tests of flexible and rigid monopile foundations in clay soil, results computed using the FE model were found to give a much more accurate prediction of the lateral behaviour of monopile foundation in clay soil as compared to the prediction computed by existing p-y models. In turn, proving the more accurate assessment of the lateral behaviour of monopile foundation in clay soil with the use of the FE model.

Sub-research question: *"How does the lateral response of rigid monopile in clay soil differ with load eccentricity?"*

- Computed results regarding lateral load-displacement curves suggest that an increase in applied loading eccentricity results in a decrease of the lateral capacity of the rigid monopile in clay soil. This interpretation held true for all clay soil conditions analyzed. The computed result is in line with conclusions drawn from centrifuge test data regarding rigid pile behaviour in clay soil as presented in the literature.

- Computed results regarding moment-rotation curves suggest that an increase in applied loading eccentricity results in an increase of the moment capacity of the rigid monopile in clay soil. In addition, The FEA shows that a change in loading eccentricity leads to a fairly stable moment-rotation response at the rotation center for rigid pile in clay soil. This interpretation held true for all clay soil conditions analyzed.

- Computed results regarding pile deflection curves suggest that the rotation center of the rigid pile tends to move more towards the ground surface with increasing loading eccentricity in clay soil. This interpretation held true for all clay soil conditions analyzed.

- Computed results regarding the normalized rotational stiffness degradation curves suggest that the influence of the loading eccentricity is of low value such that the influence of increasing loading eccentricity on the rotational stiffness can be considered negligible for a rigid pile in clay soil. This interpretation held true for all clay soil conditions analyzed.

Sub-research question: *"How does the lateral response of rigid monopile in clay soil differ with different clay soil conditions?"*

- Results regarding lateral load-displacement and moment-rotation curves suggest that a stiffer OC clay soil condition increases the lateral and moment capacity of rigid monopile. This interpretation held true for all loading eccentricities analyzed.

- Results regarding lateral load-displacement and moment-rotation curves suggest that the resulting change in lateral and moment capacity due to an increase in loading eccentricity is similar regardless of the clay soil condition of the rigid monopile.

- Results regarding pile deflection curves suggest that the position of the rotation center of the rigid monopile stabilizes more towards the ground surface in OC clay soil as compared to in NC clay soil. In NC clay soil, the position of the rotation center tends to stabilize between ranges of 0.85-0.80L depending on the loading eccentricity. In OC clay soil, the position of the rotation center tends to stabilize between ranges of 0.76-0.64L depending on the loading eccentricity. In addition, the influence of the loading eccentricity on the movement of the rotation center is more prevalent in OC clay soil conditions as compared to in NC clay soil condition.

6.1.2. COMBINED LOADING
Interpretations and key findings regarding sub-questions concerning the combined loading scenario are addressed below.

Sub-research question: *"What is the influence of the vertical load magnitude on the lateral behaviour of rigid monopile in clay soil?"*

- Results regarding lateral load-displacement and moment-rotation curves suggest that increasing the applied vertical load magnitude causes a decrease of the lateral and moment capacity. At applied vertical load magnitudes below 0.50V_{ult}, the resultant decrease of the lateral and moment capacity was found to be of low value with an observed decrease in lateral and moment capacity up to 11% and 14% respectively. The results suggest a more obvious influence of the applied vertical load at magnitudes higher than 0.50V_{ult}. At an applied vertical load equal to 0.75V_{ult}, the resultant decrease of the lateral and moment capacity was found to be up to 24% and 28% respectively.

- Results regarding pile deflection curves suggest that that the rotation center of the rigid pile tends to move slightly more towards the ground surface due to the

applied vertical load at magnitudes larger than $0.50V_{ult}$. Below a magnitude of $0.50V_{ult}$, the influence of the vertical load on the position of the rotation center can be considered non-existent. This interpretation held true for all clay soil conditions and applied loading eccentricities analyzed.

- Computed results regarding the normalized rotational stiffness degradation curves suggest that the influence of the vertical load is of low value such that the influence of increasing vertical load magnitude on the rotational stiffness can be considered negligible for a rigid pile in clay soil. This interpretation held true for all clay soil conditions and applied loading eccentricities analyzed.

- Results regarding normalized H-M curves suggest that H-M contours of short rigid monopile foundations in clay soil tend to move towards the origin with increasing applied vertical load magnitude. The result tends to be more obvious at applied vertical load magnitudes larger than $0.50V_{ult}$. This interpretation held true for both clay soil conditions analyzed

Sub-research question: *"Is the influence of the vertical load on the lateral behaviour of rigid monopile in clay soil affected by different applications of lateral load eccentricity?"*

6

- Results regarding lateral load-displacement and moment-rotation curves suggest that the influence of the vertical load on the pile and moment capacity is not affected by different applications of lateral load eccentricity in NC clay soil conditions. In OC clay soil conditions, higher applications of load eccentricity tend to amplify the influence of the applied vertical load at magnitudes larger than $0.50V_{ult}$. At an applied vertical load of $0.75V_{ult}$ in OC clay soil conditions, the decrease of the lateral and moment capacity ranges between 13-24% and 14-28% respectively due to increasing loading eccentricity.

- Results regarding the influence of the vertical load on pile deflection, normalized rotational stiffness degradation and normalized H-M curves seem unaffected by different applications of loading eccentricity.

Sub-research question: *"Is the influence of the vertical load on the lateral behaviour of rigid monopile in clay soil affected by different clay soil conditions?"*

- Results regarding lateral load-displacement and moment-rotation curves suggest that OC clay soil conditions tend to amplify the influence of loading eccentricity on the applied vertical load. This amplification was more obvious at vertical load magnitudes larger than $0.50V_{ult}$. In NC clay soil conditions, this correlation was not present.

- Results regarding the influence of the vertical load on pile deflection, normalized rotational stiffness degradation and normalized H-M curves are unaffected by different clay soil conditions.

6.2. IMPLICATION OF RESULTS

6.2.1. REAL TURBINE ANALYSIS: OFFSHORE WIND TURBINE IN LONDON CLAY SOIL

To analyse the impact of combined loading on lateral loading design of a rigid pile in clay soil, a real turbine analysis is performed to gain a realistic estimate of the amount of vertical loading present on a rigid monopile in clay soil. Considered in the analysis is a rigid monopile installed in London Clay soil. Deposits of London Clay soil are abundantly present in the southern North Sea in the Thames Estuary, which is home to several offshore wind farms such as the Kentish Flats and the London Array wind farms (Vattenfall, 2022 and London Array, 2022). The NREL 5 MW turbine is considered for the analysis due to its common use in literature and similarity to turbines installed in the North Sea (Vattenfall, 2022 and London Array, 2022).

A realistic monopile design used for a 5 MW turbine installed in London Clay soil deposits is outlined in Table 6.1. The monopile design considered in the analysis is sim-

Pile Property	Value	Unit
Embedded Length, L	25	m
Pile Diameter, D	6	m
Wall Thickness, t	0.09	m
Loading eccentricity, e	30	m
Aspect Ratio, L/D	4.2	-
Young's Modulus Pile, E_p	210	GPa
Poisson's Ratio, ν_p	0.25	-
Unit Weight, γ	78	kN/m^3
Solid Density, ρ_s	8500	kg/m^3

Table 6.1: Pile properties and geometries of the simulated monopile in London Clay soil (Carswell et al., 2016 and Charlton and Rouainia, 2022).

Input Parameter	Input Value	Unit
γ_{sat}	19.2	kN/m^3
e_{ini}	0.74	-
G_{ur}/S_u^a	560	-
γ_f^C	4.999	%
γ_f^E	5.001	%
γ_f^{DSS}	5	%
$S_{u,ref}^a$	10	kN/m^2
z_{ref}	0	m
$S_{u,inc}^a$	2.4	kN/m^2/m
S_u^p/S_u^a	1	-
τ_0/S_u^a	0	-
S_u^{DSS}/S_u^a	1	-
ν_u	0.495	-
R_{inter}	0.67	-
$K_{0,x}$	1	-
$K_{0,y}$	1	-

Table 6.2: Input parameters for the simulated London Clay soil in the FE model (Viggiani and Atkinson, 1995, Carswell et al., 2016 and Charlton and Rouainia, 2022).
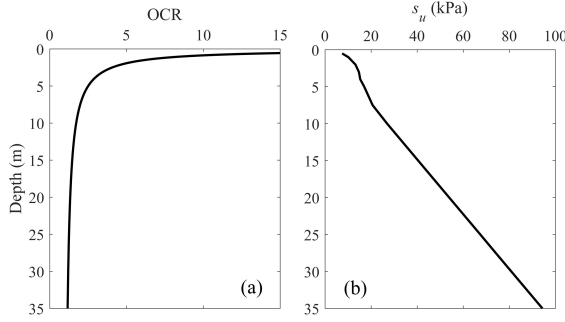
Figure 6.1: (a) OCR and (b) undrained shear strength profile of the simulated London Clay soil (Charlton & Rouainia, 2022).

ilar to those found in literature of other monopile foundations hosting a NREL generic 5 MW tubine (Carswell et al., 2016) and to monopile foundations installed in the North Sea (Damgaard et al., 2014 and London Array, 2022). The input for the London Clay soil for the FE model is summarized in Table 6.2. The input is based on several studies and experimental tests performed on London Clay soil (Viggiani and Atkinson, 1995, Carswell et al., 2016 and Charlton and Rouainia, 2022). The OCR and undrained shear strength profile of the simulated London Clay soil is illustrated in Figure 6.1. It is noted that the OCR profile illustrated in Figure 6.1 bears similarity to that of the OC clay soil analyzed in this research (Figure 3.5c). Based on the mass properties of the NREL generic 5MW turbine (Jonkman et al., 2009), mass of the monopile and the computed bearing capacity of the monopile in the London Clay soil, a realistic percentage of the bearing capacity occupied by aforementioned mass can be determined. The result of the analysis is outlined in Table 6.3. Assumed is the presence of a soil plug due the high internal skin friction present. As is shown in the table, a realistic design of a monopile in clay soil takes into account that ~27% of the bearing capacity is occupied by vertical loading due to the mass of the turbine and monopile foundation. Based on results from the combined loading scenario and the real turbine analysis, it can be concluded that the vertical loading of offshore wind turbines will be of limited influence on the lateral behaviour of a rigid pile in clay soil and the influence can be considered negligible.

Parameter of interest	Value	Unit
Tower Mass, m_t	347,460	kg
Blade Mass, m_b	17,740	kg
Rotor Nacelle Mass, m_{rn}	350,000	kg
Monopile Mass, m_p	355,090	kg
Buoyant Weight Soil Plug, W_s'	6119	kN
Buoyant Weight Monopile, W_p'	2841	kN
Total Weight Applied, W	15,976	kN
Bearing Capacity, V_{ult}	58,254	kN
% of V_{ult} occupied	27	%

Table 6.3: Results of the real turbine analysis regarding 5 MW NREL turbine in London Clay soil.

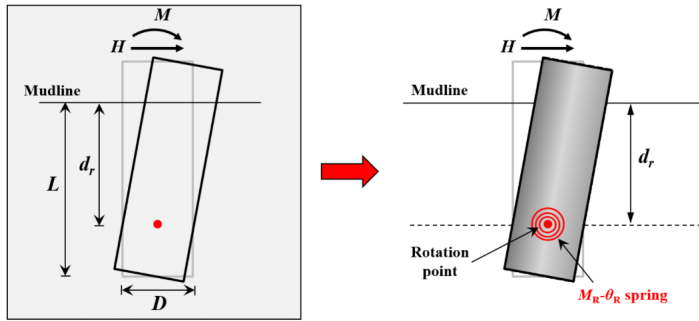### 6.2.2. FOUNDATION DESIGN OF RIGID MONOPILE IN CLAY SOIL

Figure 6.2: Concept of the rotational spring model (Wang et al., 2022)).

Based on the results of the pure lateral loading scenario, it can be concluded that existing p-y models heavily underestimate the lateral load response of rigid monopile in clay soil and are not fit to provide an accurate assessment. As concluded from the literature review, this is likely due to the existing p-y models being either calibrated on flexible pile behaviour and/or deviating monopile dimensions. Existing p-y models also do not take into account vertical shear tractions induced on the pile-soil interface which, as suggested by the results of the research, play a prominent role in the lateral load response of rigid monopile in clay soil. Based on the research, the following models are suggested to correctly assess the lateral load response of rigid monopile in clay soil:

- A 3D finite element model akin to model used in the research.

- The PISA design model for offshore monopiles.

- 1D Rotational spring model

A drawback of the first two models is the general lack of efficiency and inaccessibility. Both models require the use and comprehensive understanding of 3D modeling and/or extensive calibration to correctly assess the lateral load response of rigid monopile foundations in clay soil. A potential alternative to both models is the 1D rotational spring model proposed by Wang et al. (2022). As illustrated in Figure 6.2, this model simplifies the laterally loaded rigid pile as a beam hinged at the rotation center. The pile-soil interaction is then represented simply by a single rotational spring. This rotational spring can then be defined by scaling the stress-strain response akin to the p-y models proposed by Jeanjean et al. (2017) and Zhang and Andersen (2017). As illustrated in Figure 6.3, results computed in the pure lateral loading scenario regarding analysis of the depth and moment response of the rotation center bear similarity to those found by Wang et al. (2022) in sandy soil. In turn, this suggest that the suggested simplification of the laterally loaded rigid pile also holds true for rigid piles embedded in clay soil. As of writing this research, the 1D rotational spring model for laterally loaded rigid pile in sandy soil is still under review.
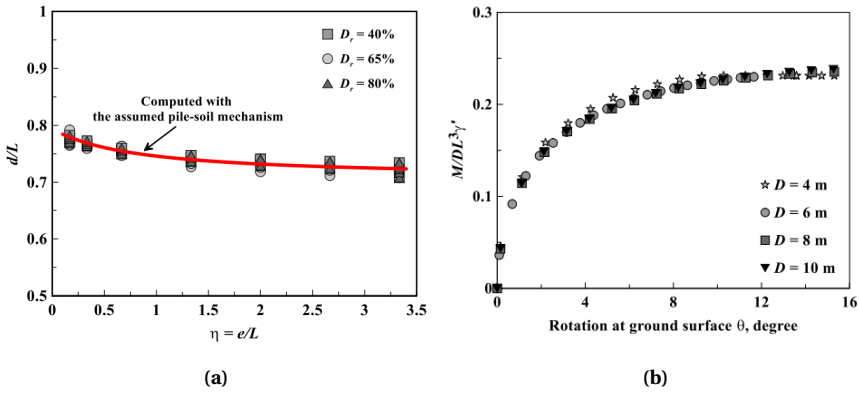
Figure 6.3: (a): Variation of rotation center at different loading eccentricity in sandy soil with varying relative density D_r. (b): Normalized moment at the rotation center of rigid pile with varying diameter in sandy soil (Wang et al., 2022).

6

7

CONCLUSION

7.1. CONCLUSION

The main objective of this research is to get a comprehensive understanding of the influence of vertical loading on the lateral behaviour of rigid monopile in clay soil. The main research objective led to the main research question, which was formulated as follows:

> *"What is the influence of vertical loading on the lateral behaviour of rigid monopile in clay soil and how does this affect current design methods regarding lateral behaviour analysis of monopile foundations?"*

An analysis using 3D finite element modeling has been conducted to answer the main research question. The answer to the main research question drawn from the results is listed below.

- The numerical analysis is performed using a 3D finite element model, which is validated by field and centrifuge data. From the numerical analysis, it can be concluded that the presence of vertical loading causes a decrease in lateral and moment capacity of the rigid pile in clay soil. In turn, H-M contours regarding short rigid monopile foundations in clay soil tend to move towards the origin under combined loading. However, the influence was found dependent on the magnitude of the vertical loading. At applied vertical load magnitudes below $0.50V_{ult}$, the described influence was found to be of low value. A more obvious influence of the applied vertical load was found at a magnitude of $0.75V_{ult}$. This conclusion held true for all clay soil conditions and loading eccentricities analyzed.

- The real turbine analysis concluded that ~27% of the bearing capacity of a rigid monopile in clay soil is occupied by vertical loading. Based on the results from the real turbine analysis and the combined loading analysis on the lateral capacity, moment capacity, pile deflection and rotational stiffness degradation of rigid pile in clay soil, it can be concluded that the vertical loading of offshore wind turbines will be of limited influence on the lateral behaviour of a rigid pile in clay

soil and the influence can be considered negligible. Thus, current design methods regarding lateral behaviour analysis of monopile foundations in clay soil remain unaffected by the influence of vertical loading.

- Results regarding pure lateral loading conclude that current design methods, such as API, heavily underestimate the lateral load response of rigid monopile foundations in clay soil and are not fit to provide an accurate assessment. In order to correctly assess the lateral load response of rigid monopile in clay soil, a method consisting of a 3D finite element model akin to the model used in the research or a PISA design model is advised.

7.2. **LIMITATIONS AND RECOMMENDATIONS**

The scope of the research is as such that several limitations arise with regards to the research topic. The limitations of the research, recommendations to resolve the limitations and starting points for future research are listed below.

- Due to the lack of experimental tests performed during the research, parameters of the modeled clay soil are based on those proposed by literature. For future numerical analysis using the NGI-ADP model, laboratory tests such as DSS or triaxial tests are recommended to determine parameters of clay soil from the field. This allows for less assumptions, and in turn, a more accurate result based on reality.

- Though the NGI-ADP model allows for modeling anisotropic behaviour of the clay soil, for simplicity it was chosen to model both clay soil conditions analyzed as such that the clay soil exhibits isotropic behaviour. With use of the NGI-ADP model, a further investigation into the influence of vertical loading on rigid monopile in clay soil exhibiting anisotropic behaviour is recommended.

- In modeling the OC clay soil using the NGI-ADP model, a simplification is made by implementing a constant undrained shear strength profile. In reality, the undrained shear strength profile of an OC clay soil varies irregularly with depth. The realistic nature cannot be implemented in a NGI-ADP model, but can be implemented in other PLAXIS 3D models (e.g.: the hardening-soil model). In conjunction with the aforementioned recommendation of laboratory testing, the proposed set-up can lead to a more accurate result regarding the influence of vertical loading of rigid monopile in OC clay soil.

- The research is performed by means of subjecting monotonic lateral loading conditions on the rigid monopile. Though this loading condition gives a good preliminary insight into the lateral behaviour of rigid monopile, imposing a cyclic loading condition instead can give a more realistic insight in regards to offshore design. It is recommended for future work to investigate the influence of vertical loading on rigid monopile in clay soil by means of subjecting a cyclic lateral loading condition. This can be done experimentally using a centrifuge set-up or numerically using ABAQUS software and/or PLAXIS 3D software using the advanced UDCAM-S model.

REFERENCES

Anagnostopoulos, C., & Georgiadis, M. C. (1993). Interaction of axial and lateral pile responses. *Journal of Geotechnical Engineering, 119*, 793–798.

Andresen, L., Saygili, G., & Grimstad, G. (2011). Finite element analysis of the saint-alban embankment failure with an anisotropic undrained strength model. *Proceedings of the 15th European Conference on Soil Mechanics and Geotechnical Engineering*, 1111–1118. https://doi.org/10.3233/978-1-60750-801-4-1111

API. (2000). Recommended practice for planning, designing and constructing fixed offshore platforms - working stresses design. *American Petroleum Institute, 21st ed.*

API. (2014). Api recommended practice 2a-wsd: Planning, designing, and constructing fixed offshore platforms—working stress design. *American Petroleum Institute, 22nd ed.*

Arshad, M., & O'Kelly, B. C. (2012). Offshore wind-turbine structures: A review. *Energy, 166*(4), 139–152. https://doi.org/https://doi.org/10.1680/ener.12.00019

Aubeny, C., & Grajales, F. (2015). Strain path analysis of setup time around piles and caissons. *Offshore Technology; Offshore Geotechnics*. https://doi.org/10.1115/OMAE2015-41088

Bentley. (2020). Plaxis 3d manual. *PLAXIS*.

Bentley. (2022). Plaxis modeto manual. *PLAXIS*.

Bjerrum, L. (1973). Problems of soil mechanics and construction on soft clays. *State of the Art Report to Session IV, The Eighth International Conference on Soil Mechanics and Foundation Engineering*, 111–159.

BP. (2021). Statistical review of world energy. *70th edition*.

Bransby, M. F. (1999). Selection of p–y curves for the design of single laterally loaded piles. *International Journal for Numerical and Analytical Methods in Geomechanics, 23*, 1909–1926. https://doi.org/10.1002/(SICI)1096-9853(19991225)23:15<1909::AID-NAG26>3.0.CO;2-L

Bransby, M. F., & Randolph, M. F. (1999). The effect of skirted foundation shape on response to combined v-m-h loadings. *International Journal of Offshore and Polar Engineering, 9*(03).

Briaud, J., Smith, T., & Meyer, B. (1984). Laterally loaded piles and the pressuremeter: Comparison of existing methods. *Laterally Loaded Deep Foundations: Analysis and Performance*, 97–111.

Budhu, M., & Davies, T. (1987). Nonlinear analysis of laterally loaded piles in cohesionless soils. *Canadian Geotechnical Journal*, *24*(2), 289–296.

Butterfield, R., & Gottardi, G. (1994). A complete three-dimensional failure envelope for shallow footings on sand. *Géotechnique*, *44*(1), 181–184. https://doi.org/10.1680/geot.1994.44.1.181

Byrne, B., Mcadam, R., Burd, H., Houlsby, G., Martin, C., Beuckelaers, W., Zdravkovic, L., Taborda, D. M. G., Potts, D., Jardine, R., Ushev, E., Liu, T., Abadias, D., Gavin, K., Igoe, D., Doherty, P., Gretlund, J., Pacheco, A. M., Wood, A., & Plummer, M. (2017). Pisa: New design methods for offshore wind turbine monopiles. *Offshore Site Investigation Geotechnics 8th International Conference Proceeding*, 142–161. https://doi.org/doi:10.3723/OSIG17.142

Byrne, B., McAdam, R. A., Burd, H. J., Houlsby, G. T., Martin, C. M., Gavin, K., Doherty, P., Igoe, D., Zdravković, L., Taborda, D. M. G., Potts, D. M., Jardine, R. J., Sideri, M., Schroeder, F. C., Wood, A. M., Kallehave, D., & Gretlund, J. S. (2015). Field testing of large diameter piles under lateral loading for offshore wind applications. *Proceedings of the XVI ECSMGE Geotechnical Engineering for Infrastructure and Development*, 1255–1260.

Carswell, W., Arwade, S. R., DeGroot, D. J., & Myers, A. T. (2016). Natural frequency degradation and permanent accumulated rotation for offshore wind turbine monopiles in clay. *Renewable Energy*, *97*, 319–330. https://doi.org/https://doi.org/10.1016/j.renene.2016.05.080

Charlton, T. S., & Rouainia, M. (2022). Geotechnical fragility analysis of monopile foundations for offshore wind turbines in extreme storms. *Renewable Energy*, *182*, 1126–1140. https://doi.org/https://doi.org/10.1016/j.renene.2021.10.092

Damgaard, M., Bayat, M., Andersen, L. V., & Ibsen, L. B. (2014). Assessment of the dynamic behaviour of saturated soil subjected to cyclic loading from offshore monopile wind turbine foundations. *Computers and Geotechnics*, *61*, 116–126. https://doi.org/https://doi.org/10.1016/j.compgeo.2014.05.008

Dijkstra, J., Broere, W., & Heeres, O. M. (2011). Numerical simulation of pile installation. *Computers and Geotechnics*, *38*(5), 612–622. https://doi.org/https://doi.org/10.1016/j.compgeo.2011.04.004

Dobry, R., O'Rourke, M., Roesset, J., & Vicente, E. (1982). Stiffness and damping of single piles. *Journal of Geotechnical Engineering*, *108*(3), 439–458.

Doherty, P., & Gavin, K. (2012). Laterally loaded monopile design for offshore wind farms. *Energy*, *165*(1), 7–17. https://doi.org/http://dx.doi.org/10.1680/ener.11.00003

European Commision. (2013). Green paper: A 2030 framework for climate and energy policies. *COM*, *169*.

Gourvenec, S., Acosta-Martinez, H. E., & Randolph, M. F. (2009). Experimental study of uplift resistance of shallow skirted foundations in clay under transient and sus-

tained concentric loading. *Géotechnique*, *59*(6), 525–537. https://doi.org/10.1680/geot.2007.00108

Grimstad, G., Andresen, L., & Jostad, P. H. (2012). Ngi-adp: Anisotropic shear strength model for clay. *International Journal for Numerical and Analytical Methods in Geomechanics*, *36*(4), 483–497. https://doi.org/https://doi.org/10.1002/nag.1016

Hazzar, L., Hussien, M. N., & Karray, M. (2017). Vertical load effects on the lateral response of piles in layered media. *International Journal of Geomechanics*, *17*(9), 291–304. https://doi.org/10.1061/(ASCE)GM.1943-5622.0000970

He, B., Kanmin, S., Hong, Y., & Wang, L. (2018). Effect of vertical load on lateral behavior of pile in clay. *Proceedings of China-Europe Conference on Geotechnical Engineering*, 942–946.

IEA. (2019). Offshore wind outlook 2019. *International Energy Association*. https://www.iea.org/reports/offshore-wind-outlook-2019

Igoe, D., Gavin, K., & O'Kelly, B. (2013). An investigation into the use of push-in pile foundations by the offshore wind sector. *International Journal of Environmental Studies*, *70*(5), 777–791. https://doi.org/10.1080/00207233.2013.798496

International Energy Association. (2019). Offshore wind outlook 2019: World energy outlook special report. *IEA*.

Jeanjean, P. (2009). Re-assessment of P-Y curves for soft clays from centrifuge testing and finite element modeling. *All Days*. https://doi.org/10.4043/20158-MS

Jeanjean, P, Zhang, Y., Zakeri, A., Andersen, K. H., Gilbert, R., & Senanayake, A. I. M. J. (2017). A framework for monotonic p-y curves in clays. *Offshore Site Investigation Geotechnics 8th International Conference Proceeding*, 108–141. https://doi.org/doi:10.3723/OSIG17.108

Jonkman, J., Butterfield, S., Musial, W., & Scott, G. (2009). Definition of a 5-mw reference wind turbine for offshore system development. *National Renewable Energy Laboratory, Tech. Rep. NREL/TP-500-38060.*

Kallehave, D., Byrne, B., Thilsted, C., & Mikkelsen, K. (2015). Optimization of monopiles for offshore wind turbines. *Philosophical transactions. Series A, Mathematical, physical, and engineering sciences*, *373*(20140100). https://doi.org/http://doi.org/10.1098/rsta.2014.0100

Karthigeyan, S., Ramakrishna, V. V. G. S. T., & Rajagopal, K. (2007). Numerical investigation of the effect of vertical load on the lateral response of piles. *Journal of Geotechnical and Geoenvironmental Engineering*, *133*(5), 512–521. https://doi.org/10.1061/(ASCE)1090-0241(2007)133:5(512)

Klar, A. (2008). Upper bound for cylinder movement using "elastic" fields and its possible application to pile deformation analysis. *International Journal of Geomechanics*, *8*. https://doi.org/10.1061/(ASCE)1532-3641(2008)8:2(162)

Klar, A., & Osman, A. (2008). Load-displacement solutions for piles and shallow foundations based on deformation fields and energy conservation. *Geotechnique, 58*, 581–589. https://doi.org/10.1680/geot.2007.00128

Ladd, C. C., & Foott, R. (1974). New design procedure for stability of soft clays. *Journal of the Geotechnical Engineering Division, 100*(7), 763–786. https://doi.org/10.1061/AJGEB6.0000066

Li, Q. (2020). Response of monopiles subjected to combined vertical and lateral loads, lateral cyclic load, and scour erosion in sand. https://doi.org/10.4233/uuid:21829001-1f0f-40e8-a3cd-31ec07d30071

Li, Q., Prendergast, L. J., Askarinejad, A., & Gavin, K. (2020). Influence of vertical loading on behavior of laterally loaded foundation piles: A review. *Journal of Marine Science and Engineering, 8*(12). https://doi.org/10.3390/jmse8121029

London Array. (2022). About london array. *London Array*. https://londonarray.com/

Lynas, M., Houlton, B. Z., & Perry, S. (2021). Greater than 99% consensus on human caused climate change in the peer-reviewed scientific literature. *Environmental Research Letters, 16*(11).

Matlock, H. (1970). Correlations for design of laterally loaded piles in soft clay. *Proc. 2nd Offshore Technology Conference*, (OTC 1204), 577–594.

Murali, M., Grajales, F., Beemer, R. D., Biscontin, G., & Aubeny, C. (2015). Centrifuge and Numerical Modeling of Monopiles for Offshore Wind Towers Installed in Clay. *Volume 1: Offshore Technology; Offshore Geotechnics*. https://doi.org/10.1115/OMAE2015-41332

Murali, M., Grajales-Saavedra, F. J., Beemer, R. D., Aubeny, C. P., & Biscontin, G. (2019). Capacity of short piles and caissons in soft clay from geotechnical centrifuge tests. *Journal of Geotechnical and Geoenvironmental Engineering, 145*(10), 04019079. https://doi.org/10.1061/(ASCE)GT.1943-5606.0002091

Musial, W., & Ram, B. (2010). Large-scale offshore wind power in the united states. *NREL*.

Nova, R., & Montrasio, L. (1991). Settlements of shallow foundations on sand. *Géotechnique, 41*(2), 243–256. https://doi.org/10.1680/geot.1991.41.2.243

O'Kelly, B. C., & Arshad, M. (2016). 20 - offshore wind turbine foundations – analysis and design. In C. Ng & L. Ran (Eds.), *Offshore wind farms* (pp. 589–610). Woodhead Publishing. https://doi.org/https://doi.org/10.1016/B978-0-08-100779-2.00020-9

Poulos, H. G., & Hull, T. S. (1989). The role of analytical geomechanics in foundation engineering. *Foundation Engineering: Current Principles and Practices, 2*, 1578–1606.

Randolph, M. F., & Gourvenec, S. (2011). *Offshore geotechnical engineering*. Spon Press Abingdon, Oxon.

Randolph, M. F., & Houlsby, G. T. (1984). The limiting pressure on a circular pile loaded laterally in cohesive soil. *Géotechnique, 34*(4), 613–623. https://doi.org/10.1680/geot.1984.34.4.613

Reese, L., Cox, W., & Koop, F. (1975). Field testing and analysis of laterally loaded piles in stiff clay. *Proc. 7th Offshore Technology Conference, 2*(OTC 2312), 671–690.

Ritchie, H., & Roser, M. (2020). Energy [https://ourworldindata.org/energy]. *Our World in Data*.

Sørensen, S. P. H., Brødbæk, K. T., Møller, M., & Augustesen, A. H. (2012). *Review of laterally loaded monopiles employed as the foundation for offshore wind turbines*. Department of Civil Engineering, Aalborg University.

Stehly, T., Beiter, P., & Duffy, P. (2019). 2019 cost of wind energy review. *National Renewable Energy Laboratory*.

U.S. Energy Information Administration. (2021). International energy outlook 2021. *EIA*.

U.S. Nuclear Regulatory Commission. (2021). *Capacity factor (net)*. Retrieved September 3, 2021, from https://www.nrc.gov/reading-rm/basic-ref/glossary/capacity-factor-net.html

Vattenfall. (2022). Kentish flats. *Vattenfall*. https://powerplants.vattenfall.com/kentish-flats/

Viggiani, G., & Atkinson, J. H. (1995). Stiffness of fine-grained soil at very small strains. *Géotechnique, 45*(2), 249–265. https://doi.org/10.1680/geot.1995.45.2.249

Wang, H., Lehane, B. M., Bransby, M. F., Askarinejad, A., Wang, L. Z., & Hong, Y. (2022). A simple rotational spring model for laterally loaded rigid piles in sand. *Marine Structures, in-press*.

Wang, H., Wang, L., Hong, Y., Askarinejad, A., He, B., & Pan, H. (2021). Influence of pile diameter and aspect ratio on the lateral response of monopiles in sand with different relative densities. *Journal of Marine Science and Engineering, 9*(6). https://doi.org/10.3390/jmse9060618

Welch, R. C., & Reese, L. C. (1972). Laterally loaded behavior of drilled shafts.

WindEurope. (2020). Offshore wind in europe: Key trends and statistics 2019. *WindEurope*.

WindEurope. (2021a). Offshore wind in europe: Key trends and statistics 2020. *WindEurope*.

WindEurope. (2021b). Wind energy in europe: 2020 statistics and the outlook for 2021-2025. *WindEurope*.

Zhang, Y., & Andersen, K. (2017). Scaling of lateral pile p-y response in clay from laboratory stress-strain curves. *Marine Structures, 53*, 124–135. https://doi.org/10.1016/j.marstruc.2017.02.002

Zhu, B., Zhu, Z., Li, T., Liu, J., & Liu, Y. (2017). Field tests of offshore driven piles subjected to lateral monotonic and cyclic loads in soft clay. *Journal of Waterway, Port, Coastal, and Ocean Engineering, 143*(5), 05017003. https://doi.org/10.1061/(ASCE)WW.1943-5460.0000399

A

γ_f^{DSS} ANALYSIS

A.1. ANALYSIS REGARDING NC CLAY SOIL
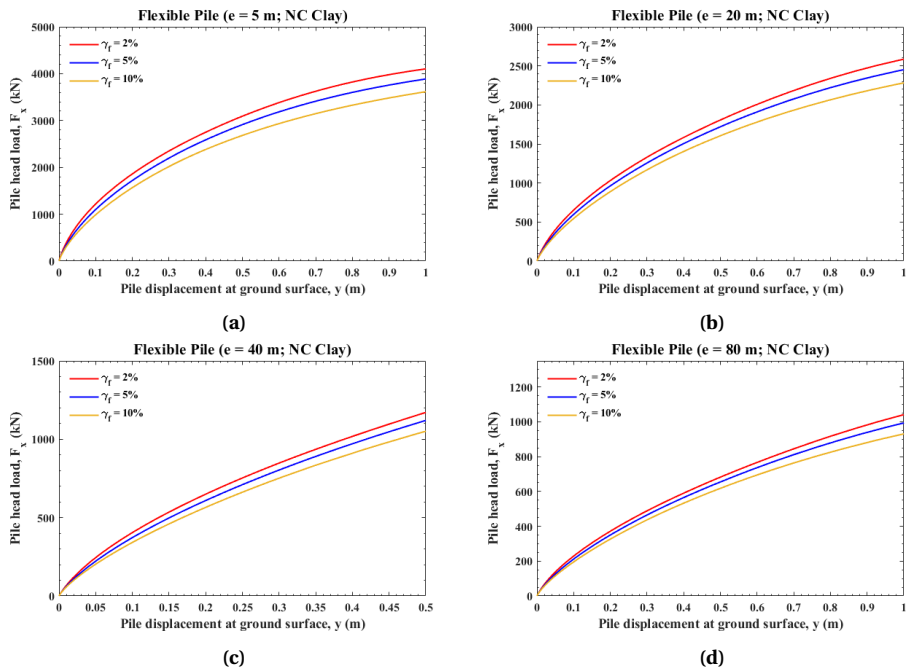
Figure A.1: Response of flexible pile under lateral load in NC clay soil with varying γ_f^{DSS} input ($\gamma_f^{DSS} = 2\%, 5\%, 10\%$) with loading eccentricity: (a) $e = 5$ m (b) $e = 20$ m (c) $e = 40$ m (d) $e = 80$ m.
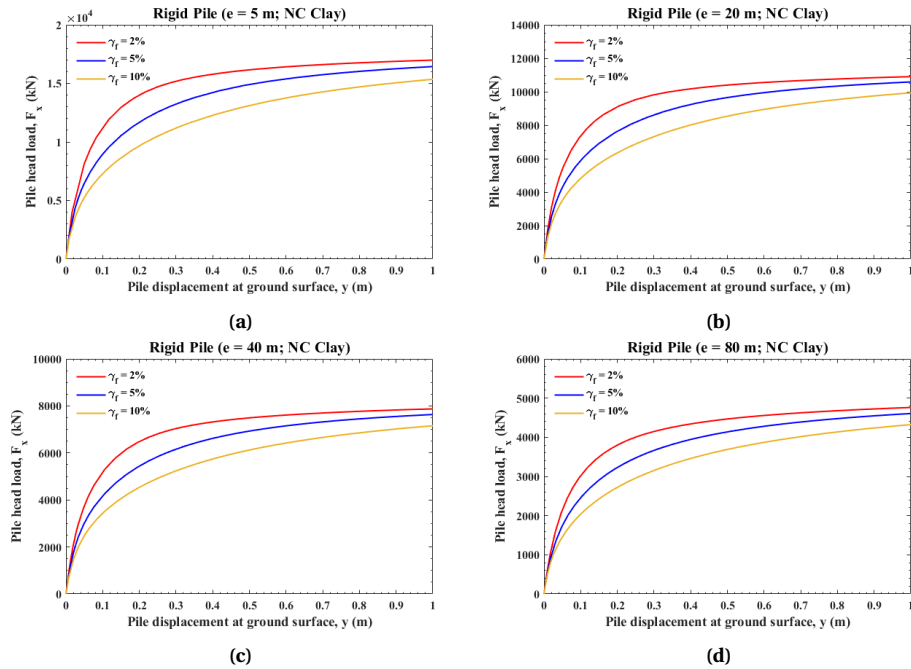
Figure A.2: Response of rigid pile under lateral load in NC clay soil with varying γ_f^{DSS} input ($\gamma_f^{DSS} = 2\%, 5\%, 10\%$) with loading eccentricity: (a) $e = 5$ m (b) $e = 20$ m (c) $e = 40$ m (d) $e = 80$ m.

A.2. ANALYSIS REGARDING OC CLAY SOIL
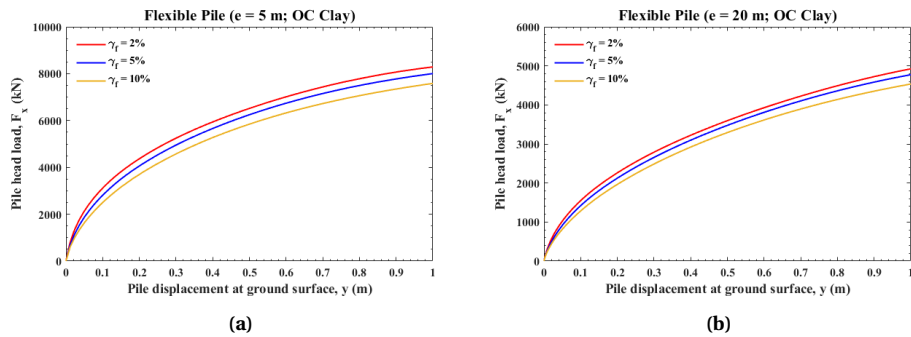
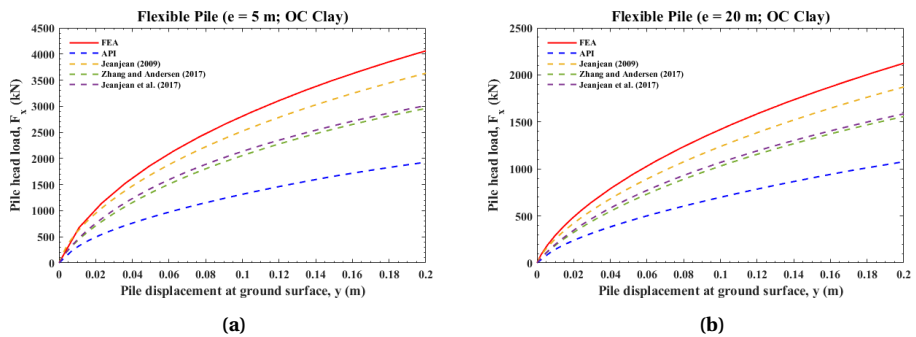**Figure A.3:** Response of flexible pile under lateral load in OC clay soil with varying γ_f^{DSS} input ($\gamma_f^{DSS} = 2\%, 5\%, 10\%$) with loading eccentricity: (a) $e = 5$ m (b) $e = 20$ m (c) $e = 40$ m (d) $e = 80$ m.
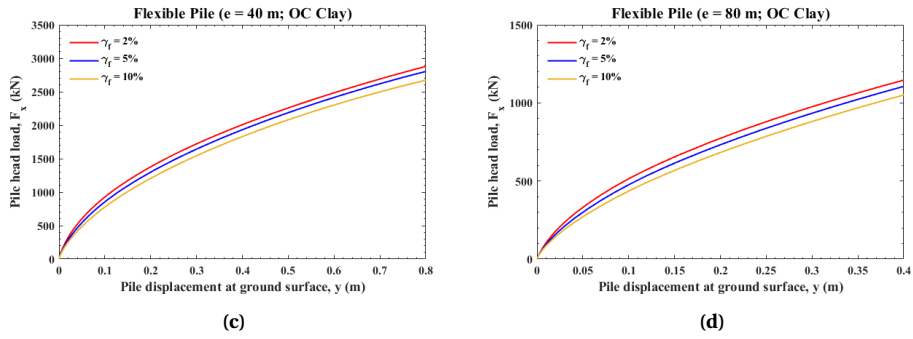
Figure A.3: (cont.) Response of flexible pile under lateral load in OC clay soil with varying γ_f^{DSS} input ($\gamma_f^{DSS} = 2\%, 5\%, 10\%$) with loading eccentricity: (a) $e = 5$ m (b) $e = 20$ m (c) $e = 40$ m (d) $e = 80$ m.
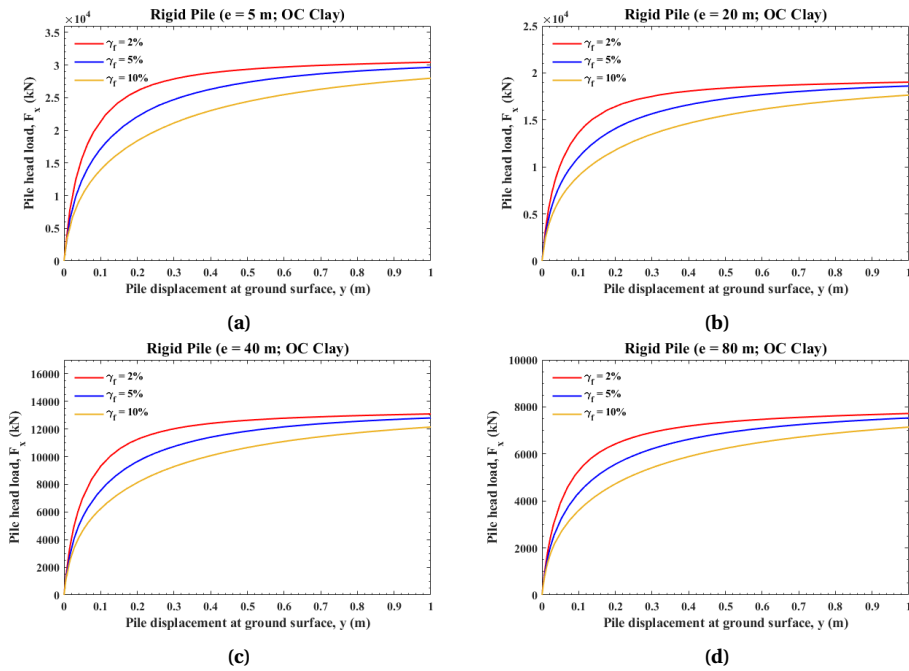
Figure A.4: Response of rigid pile under lateral load in OC clay soil with varying γ_f^{DSS} input ($\gamma_f^{DSS} = 2\%, 5\%, 10\%$) with loading eccentricity: (a) $e = 5$ m (b) $e = 20$ m (c) $e = 40$ m (d) $e = 80$ m.

B

P-Y COMPARISON

B.1. ANALYSIS REGARDING NC CLAY SOIL
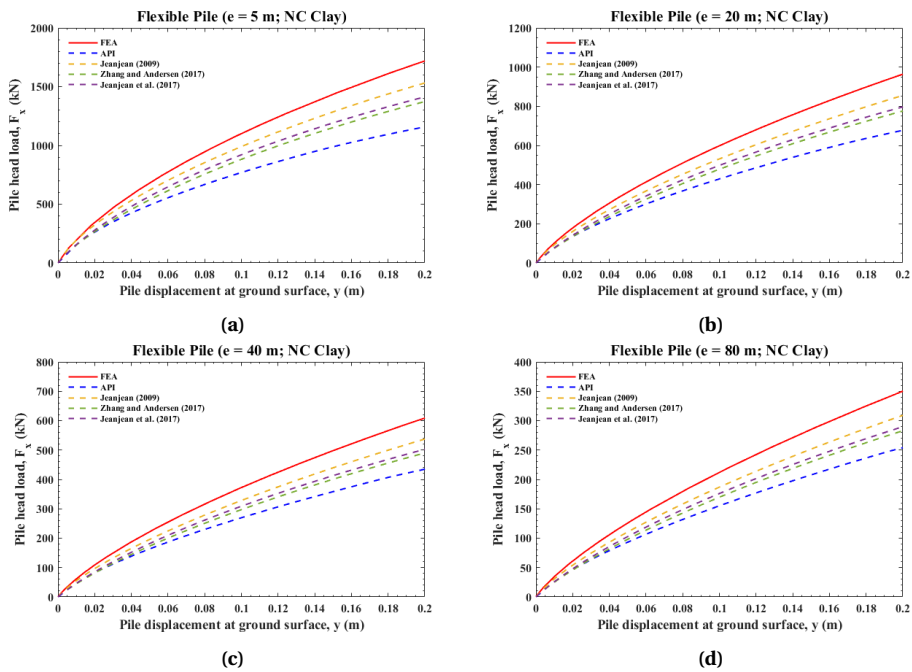
Figure B.1: Predicted response of flexible pile under lateral load per model in NC clay soil with loading eccentricity: (a) $e = 5$ m (b) $e = 20$ m (c) $e = 40$ m (d) $e = 80$ m.
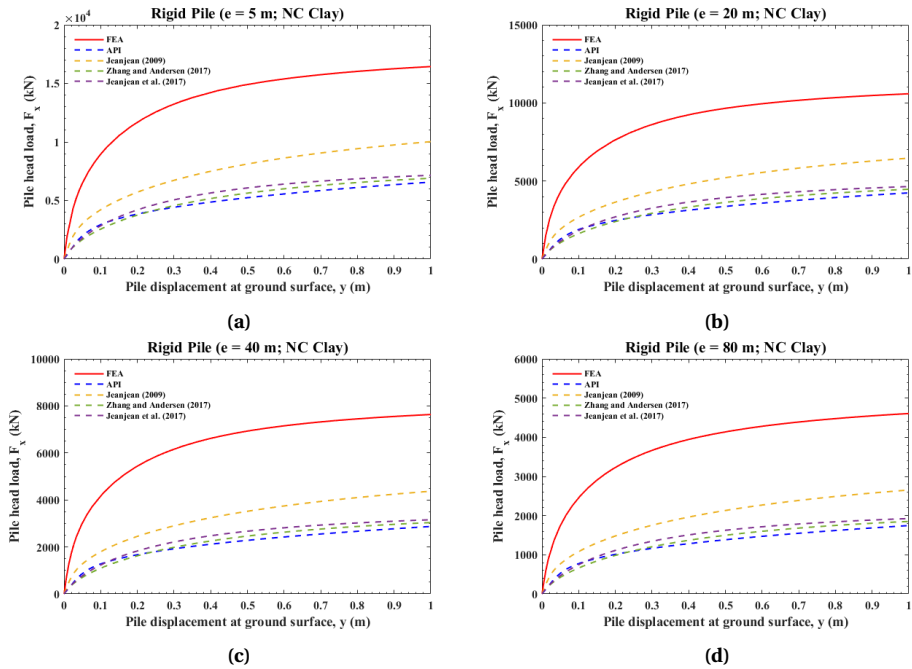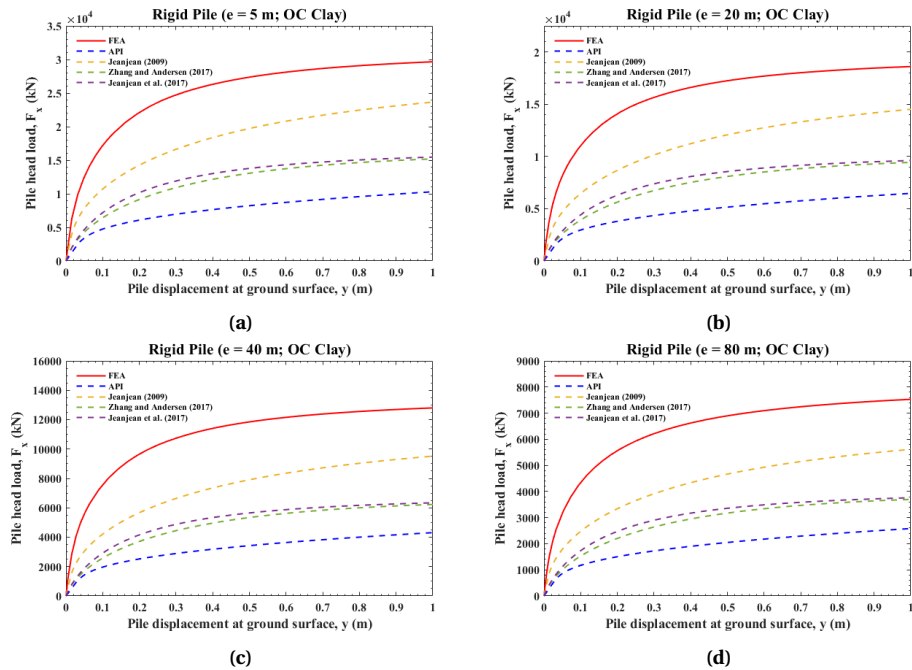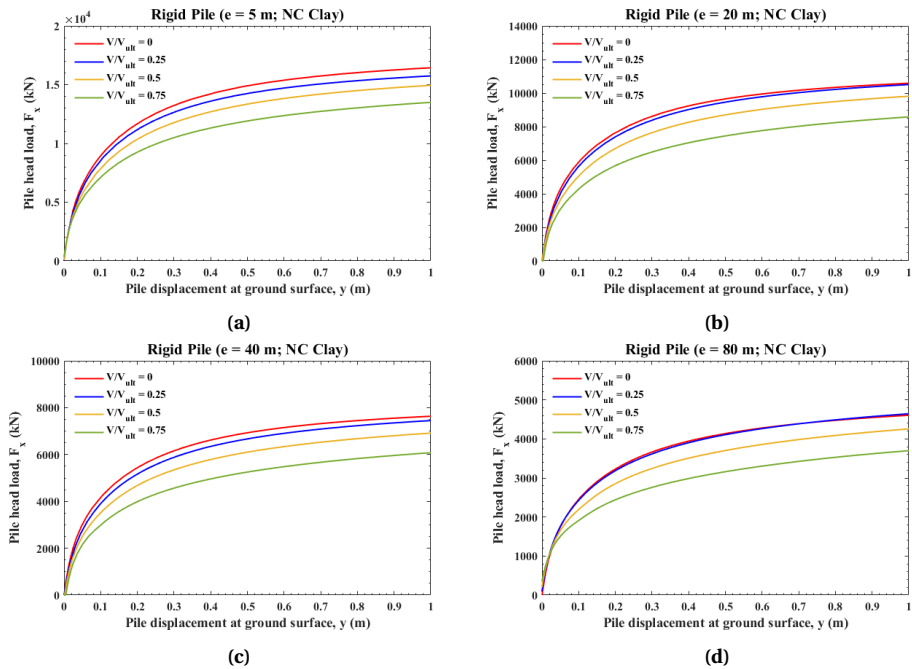
Figure B.2: Predicted response of rigid pile under lateral load per model in NC clay soil with loading eccentricity: (a) e = 5 m (b) e = 20 m (c) e = 40 m (d) e = 80 m.
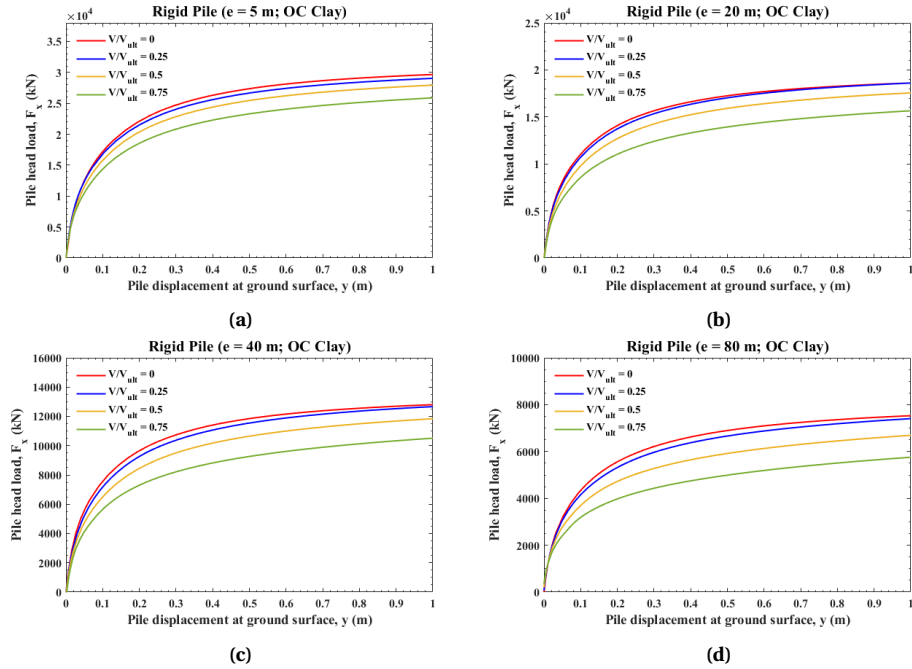
B.2. ANALYSIS REGARDING OC CLAY SOIL

Figure B.3: Predicted response of flexible pile under lateral load per model in OC clay soil with loading eccentricity: (a) e = 5 m (b) e = 20 m (c) e = 40 m (d) e = 80 m.
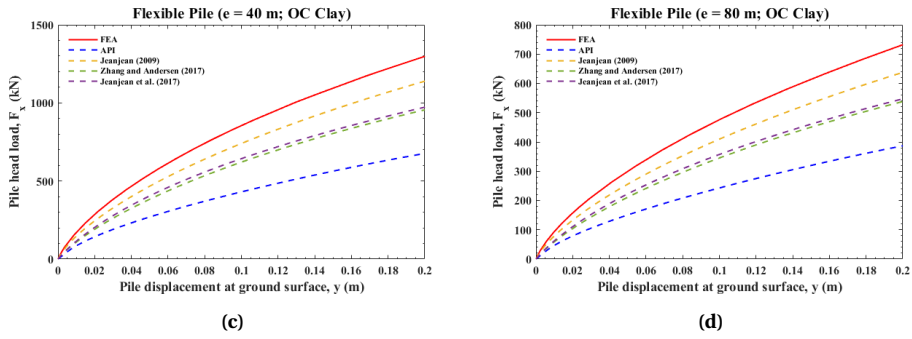
Figure B.3: (cont.) Predicted response of flexible pile under lateral load per model in OC clay soil with loading eccentricity: (a) $e = 5$ m (b) $e = 20$ m (c) $e = 40$ m (d) $e = 80$ m.

Figure B.4: Predicted response of rigid pile under lateral load per model in OC clay soil with loading eccentricity: (a) $e = 5$ m (b) $e = 20$ m (c) $e = 40$ m (d) $e = 80$ m.

C

LATERAL LOAD-LATERAL DISPLACEMENT CURVES

C.1. ANALYSIS REGARDING NC CLAY SOIL

Figure C.1: Response of rigid pile under combined loading in NC clay soil with loading eccentricity: (a) e = 5 m (b) e = 20 m (c) e = 40 m (d) e = 80 m.
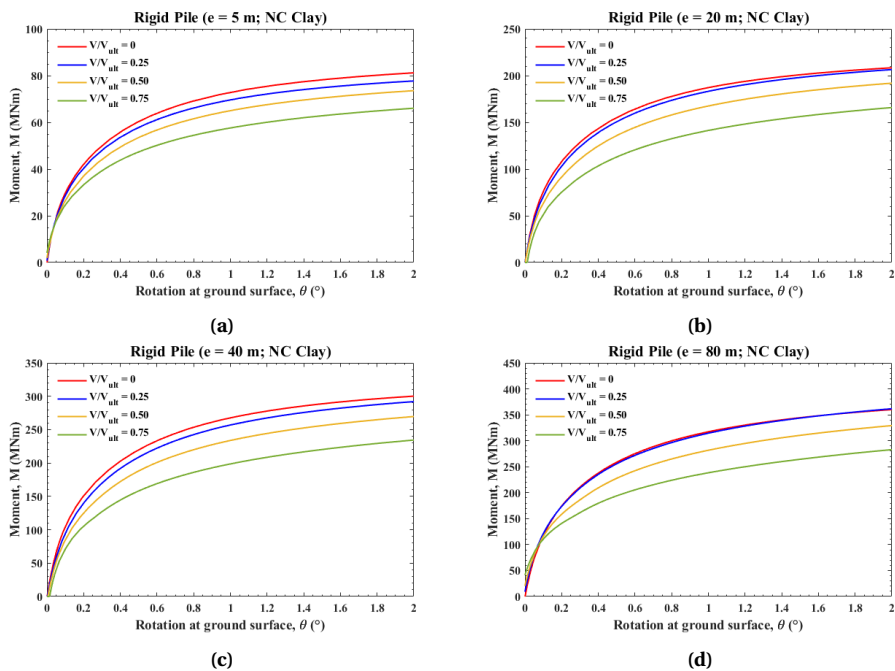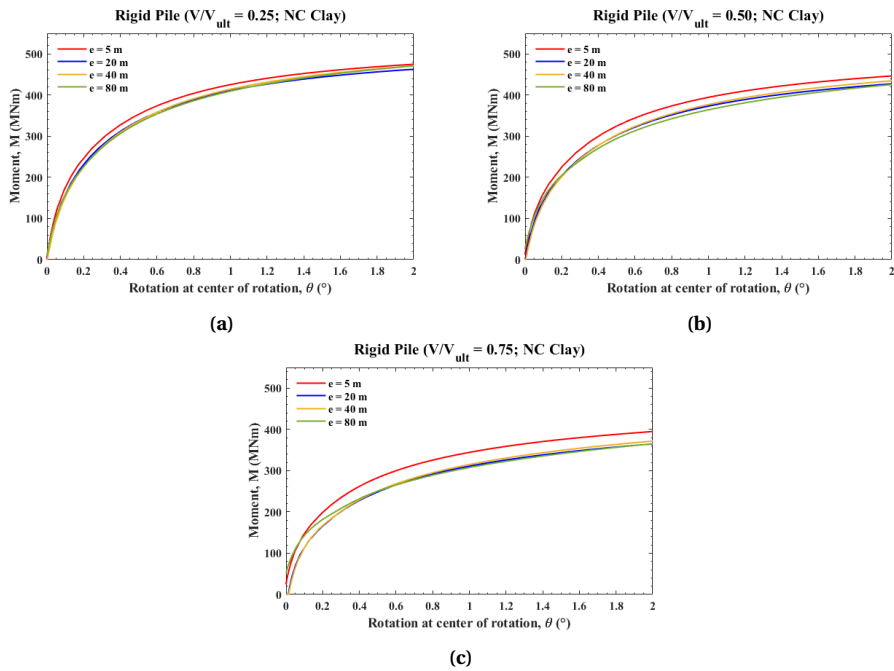
C.2. Analysis regarding OC clay soil

Figure C.2: Response of rigid pile under combined loading in OC clay soil with loading eccentricity: (a) $e = 5$ m (b) $e = 20$ m (c) $e = 40$ m (d) $e = 80$ m.

D

MOMENT-ROTATION CURVES
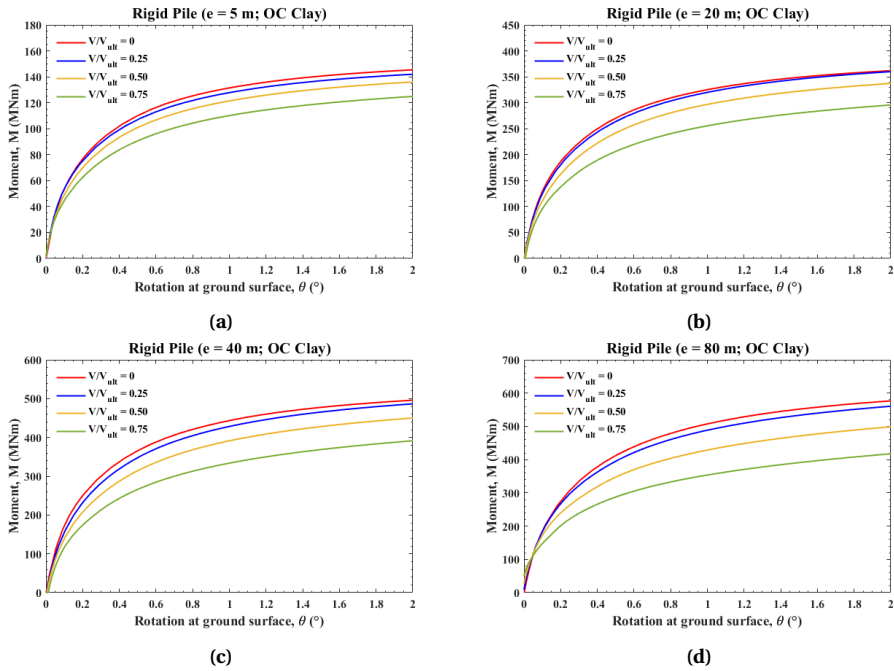
D.1. ANALYSIS REGARDING NC CLAY SOIL

Figure D.1: Moment-rotation curve at the ground surface of rigid pile under combined loading in NC clay soil with loading eccentricity: (a) *e* = 5 m (b) *e* = 20 m (c) *e* = 40 m (d) *e* = 80 m.
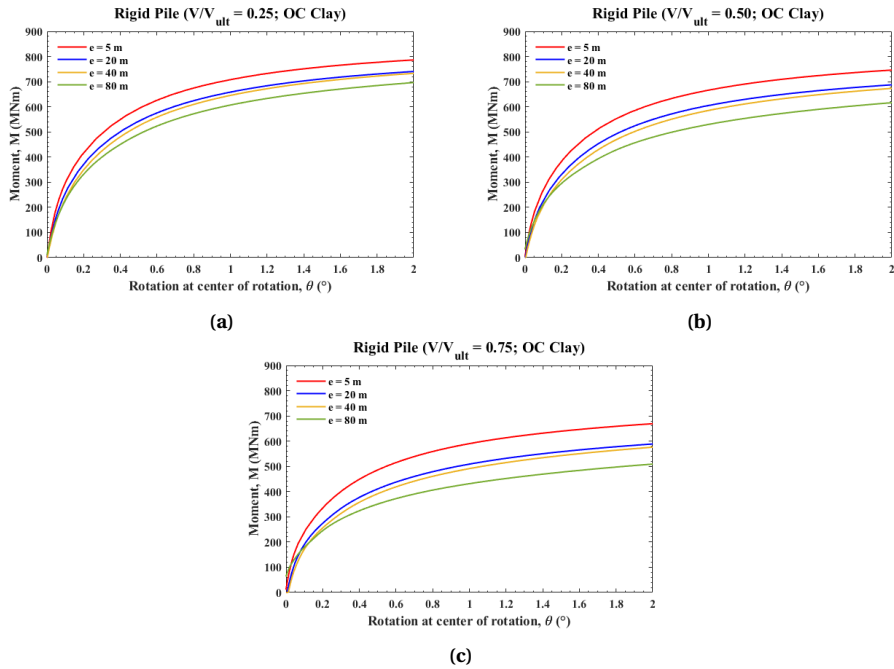
Figure D.2: Moment-rotation curve at the center of rotation of rigid pile under combined loading in NC clay soil with varying loading eccentricity and applied vertical load: (a) $V/V_{ult} = 0.25$ (b) $V/V_{ult} = 0.50$ (c) $V/V_{ult} = 0.75$.

D.2. ANALYSIS REGARDING OC CLAY SOIL

Figure D.3: Moment-rotation curve at the ground surface of rigid pile under combined loading in OC clay soil with loading eccentricity: (a) $e = 5$ m (b) $e = 20$ m (c) $e = 40$ m (d) $e = 80$ m.

Figure D.4: Moment-rotation curve at the center of rotation of rigid pile under combined loading in OC clay soil with varying loading eccentricity and applied vertical load: (a) $V/V_{ult} = 0.25$ (b) $V/V_{ult} = 0.50$ (c) $V/V_{ult} = 0.75$.

E

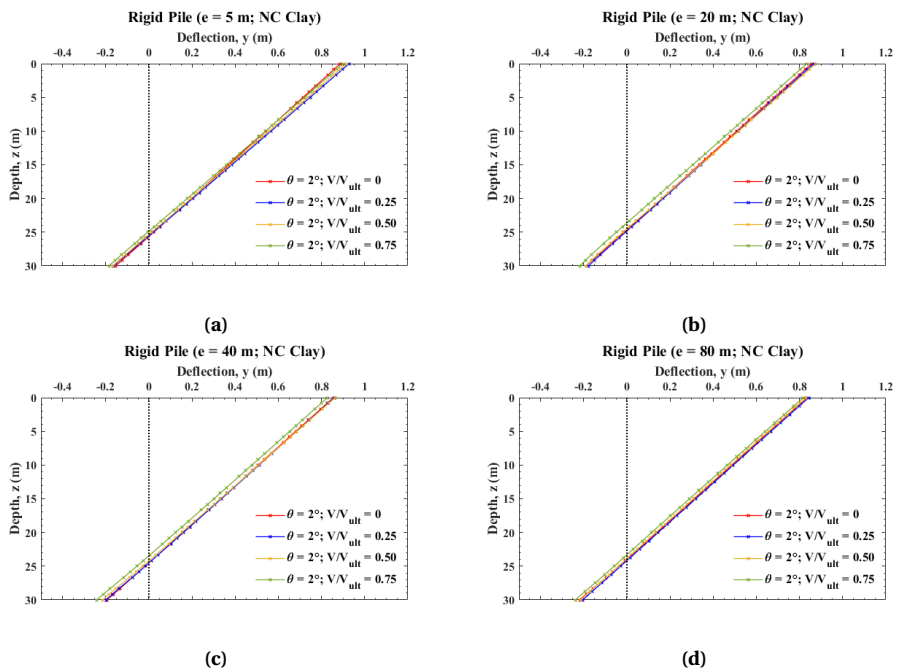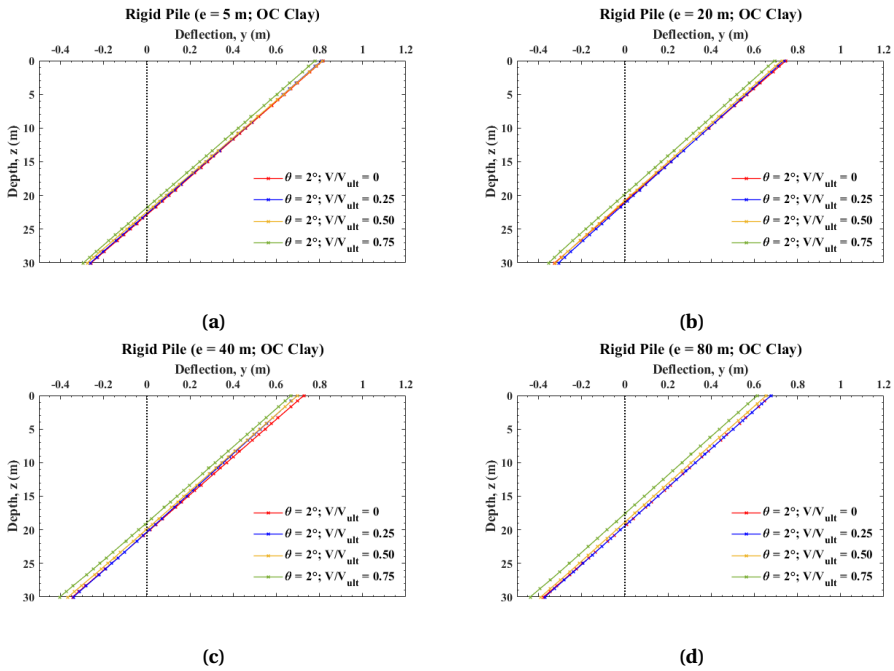## PILE DEFLECTION CURVES

E.1. ANALYSIS REGARDING NC CLAY SOIL

Figure E.1: Deflection profile of rigid pile under combined loading in NC clay soil with rotation θ = 2° and applied loading eccentricity: (a) e = 5 m (b) e = 20 m (c) e = 40 m (d) e = 80 m.

E.2. ANALYSIS REGARDING OC CLAY SOIL

(a)

(b)

(c)

(d)

Figure E.2: Deflection profile of rigid pile under combined loading in OC clay soil with rotation θ = 2° and applied loading eccentricity: (a) e = 5 m (b) e = 20 m (c) e = 40 m (d) e = 80 m.

F

ROTATIONAL STIFFNESS DEGRADATION CURVES

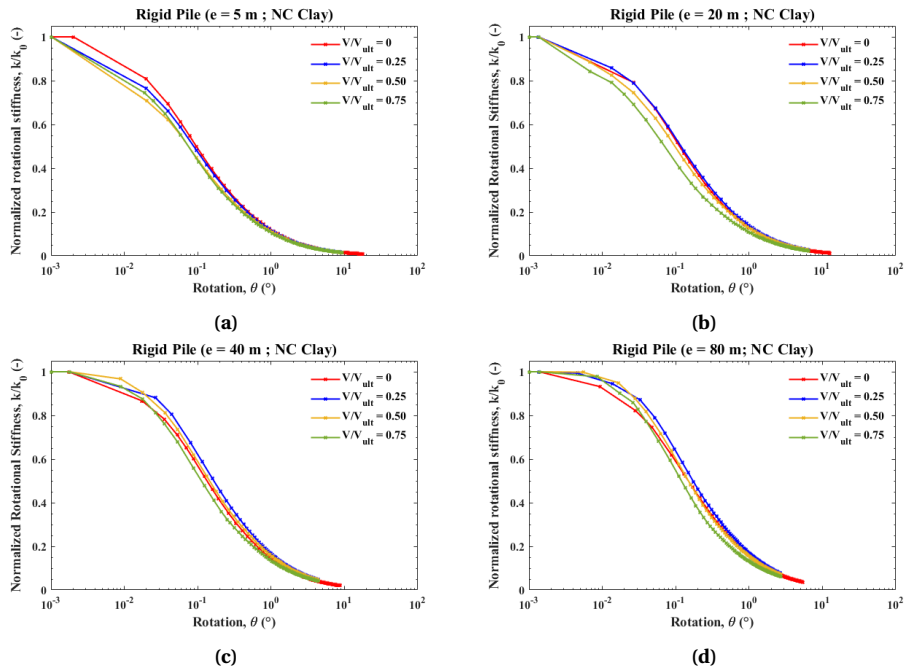### F.1. ANALYSIS REGARDING NC CLAY SOIL

Figure F.1: Normalized rotational stiffness degradation curve of rigid pile under combined loading in NC clay soil with loading eccentricity: (a) $e = 5$ m (b) $e = 20$ m (c) $e = 40$ m (d) $e = 80$ m.
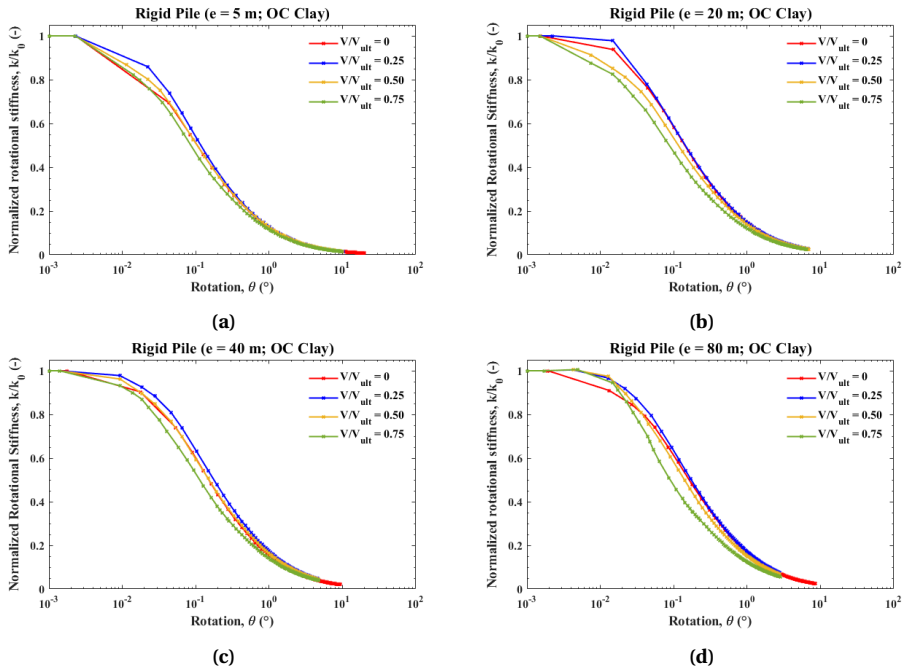
F.2. ANALYSIS REGARDING OC CLAY SOIL

Figure F.2: Normalized rotational stiffness degradation curve of rigid pile under combined loading in OC clay soil with loading eccentricity: (a) $e = 5$ m (b) $e = 20$ m (c) $e = 40$ m (d) $e = 80$ m.
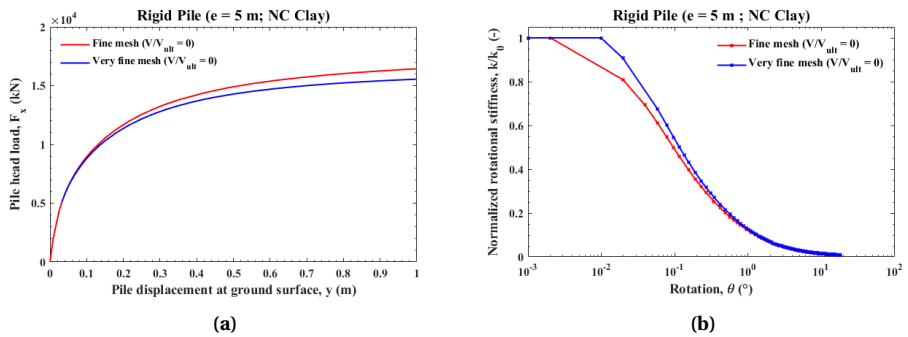
G

MESH ANALYSIS

Figure G.1: Mesh analysis on rigid pile with loading eccentricity e = 5 m in NC clay soil regarding: (a) lateral-load displacement and (b) stiffness degradation curve.